Stealth properties of nanoparticles against cancer

Surface modification of nanoparticles for passive targeting to human cancer tissue in zebrafish embryos

Patrick Lie Johansen

Thesis for Master's degree in Molecular Biosciences
Faculty of Mathematics and Natural sciences

UNIVERSITY OF OSLO

[May 2015]

II

Acknowledgments

Oslo, May 2015

Patrick Lie Johansen

IV

v

Abstract

The prospect of using nanoparticles (NPs) as carriers of drugs for use in treatment of diseases is becoming progressively more evident. The concept of NPs is in principle very simple; the encapsulation of drugs in NPs protects the drug, thereby increasing its blood half-life. The process of encapsulation also increases drug concentration at the target sites and lowers toxicity, thereby reducing side effects, an aspect that is very important for patient compliance. Current nanotherapies however, are not reaching these goals, at least not to their full potential. Clearance of NPs from circulation via organs such as the liver and spleen, as well as clearance from the body by macrophages of the mononuclear phagocyte system (MPS) represents major problems needing to be solved before NPs can be reliably used in cancer therapy. In this thesis, the zebrafish (ZF) embryo is introduced as a transparent vertebrate system for characterization of nanoparticles for use in cancer therapy. Via microinjections of a human cancer cell line, tumor-like structures were established in the ZF embryo. This transplantation process of human cancer cells via microinjections is made possible by the fact that the ZF is devoid of an adaptive immune system for the first 4 to 6 weeks after fertilization, and will not reject the foreign cells. The formation of these tumor-like structures can be followed in real time by fluorescent microscopy. By injecting fluorescent NPs, here made of polystyrene or liposomes into the ZF embryos, these can also be imaged in real-time, with a high spatial and temporal resolution *in vivo*. This ZF system is proposed as a quick and easy model for evaluating the properties of different NPs, as well as how different NPs interact with human tumor-like structures *in vivo*. In this thesis it is demonstrated that NPs have the capacity to co-localize with these tumor-like structures via passive accumulation, and a mechanisms for this passive co-localization is proposed based on fluorescent imaging using transgenic ZF lines. By applying a poly ethylene glycol (PEG) surface coating to the NPs, PEG was shown to decrease the uptake of NPs into macrophages *in vivo*. This PEG-effect was also shown using optical tweezers to quantify the interactions between NPs and macrophages, as well as cancer cells. The zebrafish embryos also give us the opportunity to investigate NP interaction with a biological interface in a more direct manner. By injecting the zebrafish with polystyrene NPs, and using the optical tweezers, we have established a protocol for *in vivo* manipulation of NPs. By combining the transparency of the zebrafish embryo with an optical tweezers setup, it is possible to manipulate NPs inside a living embryo, giving never before seen opportunities to investigate the interactions between NPs and biological systems. Due to the ZF systems imaging qualities this platform is suggested as a powerful system for screening of NPs before moving on to more clinical vertebrate systems, such as mice.

Selected abbreviations

ABC	**Accelerated blood clearance**
ATP	**Adenosine triphosphate**
DLAV	**Dorsal longitudinal anastomotic vessel**
DNA	**Deoxyribonucleic acid**
dpf	**Days post fertlization**
dpi	**Days post injection**
FGF-T-MAE	**fibroblast growth factor-overexpressing murine aortic endothelial cells**
FPC	**Fluorescent pixel count**
GF	**Growth factor**
GFP	**Green fluorescent protein**
HEK 293	**Human embryonic kidney 293 cells**
hpi	**Hours post Injection**
ISV	**Intersegmental vessels**
M*m*	**Mycobacterium *marinum***
MPS	**Mononuclear phagocyte system**
NP	**Nanoparticles**
OT	**Optical tweezers**
PEG	**Polyethylene glycol**

PSNP	**Polystyrene nanoparticle**
RES	**Reticuloendothelial system**
SEM	**Scanning electron microscopy**
TEM	**Transmission electron microscopy**
WCRF	**World Cancer Research Fund**
WHO	**World Health Organization**
ZF	**Zebrafish**

Table of contents

1 Introduction

1.1 Cancer

1.1.1 A brief introduction to cancer

Cancer is a generic term describing a larger group of diseases. This group of diseases can affect any part of the body and is defined by abnormal cell growth both in the organ or part of the body it resides in and beyond their usual boundaries.

Many types of cancer have their origin in cells and natural mutations of the DNA. However external factors is also known to be involved in the development of cancer, such as environmental toxins, radiation, exposure to certain chemicals and more[1-3].

The cause of cancer is now known to be damage, known as mutations, to the basic building blocks of all life, DNA. When these mutations accumulate in the DNA over time, it will cause the cell to lose and gain certain traits. If the acquired mutations affect control of cell growth or the cells ability to communicate with its surroundings it can lead to uncontrollable growth of the cell (the trait) and give rise to cancer.

After rapid advances in cancer research and medicine through the19th century a rich body of knowledge have been accumulated regarding cancer [4-9]. These discoveries have shown cancer to be a disease largely involving changes in genome dynamics. Oncogenes with gain of function and tumor suppressor genes with loss of function have been identified as being involved in the progressive transformation of normal cells to cancer cells[10].

1.1.2 Causes of cancer and geographical distribution

Despite the remarkable pace at which knowledge and understanding of cancer have been gained the development of new and more effective treatments is still a challenge. Mechanisms behind cancer initiation are still elusive and poor diagnostic tools to detect the disease at its earliest phases makes cancer still one of the leading causes of death world wide, with 14 million new cancer cases in 2012 and 8.2 millions deaths caused by cancer the same year according to the World Health Organization (WHO).

Some forms of cancer have higher incidence rates than other (Table 1). Liver, lung, breast, colorectal and stomach cancer are the dominant cancers leading to mortality. The leading causes of cancer according to WHO can be associated with five risk factors: high body mass index (obesity), low fruit and vegetable intake, lack of physical activity, tobacco use and excessive alcohol intake. All of which are global occurrences across populations, making cancer an illness with high incidence rates worldwide, although regional differences in both type of cancers and incidence are observed.

Table 1: World Cancer statistics for the most common cancers (2012) in both sexes.
Source: www.wcrf.org

World cancer statistics for the most common cancers(2012) in both sexes			
Rank	Cancer	New cases diagnosed in 2012 (1,000s)	Per cent of all cancers
1	Lung	1,825	13,0
2	Breast	1,677	11,9
3	Colorectum	1,361	9,7
4	Prostate	1,112	7,9
5	Stomach	952	6,8
6	Liver	782	5,6
7	Cervix uteri	528	3,7
8	Oesophagus	456	3,2
9	Bladder	430	3,1
10	Non-Hodgkin lymphoma	386	2,7

Table 2: Cancer frequency by country. *Source: www.wcrf.org*

Cancer frequency by country		
Rank	Country	Age-Standardized Rate per 100,000
1	Denmark	338,1
2	France	324,6
3	Australia	323,0
4	Belgium	321,1
5	Norway	318,3
6	United States of America	318,0
7	Ireland	307,9
8	Republic of Korea	307,8
9	The Netherlands	304,8
10	New Caledonia	297,9
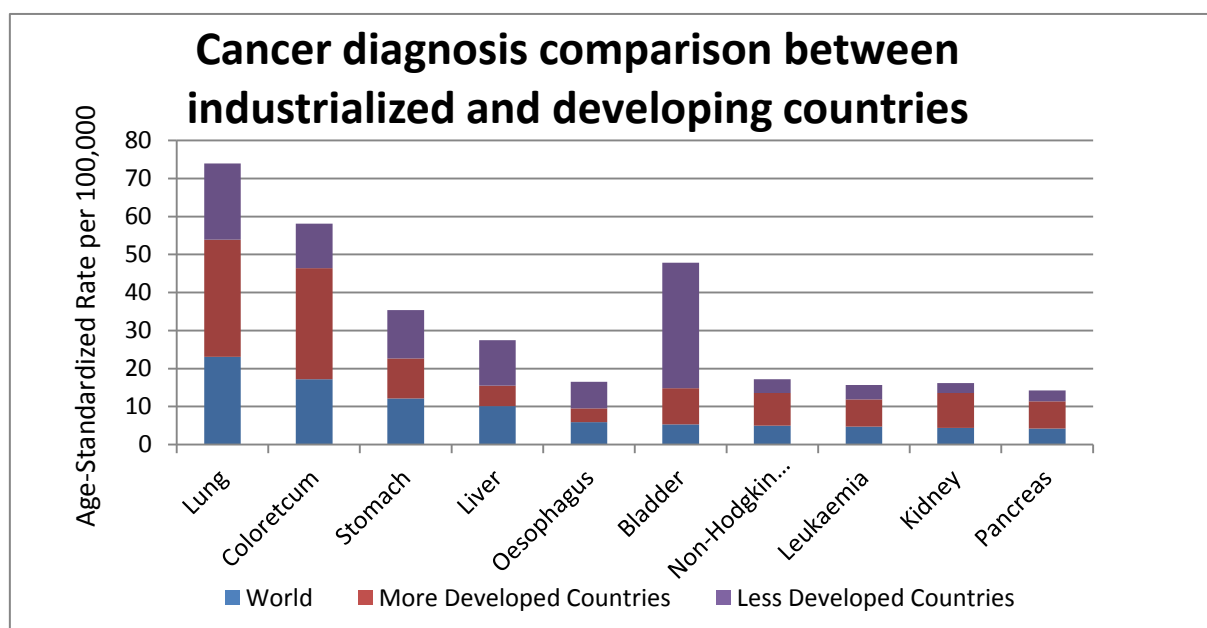
Figure 1: Comparison of cancer diagnosis between industrialized countries and developing countries. *Source: www.wcrf.org*

Numbers from the World Cancer Research Fund International (WCRF) (Table 1) show that the ten most common cancer types in the world are responsible for over 67% of the world cancer cases.

Data in Table 2 shows that the countries with the highest incidents of cancer are developed countries in the west, and most of them in Europe. The regional differences in types of cancer presented in Figure 1 shows a divergence in the types of cancer afflicting more, and less developed countries. Developed countries have a disproportionate affliction with regards to cancer, but as health care in undeveloped countries gets better and average life expectancy gets higher, the incidents of cancer will likely increase also there.

1.1.3 How Cancer Kills

Given the diversity of cancer as an illness, with regards to how the mechanics of different cancers function one would perhaps expect several different ways of cancer becoming lethal. However cancer only generally becomes lethal in one of two ways: (1) The location of a solid tumor can be fatal, such as brain or heart tumors, as it interferes with the organs ability to function normally[11], or (2) by metastasis[12]. Metastasis is the process whereby cancer cells separate from the primary tumor and migrate though the body via the lymph- or blood circulatory system and then settle in other locations, where they have the opportunity to develop into a malignant tumor[12]. Different types of malignant tumors have tendencies to metastasize in specific organs, with bone, lungs and the liver being the most common locations for where cancer metastases are found[13]. The human body cannot support the growth of several tumors simultaneously and the tumors can affect the function of the affected organs. Treatment of metastatic tumors is mainly aimed at controlling tumor growth, or simply to relieve symptoms. Most cancer related deaths are caused by metastatic cancer, and not by primary tumors interfering with organ function[12].

The aggressiveness, or metastatic potential of cancer is related to alterations in tumor suppressor genes and oncogenes that accumulate during the progression from a normal cell to a cancer cell[14], and much research has been done to get a better understanding of these alterations that give rise to traits associated with cancer cells.

4

1.1.4 Essential traits of cancer cells

In the 2000 paper by Douglas Hanahan and Robert Weinberg entitled 'Hallmarks of Cancer'[10] they proposed that cancer can best be understood by considering a few key underlying principals. These principals have to do with the rules that govern the transformation of normal cells into malignant cells. They proposed six hallmarks that are novel cellular capabilities. These are acquired during the stepwise progression from a normal cell to a cancer cell and consist of defects in the cells regulatory circuits that confer a type of growth advantage or metastatic property[10]. This idea was derived from the fact that virtually all mammalian cells have the same molecular machinery regulating three essential processes for normal cells and that are especially important in the progression into cancer cells; proliferation, differentiation and apoptosis. An overview of the six original hallmarks can be seen in Table 3.

Table 3: Overview of the 6 original cancer hallmarks as presented in Hallmarks of Cancer[10]

Hallmarks of cancer according to Hanahan and Weinbeberg
Self-sufficiency in growth signals
Insensitivity to antigrowth signals
Evasion of apoptosis
Limitless replicative potential
Sustained angiogenesis
Tissue invasion and metastasis

In addition to these six hallmarks, two more potential hallmarks are emerging as important traits in many forms of cancer. These are the reprogramming of the cancer cells energy metabolism and the cancer cells ability to evade destruction by the hosts immune system[15].

The uncontrollable proliferation of cancer cells resulting in their insensitivity to antigrowth signal and self-sufficiency in growth factors (GF) is sustained by

adjustment of the cells' energy metabolism. Cancer cells have a reprogrammed metabolism, making them largely favor aerobic glycolysis, meaning their energy production even in the presence of oxygen is limited to glycolysis[16, 17]. Since glycolysis has a much lower efficiency in ATP production compared to oxidative phosphorylation the cancer cells up-regulate the import of glucose via the GLUT1 transporter[18-20]. This form of energy production is believed to allow the cancer cells to divert glycolytic intermediates into biosynthetic pathways. This is a way for the cancer cells to support the rapid pace at which they divide, giving them an increased need for macromolecule and organelle production[21, 22]. The population of cancer cells also supplements their need for energy and their increased macromolecule and organelle production by diving into two subpopulations that function symbiotically. One subpopulation is the aerobic glycolysis cells secreting lactate and the other subpopulation import and utilizes the lactate as their main energy source [23, 24].

The immune systems role in tumor formation is another potential hallmark of cancer[15]. Anti-tumoral immune response is gaining increased viability as a concept and can possibly work as a significant barrier for metastasis and formation of tumors[25]. The theory that all tissue and cells are under constant monitoring by the immune system leads to the conclusion that tumors that do form have somehow evaded destruction by the immune system, and the increased incidence rate of cancer in immune-deprived patients seems to provide support for this theory[26]. Immunoevasion may therefore also be an important trait acquired by many forms of cancer.

The traits of cancer discussed above are achieved by different forms of the diseases classified as cancer in a myriad of different ways. The ones described briefly above are only a few examples. This diversity is what makes cancer so hard to effectively fight or cure. It is therefore necessary to constantly improve on both diagnostics and treatment options for cancer.

1.2 Current diagnostics and treatments of cancer

1.2.1 Diagnosis

If diagnosed early and correctly, treatment of cancer has a higher probability to end in remission of the cancer, while more advanced cases can get an increased lifespan [27, 28]. Therefore developing and researching diagnostic tools and methods for cancer has received a lot of attention. Methods span from non-invasive procedures like x-ray imaging, CT- and MRI scans, and ultrasound, to more invasive methods like endoscopy, tissue biopsies, surgery and blood and fluid samples.

From these tests the diagnosis will determine the type and grade of cancer, a process called cancer staging. This cancer staging in turn determines the prognosis and treatment options for each individual patient[29]. For optimal treatment an accurate diagnosis is important [30]. New and novel options have emerged during the last decade, utilizing new technology, making faster and more accurate diagnosis possible.

Among these techniques are molecular classification, using oligonucleotide microarray gene expression analysis to diagnose multiple, different well-differentiated cancer types[31]. Biomarkers provide another useful diagnosis and prognosis tool. Although different biomarkers have been used in diagnosis for some time, many used today have limitations. The ideal biomarker should have a high degree of specificity and sensitivity for a specific cancer; they should not be expressed by normal cells. These abilities enable biomarkers to track both progress of tumors, but also regression. They are therefore valuable in both diagnosis and prognosis settings. To find these ideal biomarkers high-throughput proteomics are now being used to research structure and function of possible biomarkers in cancerous tissue and associated fluids[32].

These new diagnostic tools allow scientists to stratify cancers in a new way. The more detailed subdivision and arrangement of cancer based on their biological properties and molecular make up is an important part in treatment and in advances in research into new treatment options. These new diagnostic tools will give doctors

and scientists a more detailed insight into the type of cancer they are looking at than the histological approach favored for many decades now[32].

One clinical example of the use and the importance of such diagnostic tools can be found in breast cancer. Some primary breast tumors are more likely than others to metastasize. The tools to differentiate between the tumors that are likely to become malignant and those likely to remain indolent for the remainder of the patients life will spare several women surgery and chemotherapy treatments. The use of gene expression arrays combined with bioinformatics has provided the capability of predicting the clinical course of breast cancer progression[33], a huge step forwards for the field of cancer diagnostics.

1.2.2 Treatment

Cancer treatment varies for different cancer types. Many cancer drugs target one or more of the essential traits of cancer cells described by Hanahan and. Weinberg[10]. Figure 2 illustrates example drugs and treatments aimed at attacking these traits in cancer, like telomerase inhibitors meant to stop cancer cells from having a limitless replicative potential.
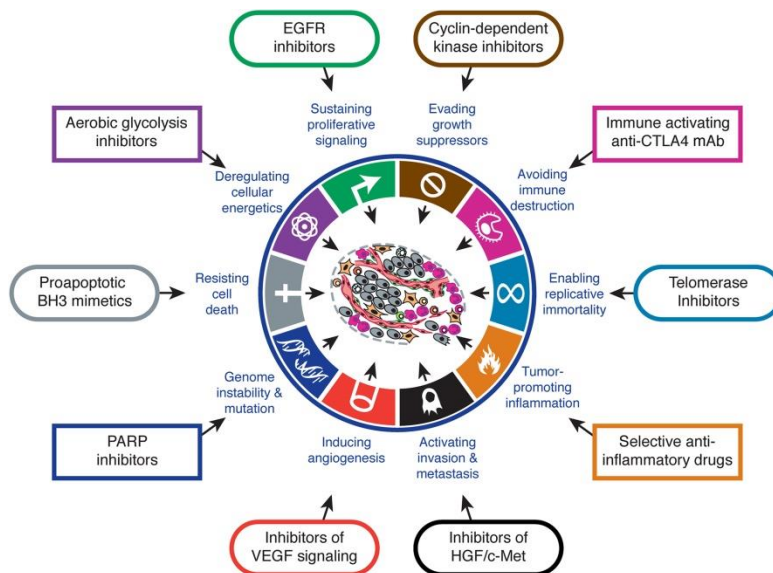

Figure 2: Overview of therapeutic targets of the cancer hallmarks. *Source: Cell 2011 144, 646-674DOI: (10.1016/j.cell.2011.02.013)*

Some types of cancer have a fairly high survival rate, especially if diagnosed early and the patient receives the appropriate treatment. Among these are prostate cancer, the 4th most common cancer in the world (Table 1), with a survival rate of over 98 per cent within 5 years of being diagnosed[34]. Other types of cancer do not have the same prognosis. Liver cancer, the 6th most common cancer in the world (Table 1), has a survival rate of only 16 per cent within 5 years of being diagnosed[35].

Early detection of colon cancer using new detection methods has caused a fall in death rates for this cancer type. However colon cancer in more advanced stages still kills most afflicted patients. This shows the inadequacy of chemotherapy and radiation in treatment of metastasized cancer cases [36].

There is also shown little decline in mortality rates in most other tumor types over the years. This indicates that the traditional therapies have stagnated and reached their peak potential in cancer treatment, at least in severe and advanced cases of malignancy[37].

Although the traditional therapies can be effective in reducing disease progression and reducing deaths associated with cancer within the first 5 years of diagnosis[37], new and more effective treatments are needed to increase survival of cancer patients and also increase the incidences of full remission in cancer. Although numerous treatment alternatives are available today, such as surgery, chemotherapy, radiation therapy, immunotherapy and stem cell transplants, these methods are collectively not effective in treating most cancers and more often than not entail varying degrees of side effects, some of them lethal by themselves for patients weak from disease[38, 39].

The reduction of side effects is important, not only for the patients' well-being, but also for the overall cost of treatment. With fewer and less severe side effects the rate of patients not needing to be admitted for longer periods of time (outpatients) can be higher, and the total of days spent in hospital can be reduced, thereby reducing treatment cost. With the possible future implementation of nanotechnology in the administration of anti-cancer drugs the total treatments and amount of drugs needed per treatment can possibly also be reduced, further reducing the cost.

Over the last 60 to 70 years the number of cancer cases has grown not only on an international level, but also in Norway (Figure 3), making the curing of cancer more important than ever. Moreover, the reduction of treatment costs and improvement of life quality of patients is also of major relevance, and more viable in the short term. Nanotechnology, including the use of nanoparticles in fighting cancer, like those used in this thesis offers a promising course of action to achieve these goals in the future.
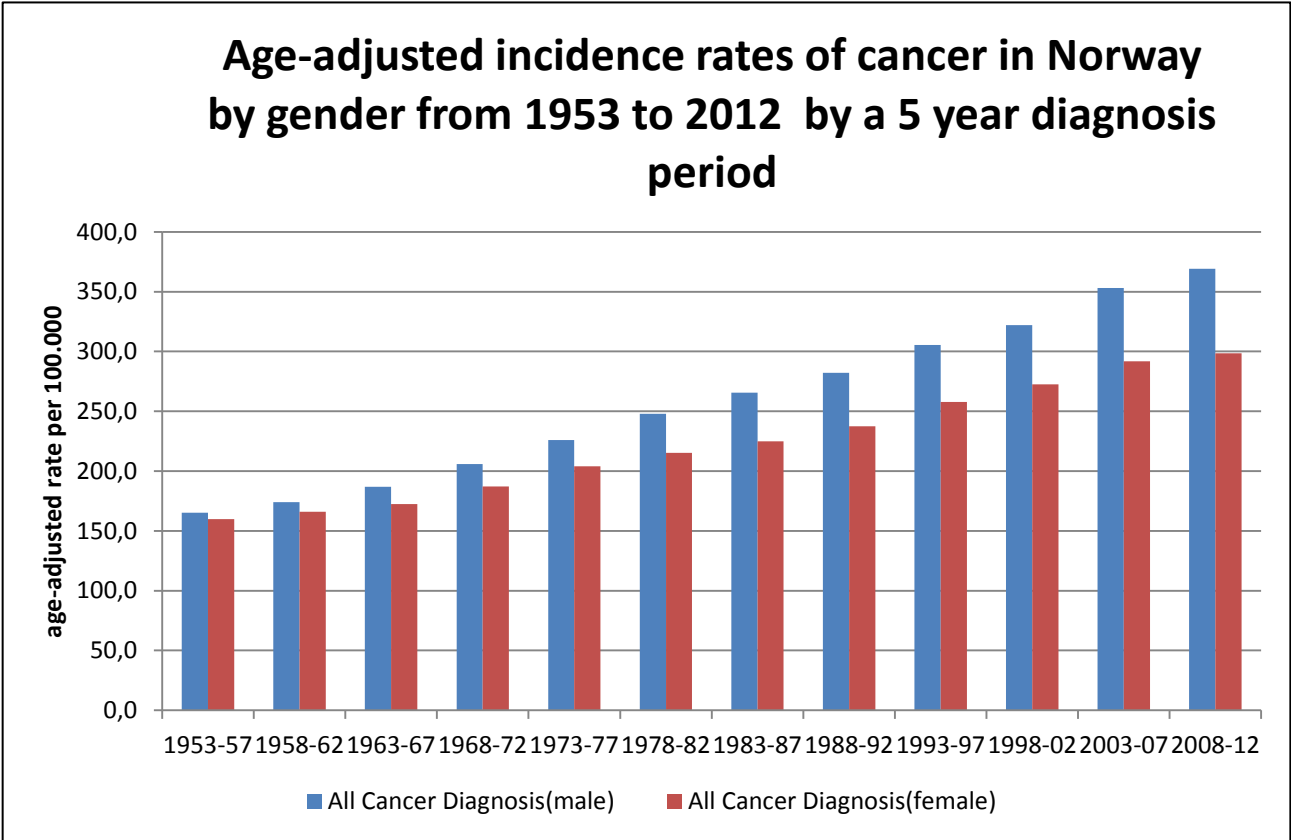

Figure 3: incidence rates of cancer in Norway, sorted by gender in the timespan of 1953 to 2012. *Source: Kreftregisteret / Cancer Registry of Norway*

1.3 Nanoparticles and their potential in treatment of cancer

1.3.1 Nanoparticles for use in cancer treatment

Since Richard Feynman's famous lecture 'There's plenty of room at the bottom' in 1959, when the field of nanotechnology was introduced, it has influenced almost every part of modern society. Nanotechnology as a field has existed since the 1960s, when liposomes was first described[40], but perhaps became more known to the public in the 1980s in part because of the advances made in integrated circuits and computer technology. Since its emergence the field has seen major growth and development, largely because of its high potential for commercial product development but also because of an academic interest in this novel field merging research disciplines such as biology, physics and chemistry.

One of many fields to spring from the emergence of nanotechnology was bionanoscience, where the focus is on how nanostructures and materials interact with biological specimens. A subfield of bionanoscience is the perhaps more known field of nanomedicine. Nanomedicine aims at using nanotechnology for treatment and diagnostics of diseases both in human and agricultural divisions [41-43]. The use of nanotechnology in medicine is meant to provide precise treatment and diagnostics by means not available with methods available today. These nanomedicines is also meant to provide faster, more accurate, higher yield and lower- cost treatments compared to the traditional treatment options. In this thesis the applications and ambitions of nanomedicine is exemplified by cancer and cancer treatment, and the use of nanoparticles (NPs) as a drug-delivery system in particular.

The ambition with the introduction of NPs in cancer research is to improve cancer therapy by increasing anti-cancer drugs efficiency and bioavailability, and at the same time decrease the toxicity [44-46]. The principle of current chemotherapy treatment is to distribute the drug to the whole body via the bloodstream. With this form of treatment mainly healthy tissue is exposed to the drug and only small amounts of drug reach the cancerous tissue. There is also a problem with the side effects of anti-cancer drugs. These side effects make the administration of optimal

doses impossible in a clinical situation. When the side-effects include vomiting, fatigue, depression, memory loss and more [47, 48], it is important that these are kept to a minimum.

The purpose of any pharmacological delivery system is to facilitate the effect of the drug, but also to enhance its potential for successful treatment. The drug must be delivered specifically to the correct location, the drug's site of action (the tumor). But it is also important that when the drug arrives at this location it is in the appropriate concentration and that it has the correct rate of delivery to maximize the therapeutic effects, but also to minimize side-effects.

An ideal delivery system could deliver the correct amount of drug to the exact site where it is needed at an appropriate and stable rate. If this can be done at the optimal time, or over a prolonged time period, with as few treatments, i.e. injections, pills or oral formulations as possible the effect of each treatment is increased and the side-effects are decreased giving the patients a more comfortable treatment course and better general health.

Several publications have described the promising results from using NPs as an approach for delivering drugs, and how modifications to these NPs, with for example polyethylene glycol (PEG), can further improve the efficacy of NP application to disease treatment[49-52].

The use of nanotechnological advances can increase the effectiveness of current drugs via active targeting and direct administration/targeted delivery of drugs. These advantages will also allow for smaller amounts of drugs to be administered, due to higher co-localization rates of drugs and cancer cells. The use of nanotechnology in cancer treatment, i.e. NPs will also be compatible with current effective anti-cancer drugs, meaning the anti cancer drugs already on the marked can be used to their full potential.

The use of these NPs can therefore increase bioavailability, reduce side effects due to delivery directly to the site of action and therefore lower dosages can be used and other healthy cells and tissue remain unaffected by the toxic drugs to a larger extent than before. Drug absorption onto the NPs can also be adjusted by coating the

12

surface of the NPs and distribution of the drugs in the body can also be adjusted by surface coating that facilitate targeting to specific locations[53, 54]. Surface coating can also contribute to an increase in uptake into cancer cells compared to non-coated NPs [55].

NPs can also offer sustained release of drugs over a prolonged time period, up to several days or even weeks[56]. This can be achieved by making the NPs biodegradable, meaning they break down slowly over time and by controlling the diffusion of the drugs from the NPs[57]. By further refining these parameters of diffusion and breakdown a more sustained release of drugs can also be possible, to ensure the minimal therapeutic dose of the drug is sustained for longer periods of time at the drugs site of action[56].

With the possibilities NPs offer, like sustained release, rate-controlled release, and targeted drug delivery, they can have significant potential for the future of cancer treatment. NPs are not however inert carriers when introduced to the circulatory system of an animal[58]. For the successful implementation of NPs in therapy several aspects of the NPs and the immune system and physiological environment of the host must be considered, including clearance by the renal system, immune system activation and potential toxicity[58-60] and the NPs designed accordingly.

1.3.2 Types of cancer eligible for nanoparticle treatment

Cancers eligible for treatment regiments using NP, such as those used in this thesis will be solid tumors, i.e. tumors not usually containing cysts or liquid areas and tumors consisting of groups of cancer cells that can be reached by NPs either through circulation in the blood or direct injections. NP treatments are also being pursued for use against cancer that is not classified as solid tumors, such as acute lymphoblastic leukemia or acute myeloid leukemia as well[61]. However these types of cancer is outside the scope of this thesis, seeing as treatment of these cancers using NPs in the form this thesis focuses on will demand more targeting functions to achieve co-localization with the cancer.

Solid tumors are among the most common, appearing in over 80 percent of cancer cases (Table 1). The five cancer types that accounts for the most cases in both men

and women in Norway are cancers that most commonly take the form of solid tumors (Figure 4). Among these are adenocarcinoma, which appears in 95 percent of colorectal cancer cases, as well as cancer of the bladder, lung and skin.

The most important traits of cancer eligible for NP treatment will be that the cancer cells are grouped together, forming a tumor, and that the NP can reach them through the circulation. For this process to be successful it is believed to be important that the tumors manipulate the vasculature, either by physical force or growth factor secretion[62]. These factors should make the endothelial lining of the vessels more permeable to the NPs, so that they can leak out from the blood stream and into the proximity of the tumor[63].

For a higher effect of NP treatment the particles should ideally be taken up by the cancer cells or be located in close proximity to them [64]. This will result in that the anti-cancer drugs being contained within these particles will be released inside of or right outside of the cancerous cells[65, 66]. This will not only increase the amount of drug that reach the cancer tissue, but also reduce the amount of healthy tissue exposed to the drug.
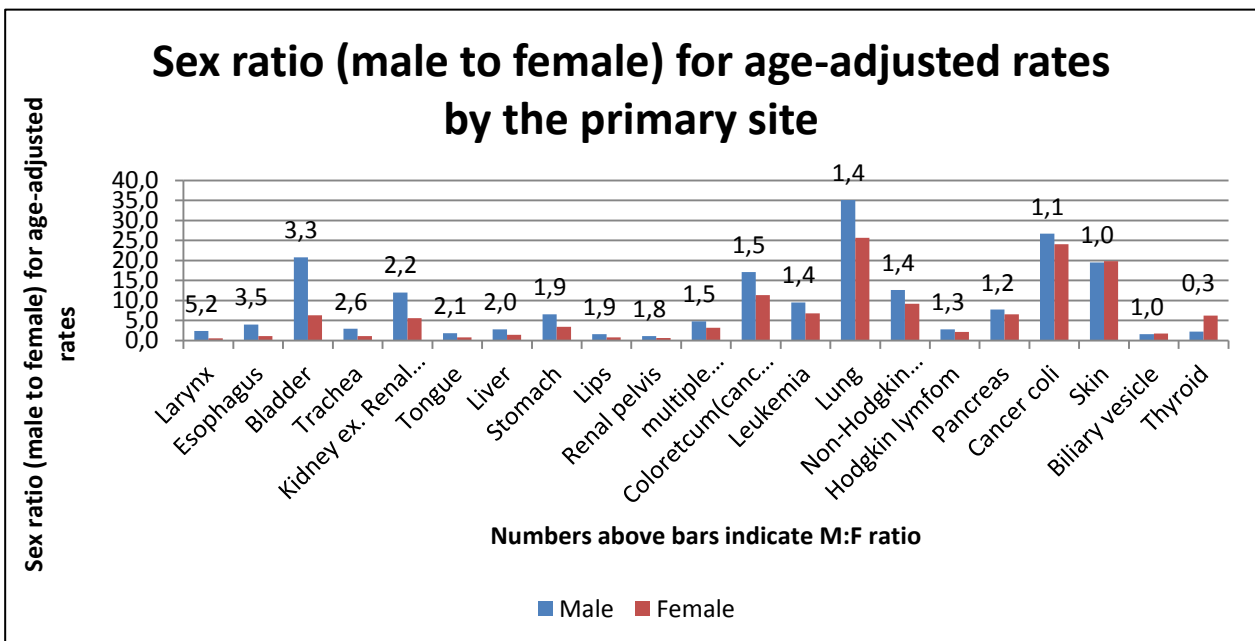

Figure 4: sex ratio (male to female) rates shown by primary site. *Source: Kreftregisteret / Cancer Registry of Norway*

14

1.3.3 Enhanced permeability and retention (EPR) effect

Taking advantage of the enhanced permeability and retention effect (EPR), described by Madea et al in 1986, co-localization between solid tumors and NPs is believed to be possible[67]. The EPR effect can be used to overcome a major problem affecting almost every type of cancer treatment in use today; a lack of tumor selectivity. The use of "selectivity" may however be misleading. When NPs are injected into the circulation, there is no "selectivity" *per se* when talking about the EPR effect. There is a distribution of NPs throughout the body, with the goal of "passive targeting" trough the EPR effect to achieve a disproportionate distribution of the NPs with regards to the tumors.

The EPR effect is a result of tumor vasculature abnormalities, like increased production of vascular permeability factors and hyper vascularization [68] .Vascular endothelial growth factor (VEGF) and other growth factors (GF) stimulate the formation of neovasculature and angiogenesis. This newly formed tumor vasculature is abnormal in form and architecture, giving fenestrations in the vessels caused by poorly aligned endothelial cells, a lack of smooth muscle and increased levels of vascular permeability factors[69, 70]. Also, hyperproduction of vascular mediators in addition to VEGF, like bradykinin, nitric oxide, peroxynitrite, prostaglandins, and matrix metalloproteinases contribute to the enhanced vascular permeability of vasculature in tumors tissue[71-73].

It is also possible that a decrease in circumference of tumor-affected vasculature, achieved by the tumor physically pushing or otherwise restricting the vessel, may lead to a higher hydrostatic pressure locally. It has been shown that an increase in fluid pressure in vasculature increases the deposition of particles on endothelial cells *ex vivo* [74, 75]. It is therefore possible that through this pressure-deposition mechanism NPs will have a higher degree of adhesion to the tumor vasculature, leading to NPs adhering more frequently to endothelial cells in these tumor affected areas; this facilitates NP co-localization with tumors. This pressure-deposition mechanism together with increased fenestration due to GF expression from the tumor may be part of what is called the EPR effect.

These fenestrations coupled with the fact that tumor tissue usually lack effective lymphatic drainage allow molecules of a certain sizes to escape the circulation locally and accumulate in the surrounding tissue, avoiding clearance [68]. NPs can also avoid renal clearance due to the size factor; it is generally stated that only molecules below 6-8 nm are excreted by the kidneys[76]. By also not being able to penetrate tight endothelial junctions present in healthy vasculature and avoiding clearance by the mononuclear phagocyte system (MPS) NPs can stay in circulation for a prolonged period of time. This facilitates for the EPR effect to cause something akin to passive targeting to solid tumors of NPs loaded with anticancer drugs. These factors make tumor vasculature a valid target for cancer treatment using NPs. By targeting the tumor vasculature, the tumor itself is also targeted indirectly, or the tumors supply line of nutrients and routes for metastasis can be affected.

1.3.4 The immune system

The mononuclear phagocytic system (MPS), or sometimes called the reticuloendothelial system (RES), is a part of the immune system. The MPS consists of both fixed and mobile cells and serves to remove and destroy bacteria, denatured proteins, antigen processing and presentation, storage of inert colloids and toxicity control from cellular debris as a result of apoptosis. The fixed cells consist of liver macrophages, the Kupffer cells, as well as macrophages in the spleen, lung, bone marrow and lymph nodes. The mobile cells are the blood monocytes and tissue macrophages[77].

As the cells making up the MPS are always 'looking' for "foreign objects" in the host body, the use of NPs in treatment of cancer needs to avoid clearance from the body both by the MPS and via the renal system. The later is achieved by the size of the NP used, considering a cut of size in the renal system of 6-8 nm [78, 79]. The MPS is harder to avoid, but still possible to elude over shorter time frames [80]. In some instances however, uptake by the MPS is desirable to treatment, like in TB treatment[81], described in section 1.4.3.

The clearance kinetics by the MPS is depended on multiple factors, including physiochemical properties such as size, charge and the hydrophobicity of the objects[80]. These factors also contribute greatly to the behavior of the objects when

16

introduced into the host. With NPs a build up of a 'corona', which refers to an aggregate of plasma proteins also known as opsonization, around the NPs is common. This corona can influence the behavior and interaction of the NPs with the host system[58, 82]. It has been noted that NPs with positive surface charges are quickly aggregated to serum proteins *in vivo*, and cleared by the MPS[58].

Macrophages are the main obstacle for obtaining longer circulation times of NPs *in vivo*. Macrophages being specialized in uptake of foreign objects in their host, and being distributed widely and in key locations make avoiding macrophages important for efficient NP treatment[83]. Different surface modifications (see section 1.3.5) and physical shapes and size variants of NPs and other delivery system have been tried to achieve this stealth factor [58, 84].

In this thesis the effect of PEGylation of NPs has been a focus, both to avoid uptake in macrophages but also to see the effect of PEG on possible uptake of NPs in cancer cells and general interaction with the host. Using RAW macrophages, the effect of PEG *in vitro* was investigated, and using different ZF lines the NP interaction with the host *in vivo* was studied.

1.3.5 Nanoparticle surface modification and optimization

To avoid uptake by the MPS, polyethylene glycol (PEG) is one possible surface coating that can be used. With the addition of PEG, opsonization is prevented, and the time the NPs spend in circulation is increased [58, 85]. These effects combined are called the "stealth effect". This "stealth effect" is reported to increase systemic circulation time of NPs of different materials and composition [86, 87].

PEGylation reduces the hydrophobic interactions of the NP with the MPS by steric hindrance. By preventing opsonization of molecules and proteins related to the MPS on the NP surface, the stealth mechanic is enabled and results in longer circulation times [86, 88-90]. The PEGylation also increases the size of the NP, which is also a factor in clearance[91].

Multiple factors of the NPs and their surface influence their behavior with the host and its immune system. Size, shape and charge are amongst the most prevalent[58].

NPs with a positive surface charge are reported to be taken up at a faster rate in non-phagocytic cells compared to neutral or negatively charged NPs[92]. In phagocytic cells however, uptake of negatively charged NPs seems to be preferred[82] .

1.3.6 Accelerated Blood Clearance and other problems to address with NPs and PEG

PEG has been suspected as a cause of a phenomenon known as Accelerated Blood Clearance (ABC) phenomenon[93]. This immunogenic response has been observed after repeated administration of PEGylated carriers such as NP or PEG conjugated liposomes, and refers to a process whereby PEGylated carriers such as these experience an accelerated clearance and reduced efficacy[94]. Phenomenon like accelerated blood clearance, macrophage uptake and adherence to endothelial cells are some problems needing to be addressed before NPs can be effectively used in cancer therapy. To address issues such as these, new systems and methods for testing and evaluating NPs is needed.

1.4 Zebrafish as a vertebrate model for human cancer and nanoparticles

1.4.1 Zebrafish as a model in general

The zebrafish (ZF) (*Danio rerio*) holds several appealing properties as a model organism. The ZF is relatively cheap to keep, they are small, fast to develop and have a high fecundity. The embryos and larvae are optically translucent and they have a sequenced genome [95-99]. Moreover, a comparison between human and ZF genomes indicates a high number of orthologue genes (Figure 5) [97]. They also come in a variety of transgenic lines, with reporter genes for fluorescent macrophages, endothelial and lymphatic systems, and there are several genetic tools available to mutate the fish, like knockdown via morpholino anti-sense oligonucleotides and zinc finger nucleases [100, 101]. All these properties have made the ZF model increasingly popular in the scientific community, as is evident by the increase in publications using the ZF as a model system over the last 15-20

years as reported by Kinth et al 2013, going from 226 publications in 1996 to 1929 publications in 2012[102].
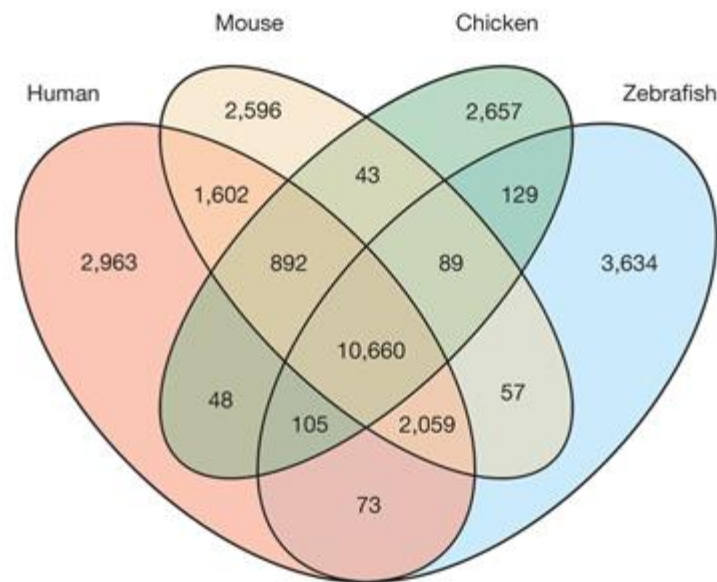
Figure 5: Orthologue genes mutual to ZF, chicken, mouse and human. Source: The zebrafish reference genome sequence and its relationship to the human genome, Nature 496, 498–503 (25 April 2013) doi:10.1038/nature12111. Modified for use.

1.4.2 Zebrafish as a model for human cancer

The ZF is a diverse model for human cancer. This is mainly due to transgenic methodologies and zebrafish lines with gene-specific mutations, yielding models for melanomas, rhabdomyosarcoma and many other solid tumors[103].

Xenograft transplantation of human cancer cells into the ZF embryo is another valuable method for cancer studies. By transplanting fluorescently labeled human cancer cells using microinjections one can establish tumor-like structures in the ZF [104, 105]. After transplantation one can follow the growth/proliferation, migration, invasiveness and neovascularization of the transplanted cells[106]. This translucency combined with xenotransplantation of fluorescent cells and confocal and stereo fluorescent imaging makes the ZF an excellent model organism for studying cancer cells *in vivo*. The ZF system gives several advantages over mouse or other

mammalian models, making the use of zebrafish as a complementary model system in research a powerful tool.

ZF embryo is without an adaptive immune system until approximately four to six weeks old[107].Thus, transplanted cells will not be rejected by the ZF embryo due to the lack of a fully developed immune system. This lack of adaptive immunity allows for the transplanted human cells to establish a tumor-like structure in the embryo. The establishment of transplanted tumors is achieved 2 days post injection of the cancer cells[108]. These features make the ZF viable for cancer studies, as well as NP research *in vivo*.

1.4.3 Nanoparticles and the zebrafish model

Tumor transplantation of human cancers into the ZF has already been described in previous sections (1.4.2), as has the ZF as a model system (1.4.1, 1.4.2). The advantageous traits of the ZF allowing for *in vivo* fluorescent imaging and the ZF limited immunity at the embryo stage can be used to study not only the mechanisms of cancer, but also to study possible treatment options for cancer and other diseases[109].

The benefits of NPs in drug delivery and for diagnostic purposes can be hard to study. After injection, or other forms of delivery into most model systems, one can not readily observe how the NP interact with the host or the disease in question or how they are distributed, at least not in the higher order vertebrate model organisms such as mice and rats without laborious methods. The ZF however offers an excellent view of the NP interactions with both host and disease[81]. This way potential complications, as well as benefits of using NPs can be observed.

In the ZF larvae observations of NP "stickiness" can be made, an example of complications with specific NPs. These kinds of uncontrolled nano-bio interactions can involve a myriad of proteins in the corona surrounding the NPs [110, 111]. These kinds of interactions of NPs with living systems are poorly understood. When it comes to the use of NPs and nanomaterials in treatment in humans the physiological response of the NPs must be understood and controlled, to be seen as safe to use. For example, sticking of NPs to endothelial cells will reduce the amount of NPs

reaching its desired target and can cause other side-effects like inflammation or other immune responses to occur. Phenomenon like this can be easily observed in the ZF, even without euthanasia, under a fluorescent microscope.

One other example of the use of the ZF and its optical translucency with fluorescent imaging is found in NP and tuberculosis (TB) research. The formation of granulomas and macrophage uptake of foreign bodies, NP, in the ZF system was visualized using fluorescent NPs, fluorescent bacteria and lines of ZF with fluorescent macrophages and neutrophils illustrating the usefulness of the ZF as a model organism[81]. The NPs are loaded with antibiotic drugs, that will be taken up by the macrophages and co-localize with the Mycobacterium *marinum* (Mm) bacteria growing in granulomas inside the macrophages endosomes. In this way the antibiotic drugs are brought in close proximity to the Mm bacteria. Directly after delivery into the ZF the NPs can be observed. The interactions of the NP with the vasculature and distribution within organs and discreet compartments of the ZF can be visualized *in vivo*. This enables researches to make observations that are not possible, or at least much more complicated to achieve in other non-optically translucent systems. In these non-translucent systems the delivery into the host is made, and only after a necropsy the distribution of NPs can be quantified. The advantageous traits of the ZF model have also allowed us to develop novel *in vivo* methods for NP evaluation.

2 Aims

The aims of this thesis was three-fold; (1) Establish a transplantation protocol for human cancer in ZF embryos, (2) show that the ZF-cancer system can be used for evaluation of NPs for use in cancer treatment as well as evaluation of NP interaction with biological system using novel methods and (3) investigate the stealth-effect mediated by PEGylation of NPs both *in vivo* and *in vitro*. These aims will be investigated using the ZF model, as well as cell cultures, optical tweezers, flow cytometry, fluorescent imaging and micro-injections of cells and NPs.

3 Methods

Recipes for all cell mediums and solutions used for cell and fish work can be found in Section 8.9: Recipes.

3.1 Nanoparticle preparation and characterization

The liposomes were made by Lars Herfindel, at the University of Bergen. The liposomes that were used in this thesis consisted of hydrogenated egg phosphatidylcholine (HEPC), and polyethylene glycol (PEG) 2000 Dalton (Da) for the PEGylated liposomes. The ratio of HEPC, cholesterol and PEG for the PEGylated liposomes is 1,81:1:0,15 (PC:Chol:PEG_PE), which means 5.1 % of the total lipids or 7.7 % of phospholipids are PEGylated. For detailed explanation of liposome preparation and composition, see Myhren et al.[112] The liposomes were stored at 4$^{\mathrm{O}}$C in lightproof containers, and used for experiments for up to 2 weeks from the date of production.

Four fluorescent monodispersed Fluoresbrite® Carboxylate Microspheres (PSNPs) (PS-COOH, 2.6% solid (w/v) aqueous suspensions) were purchased from Polysciences, Inc. Two bright blue (BB) carboxylate microspheres (particles size: 0.49µm and 0.997µm) containing dyes (coumarin) with excitation maxima 360 nm. One yellow-green (YG) carboxylate microsphere (particles size: 0.19 µm) containing dyes (fluorescein) with excitation maxima 441 nm. α-Amino-ω-methoxy-poly(ethylene glycol) 5000 (MPEG5k-NH2) was synthesized according to a previous report.[113] The other chemicals, HOBt (1-hydroxybenzotrizole), EDAC (1-dimethylaminopropyl-ethylcarbodiimide hydrochloride), NHS (N-hydroxysuccinimide), barium hydroxide solution (0.05M) were purchased from Sigma-Aldrich and used without further purification, unless otherwise started.

The "brush-like" immobilization of the MPEG5000-NH2 on the surface of carboxylate microspheres was used an adapted procedure from a previous report by using EDAC in the presence of HOBt was performed in an aqueous solution at 4$^{\mathrm{o}}$C.[114, 115] The larger PEGylation particles (0.49µm and 0.997µm) suspension were purification by centrifuged at 10000g for 10 min at RT, washed once with 0.01 M HCl and three

times with PBS-buffered solution (pH 7.4) via dispersion and centrifugation. The particles were re-suspended in PBS (0.044 wt% for 0.997μm and 0.344 wt% for 0.49μm PEGylation particles) and stored at 4^oC until use. The smaller PEGylated particles (0.19μm) suspension were purified by dialysis first against distilled water and then against PBS-buffered solution (pH 7.4) at 4^oC for 3 weeks using a dialysis membrane of regenerated cellulose with a molecular weight cut-off of 8000. The suspension in PBS was stored at 4^oC (the concentration: 0.443 wt% for 0.19 μm PEGylation particles) were determined by using UV-Vis photometer (the absorbance of the maximum peak vs particles concentration according to the Beer-Lambert law).

3.2 Fish care and treatment

The ZF line AB(wt) was used for the following experiments: quantification of growth of human cancer cells, study liposome accumulation in tumor-like structures, study nanoparticle circulation time and endothelium affinity. The ZF line Tg(fli1:EGFP)y1 was used to study the relation between ZF vasculature and injected human cancer cells, and to confirm that endothelium was the tissue PSNPs adhered to. The ZF line Tg(mpeg1:mcherry) was used to study *in vivo* macrophage uptake of NPs. Embryos were kept in standard embryo water added 0.003% phenylthiourea (Aldrich) in Petri dishes at 28.5 °C, except for embryos injected with human cancer cells who were kept at 35 °C. Keeping the embryos at 35 °C gave no adverse effects on their development. The experiments were conducted in agreement with the provisions enforced by the Norwegian national animal research authority (NARA).

3.3 Cancer cell lines

The human metastatic melanoma cell line Melmet 5 was established from a lymph node biopsy of a metastatic melanoma patient at the department of Tumor Biology, The Norwegian Radiumhospital. Melmet 5 and Melmet 1 was maintained in culture in RPMI1640 medium (Lonza) completed with 10% FBS (Saveen & Werner) and 2 % penicillin-streptomycin (Lonza). Melmet 5 was transduced and stably expresses a dsRed fluorescent marker for visualization. The cells were incubated at 37°C, 5% CO_2. The growth medium was changed every third day and cells were passaged following standard protocols prior to reaching confluence. When passaged or

24

prepared for ZF injections Versene (Life Technologies) rather than trypsine were used to preserve the molecular profile on the cell membrane.

The commercial available human liver cancer cell line HepG2 were maintained in culture in DMEM (Lonza) completed with 10% fetal bovine serum and 2 % penicillin-streptomycin (Lonza), as was the FGF-T MAE cell line. HepG2 was transduced and stably express a mCherry fluorescent marker for visualization. The growth medium was changed every third day and cells were passaged following standard protocols prior to reaching confluence. When passaged or prepared for ZF injections Versene (Life Technologies) rather than trypsine were used to preserve the molecular profile on the cell membrane.

3.4 *In vitro* assay for macrophage nanoparticle uptake

The PSNPs (Polysciences Inc.) were prepared as multiplicity of infection (MOI) 100 and MOI 20 solutions. They were sonicated for 10 min before dilution. RAW macrophages were seeded in small individual dishes compatible with confocal imaging in RPMI1640 medium and left overnight for adhesion. Next morning, the following was done: PSNPs were mixed in RPMI1640 in a concentration of $2x10^8$/ml. Cell medium containing PSNPs was added to the dishes with RAW macrophages and incubated for 4 h. The cells were subsequently washed 3 times with PBS to remove free PSNPs. Next, fresh medium was added before confocal imaging was performed. For liposomes cells were seeded in the same way as described. The next morning a 1 % liposomes solution was prepared in PBS and the PBS/liposome solution was incubated on the RAW macrophages for 10 minutes. The cells were washed and imaged identical to the protocol for PSNPs. For Flow cytometry analysis RAW cells were seeded at $1x10^6$ cells per well in a 12 well dish in 1 mL medium and left for 4 h to allow adhesion. The NoPEG and PEG PSNP suspensions were added to the cells and mixed gently by swirling and incubated for 4 h. Then cells were washed twice with ice cold DPBS without Mg^{2+} and Ca^{2+} before incubation in DPBS without Mg^{2+} and Ca^{2+} in the fridge for 10 minutes. Then cells were scraped off and collected in the bottom of the dish before they were washed 3 times with ice cold DPBS without Mg^{2+} and Ca^{2+}. The cells were kept on ice until the flow analysis.

3.5 ZF injections

Embryos were injected using a glass needle (Harvard apparatus) controlled with a micromanipulator Narishige MN-153 connected to an Eppendorf FemtoJet express. Microscopic visualization of the fish during injections was facilitated by a stereomicroscope Leica DFC365FX with a 1.0X Planapo lens.

Cancer cell injections: Cancer cells were grown in a T25 flask and harvested when reaching 85% confluence. The entire cell population was centrifuged in a 15 ml Falcon tube, washed once with PBS without resuspending the pellet, PBS was removed so that the pellet barely was covered in PBS and then the cells were resuspended in this small PBS volume. Upon injection; to estimate the number of cells coming out of the needle, test injections were done in a drop of water on the lid of a petri dish. The injection pressure or injection time was adjusted to obtain the desired number of cells per injection. 2 dpf embryos were anesthetized with tricaine as described in Gao et al.[116] and 200-300 cancer cells were injected in the lower part of Duct of Cuvier (see Figure 6A). 24 hrs post injection embryos were screened for tumor-like structures in the tail and normal blood flow throughout the entire embryo.

Nanoparticle injections: To study nanoparticle behavior in ZF embryos 2 dpf embryos were anesthetized as described. A glass needle was prepared so the tip was narrower than the posterior cardinal vein; the injection site for NPs as marked in Figure 6A. Approximately 3 nanoliter of nanoparticle suspension was injected. The calibration was done at 60x magnification using the standardized graph in supplementary protocol 1.

Accumulation of NPs in tumor-like structures: To study the potential for accumulation of NPs in the tumor-like structures in the tail of ZF embryos 2 dpf embryos were injected with cancer cells as described. Tumor-like structures were allowed to grow for 2 days. Then 4 dpf embryos with tumor-like structures in the tail were injected with NPs as described. Embryos were anesthetized as described and inspected for potential accumulation of NPs in the tumor-like structures, using the Leica stereomicroscope, 2-5 h post injection of NPs.

26

3.6 ZF imaging

A Leica DFC365FX stereomicroscope with a 1.0X Planapo lens was used for quantification of growth of the fluorescent tumor-like structures in ZF embryos. It was also used for imaging of fluorescent NPs in ZF embryos and acquisition of time-lapse videos of circulating NPs in ZF embryos. Prior to imaging ZF embryos were anesthetized by adding tricaine to embryo water. Upon imaging embryos were placed on a Petri dish on a polymerized 1.5% agarose bed with just enough embryo water to avoid drying the embryo. All time-lapse videos in supplementary data are shown at 7 frames per second.

An Olympus FluoView 1000 upright BX61WI confocal microscope was used for high-resolution microscopic imaging. Prior to imaging embryos were anesthetized in tricaine (Finquel, Argent Laboratories) as described in Gao et al.[116] Subsequently, they were placed in a small dish with a glass bottom filled with low melting point agarose. Once the agarose polymerized embryo water containing tricaine was added. We used a 40x water objective in Figure 6 and a 60x water objective in Figure 10 and 11. In Figure 12 the blue dye Dextran (MW 10 000) was used. 3D view PlugIn in Fiji computer software was used in Figure 11D. The laser lines for fluorescence imaging used were 405 (blue), 488 (green), 543 (red).

3.7 Fluorescent Pixel Count (FPC)

The FPC was used to evaluate growth of injected cancer cells in the ZF embryos. The ZF was injected with cancer cells 2 dpf as described. The images were acquired at 2, 4 and 6 dpi using fluorescent stereomicroscopy with a Leica DFC365FX with a 1.0x Planapo lens. The tail region of the fish was imaged and analyzed with FPC using ImageJ software. The same zoom, gain and exposure times were used for all time points, although different setting were used for the two cancer cells lines. The fish was kept in individual wells in a 12-well plate during the experiments in order to track individual fish. The image analysis was done using Image J software. The images was changed to 16-bit formats and an pixel counting of pixel above lowest gray value of true signal was used to quantify the surface area of the tumor-like

structure over the 3 time points. See supplementary protocol 2 for detailed instructions.

3.8 *In vitro* optical tweezers experiments

Cancer cells or macrophages were seeded out in individual 35 mm glass bottom dishes coated with poly-d-lysine (MatTek). The cell suspension was diluted to contain approximately 25 000 cells/ml. 2 ml of this suspension was added to each dish. The cells must be incubated at 37^OC for at least 4 h for them to adhere to the glass bottom dish before the experiment begins. Before the experiment the medium was removed, and the cells washed 3x with PBS (Sigma). 2 ml of the solution containing the NPs were then added to the cells. 3 different solutions with NPs were used for this experiment, PBS, RPMI-1640 (Sigma) or PBS with NPs incubated in mouse serum (Innovative Research Inc) for the macrophages or human serum (Innovative Research Inc) for the Melmet 5 cells.

For those NPs incubated with either mouse serum, human serum or FBS (Saveen & Werner) 0.000065 wt % of the NPs where incubated with 0.5 ml of the respective solution for 15 min at room temperature($20\text{-}22^O$C) in a 1.5 ml Eppendorf centrifuge tube. Then the NP-serum solution was centrifuged for 15 min at 15.000x g. The supernatant was removed carefully, not to re-suspend the pellet. 0.5 ml of PBS was added, and the pellet re-suspended. The solution was centrifuged for 15 min at 15.000x g. This washing step was repeated 1 more time. After the last washing the supernatant was removed, and 0.5 ml of PBS added and the pellet was re-suspended with a pipette. 0.5 ml of the solution was then diluted in 10 ml of PBS in a 50 ml tube, and sonicated for 5min to make the solution monodisperse. Before adding the NPs who was incubated with the serum to the cells, wash the cells 3x times with 3 ml of PBS to remove residuals of the growth medium. After washing add 2 ml of the NP solution. For the samples where the NPs are not incubated with serum, follow the same protocol, but only use PBS in all the steps. The presence of protein on the surface of the NPs after incubation was confirmed running a 2 % SDS-PAGE gel electrophoresis. The NP concentration used for the gels was normalized for surface area, with a total surface area of $2.85m^2$ for both 1000 nm and 500 nm

28

PSNPs, and incubated in 0.5 ml of undiluted serum solution. The control used was also undiluted serum. The results are attached in supplementary data 5.

When performing the experiments 15 different PSNPs where used on 15 different cells. The macrophages may adhere more to the PSNPs if the same cell is probed several times, to avoid this new individual cells was used for every new PSNP. A total of 15 cells and 15 particles where used for all the experiments. The software of the OT was programed to move the sample stage in such a way that the cell was moved towards the PSNP in the trap at a speed of 10 µm per second. When the cell made contact with the PSNPs, the stage stop moving for 1 second, and then the cell was moved away from the PSNPs at 10 µm per second. The 1 second delay upon contact is to give time for adhesion.

3.9 *In vivo* optical tweezers experiments

For injections of cancer cells or NPs prior to the optical tweezers experiments see section 3.5.

The embryos were anesthetized using 0.5 ml – 2 ml of tricaine stock solution per 20 ml of EM depending on how slow blood flow was desired. On a 24 x 60 mm coverslip two parallel lines of silicon was applied. The lengths of these lines should be approximately 30 mm and the should be a approximately 20 mm apart. Within these lines the embryo is placed in 60 µl of EM-tricaine solution and mounted on a 22 x 22 mm coverslip on top of the embryo. The coverslip was gently pushed down onto the silicon lines, carefully, in order not to damage the embryo. It is important that the upper coverslip is pushed far enough down as to make sure the embryo does not float around. Remove excess fluids using a filter paper. Seal the gaps between the upper and lower cover slips using clear nail polish. Mount the cover slips on the sample stage of the optical tweezers.

The experiments were mostly performed in the caudal vein (CV) or caudal artery (CA) of the ZF embryo. This is one of the thinnest parts of the embryo, and is therefore suited for optical tweezers. The areas in or around the CV or CA are also the areas where NPs tend to stick to endothelial lining, and is also the area where

cancer cells tends to escape the circulatory system and establish the pre neoplastic structure.

A laser power between 1-3 watts where used for the experiments. Certain areas of the embryos (seen as a dark black spot under the microscope), which are probably color pigments (melanocytes) are more sensitive to the laser than other areas of the embryo. Therefore applying high laser powers on these pigmented areas often lead to damaging the embryo.

3.10 SEM and TEM imaging

The liposomes were imaged using transmission electron microscopy (TEM) using a Philips CM100. A negative stain was applied using 2 % uranyl acetate. The polystyrene NPs were imaged with scanning electron microscopy using a Hitachi S-4800. The suspension of NPs was applied to the double-sided carbon tape and air-dried under a lamp for 30min. They were then coated with a 4 nm layer of platinum.

3.11 Statistics

The statistics was done using Excel (Microsoft). For the *in vitro* optical tweezers and growth of the cancer cells after injection the Barnards exact test was used to determine p-value, as the data was regarded as binary with regards to adhesion/no adhesion or growth/no-growth respectively. The standard errors (SE) for the binary data was calculated using $SE=\sqrt{(\pi(1-\pi))/n}$, where π=sample proportion of responders. Significance level is shown as *$p<0.05$, **$p<0.01$, ***$p>0.05$.

4 Results

4.1 The ZF embryo supports growth of human cancer cells

Fluorescently labeled human cancer cells (200-300 cells, see Materials and Methods) were injected into the lower part of the Duct of Cuvier of 2 days post fertilization (dpf) ZF embryos. Subsequently, the dissemination of cancer cells via the vasculature to the tail tissue could be monitored live by microscopy (Figure 6A). Embryos injected with human cancer cells were kept at 35°C as a compromise between the optimal temperatures for ZF embryos (28^0C) and human cells (37^0C).

The human melanoma cell line Melmet 5 was chosen because of the known capacity of these cells to establish solid tumors in mice.[117, 118] Injected Melmet 5 cells extravasated from the embryo blood vessels within the first 24 h post injection. The mechanism for establishment of a tumor-like structure appeared to be extravasation of multiple cancer cells at the same location; a crucial step in the formation of these structures as a single cancer cell cannot form a sufficiently large structure within the desired time window of 2 days post injection (dpi). In the ZF model the Melmet 5 cell line established both single and multiple tumor-like structures in the tail (Figure 6B). Using the transgenic ZF line Fli1, with a GFP reporter gene expressed specifically in the endothelial cells resulting in a green fluorescent vasculature, we could monitor the cancer cells location relative to the blood vessels. At the site of extravasation and growth of the tumor-like structure the Melmet 5 cells generated "pockets" in between blood vessels as they pushed the vasculature aside (Figure 6 c-d). The blood flow was not observed to be affected by the presence of the tumor-like structure and no endothelial cells were observed to migrate into the tumor-like structure.

The growth of the tumor-like structures was quantified every second day over a period of six dpi for the Melmet 5 tumor cell types (Figure 6E) using the fluorescent pixel count (FPC) method (see Materials and Methods). The extravasated Melmet 5 cells showed an average growth of 84 % from 2 dpi to 6 dpi, with variations among the individuals ranging from 13 % decrease in size to a 162 % increase in size. The results collectively demonstrate the ZF embryos ability to support human cancer cell

survival and even expansion of the tumor-like structures. These experiments set the stage for using the ZF embryo as a system for monitoring NPs in a dynamic *in vivo* vertebrate model for human cancer.
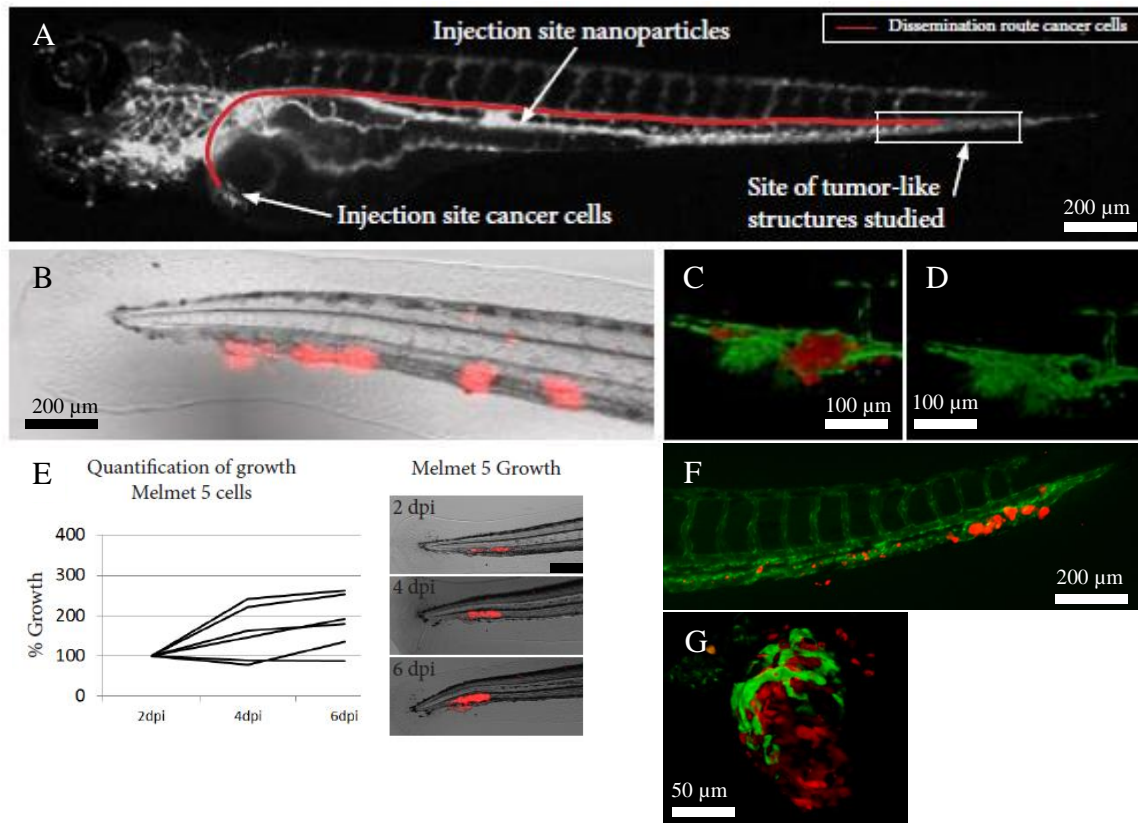

Figure 6. ZF injections and establishment of human tumor-like structures. (**A**) Illustration of injection sites for human cancer cells and NPs; Cancer cells were injected into the lower part of Duct of Cuvier and NPs were injected into the posterior cardinal vein for systemic distribution. The red line illustrates the dissemination route for cancer cells in the circulation to the preferred site of extravasation (White Square) where tumor-like structures were established. (**B**) The melanoma cell line Melmet 5 (red) had the capacity to establish multiple tumor-like structures in the tail. (**C**) A tumor-like structure comprised of Melmet 5 cells and the orientation relative to the vasculature (green). (**D**) Melmet 5 tumor-like structures reside in between blood vessels which are pushed away and excluded from the site of the cancer cells. No endothelial cells were observed to migrate into the tumor-like structure (**E**) Quantification of Melmet 5 tumor-like structure sizes in individual embryos over a period of 6 days post injection (dpi) (p<0.05). Scale bar is 200 μm. (**F**) The melanoma cell line Melmet 1 (red) had the capacity to establish multiple tumor-like strucutres along the tail region of the ZF embryo. This phenotype was similar to the one of Melmet 5. (**G**) A tumor-like structure established by transplantation of FGF-T-MAE cells into the ZF embryo. The phenotype for this cell line was different from both the Melmet 1 and 5. The tumor-like structure was established in the area of injection, rather than in the tail region. It also recruited functional blood vessel (green) trough angiogenesis. This phenotype was however not as frequently observed as the phenotypes that were readily achieved by using the Melmet cell lines.

The human liver cancer cell line HepG2 (Hepatocellular carcinoma) was also tested based on its ability to establish solid tumors in mice[119], along with Melmet 1[117] cell line and fibroblast growth factor-overexpressing murine aortic endothelial cells (FGF-T-MAE) cells [120](Figure 6 C-D).

However, these cell lines did not display a phenotype regarded as most suited for later experiments for *in vivo* testing of nanoparticles in the zebrafish model for human cancer. HepG2 had inconsistent growth, while Melmet 1 did not generate tumor-like structures, and FGF-T-MAE only grew large tumor-like structures at the site of injection.

The focus of the thesis was put on the Melmet 5, because they showed consistent growth and phenotypes after transplantation into the ZF embryos.

4.2 NPs without PEG display short circulation times *in vivo*

NPs without polyethylene glycol (PEG)-coating are known to have poor circulation times *in vivo* as they are more prone to be cleared from the circulation by macrophages.[121] The transparency of the ZF embryo model offers the possibility of fast, yet detailed *in vivo* investigation and imaging of bio-distribution of NPs.[81] By visual inspection via stereomicroscopy, we next evaluated the circulation times and bio-distribution of polystyrene nanoparticles (PSNP) and liposomes without PEG (NoPEG) in 2 dpf ZF embryo. We chose to work with these PSNPs as they have a uniform size and are easy to surface-modify because of their carboxylated surface. The liposomes were included as this type of NPs are already used for therapeutic purposes in the clinic.[122]

In order to observe the behavior of these NoPEG NPs in the ZF embryo relative to the vasculature we used the transgenic Fli1 ZF line and injected blue fluorescent 1000 nm NoPEG PSNPs (Table 4) into the posterior cardinal vein (Figure 6A). The NoPEG PSNPs stopped circulating minutes after injection. The NPs did not leave circulation and they seemed to have high affinity for the endothelium (Figure 7A) hindering circulation in the vasculature. With the aim to quantify circulation times by inspection of acquired time lapse videos, green fluorescent 200 nm NoPEG PSNPs

(Table 4) was injected into wild type ZF embryos. Twenty seconds post injection the PSNPs were in circulation (Figure 7B, asterisk) but a fraction had already adhered prominently to the endothelium (Figure 7B, red arrows, Supplementary video 1), as evident by intense green immobile dots. By 140 seconds post injection there were very low levels of NoPEG PSNPs left in the circulation (Figure 7C, white asterisk, Supplementary Video 2) compared to 20 seconds post injection, while there was increasing adhesion to the endothelium. The NoPEG PSNPs did not discriminate between the different blood vessels and adhered in comparable amounts to the caudal artery (Figure 10C, yellow asterisk), caudal vein (Figure 10C, red asterisk) and the Dorsal Longitudinal Anastomotic Vessel (DLAV) (Figure 7C, white arrow). The intersegmental vessels (ISV) are visible due to circulating NoPEG PSNPs meaning that they did not adhere to these narrow blood vessels (Figure 7C, yellow arrow).

Twenty minutes post injection there was a complete clearance of NoPEG PSNPs from the circulation, predominantly due to high affinity for the endothelium. Individual endothelial cells could be observed in the caudal vein as a speckled pattern along the vasculature to which the NoPEG PSNPs had adhered to (Figure 7D, green). The high affinity of the PSNPs for the endothelium may be toxic, since all the embryos which showed high affinity of the NPs for the endothelium died within 24 h.

We also did a parallel analysis for green fluorescent 200 nm NoPEG liposomes injected into wt embryos and embryos from a transgenic ZF line with red fluorescent macrophages (mpeg cherry, material and methods). This enables observation of the macrophages by fluorescent imaging to monitor their role in clearance of liposomes from circulation. Shortly after injection, the liposomes circulated through all blood vessels and consequently a full representation of the vasculature was visible as a green fluorescent signal (Figure 7E). The circulation time of the NoPEG liposomes was several hours, significantly longer than NoPEG PSNPs. Infrequent events of random adhesion to the endothelium could be observed (Figure 7D, arrow) but liposomes batches used within two weeks from production did in general not adhere to the endothelium. Inspection of the injected embryos the next morning, 20 h post-injection showed a total clearance of liposomes from the circulation. The injected mpeg cherry embryos showed that macrophages had cleared them from circulation.

34

Multiple yellow dots were visible in the tail referring to the red macrophages filled with green liposomes (Figure 7F, arrows). Note that very few macrophages are actively clearing liposomes from circulation as the majority is associated with other tissues and are not blood resident macrophages (Figure 7F, red). Importantly, the liposomes did not adhere to the endothelium and showed no toxicity to the ZF embryos, in stark contrast to the NoPEG PSNPs.
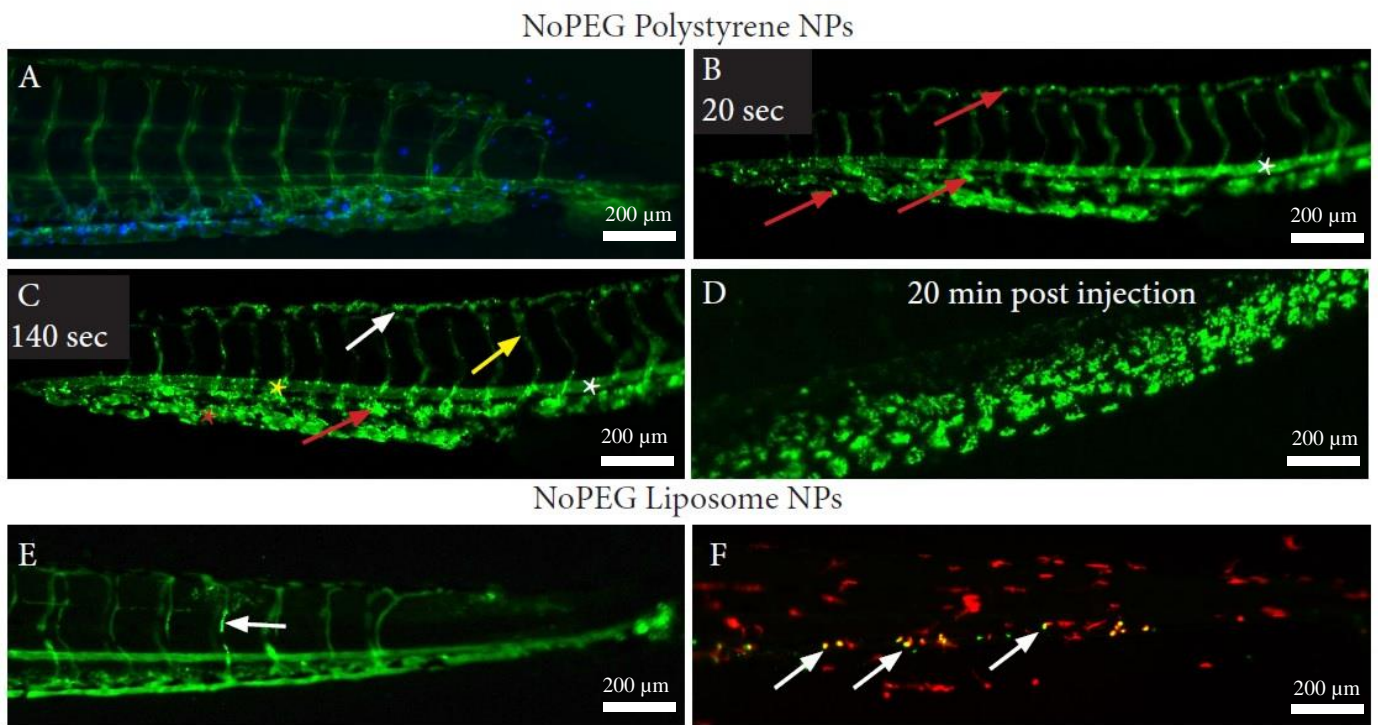
Figure 7. NoPEG NPs displays short circulation times. (A) NoPEG blue fluorescent 1000 nm PSNPs injected into Fli1 embryos show that the vasculature attracts PSNPs. **(B)** NoPEG green fluorescent 200 nm PSNPs injected into wt embryos. 20 seconds post injection NoPEG PSNPs was circulating (asterisk) but had already started to adhere to the endothelium as evident by green intense dots (red arrows). **(C)** 140 seconds post injection a relatively low level of NoPEG PSNPs was still in circulation (white asterisk). NoPEG PSNPs adhesion to the endothelium was even more evident (red arrow) and prominent adhesion was also observed in the DLAV (white arrow), caudal artery (yellow asterisk) and caudal vein (red asterisk). Very little adhesion was observed in the intersegmental vessels (yellow arrow). **(D)** 20 minutes post injection all NoPEG PSNPs was cleared from circulation and a speckled pattern appeared as a result of NoPEG PSNPs adhering to endothelial cells. **(E)** NoPEG green fluorescent liposomes right after injection circulates through the vasculature as evident by the complete representation of the vasculature in the tail. Minute levels of liposomes were occasionally observed to adhere to the endothelium (white arrow). **(F)** 20 hours post injection into mpeg cherry embryos; NoPEG green liposomes are all cleared from circulation and taken up by the red macrophages, here visible as yellow dots (arrows).

4.3 NPs coated with PEG display stealth properties *in vitro*

The paradigm in the nanoparticle field is that PEG adds stealth properties to NPs. The prevailing theory to explain this phenomenon is that this process prevents opsonization by plasma proteins and subsequent macrophage uptake and by this prolongs NP circulation time.[58, 85, 87, 123] We wanted to investigate in detail how PEG-coating affects the interaction between PSNPs and macrophages *in vitro* before testing them *in vivo*.

As an initial *in vitro* model system for analyzing the effect of PEG on PSNPs, we chose to use the mouse macrophage RAW cell line. These commonly used cells are easy to grow and display classic macrophage behavior regarding uptake of foreign particles. Green fluorescent 200 nm PEG (Figure 8A, Table 4) and NoPEG PSNP were added to the cell medium of RAW cell cultures and incubated for 4 h. After washing away unbound NPs, the cells were monitored by confocal analysis. The images clearly show that NoPEG PSNPs are taken up in high amounts as the cells displayed a clear fluorescence from the NPs (Figure 8B, left panel). In contrast, the PEGylated PSNPs could hardly be observed within cells; only minute levels were taken up (Figure 8B, right panel). To quantify the levels taken up by macrophages we performed flow cytometry showing a two-fold increase in uptake of NoPEG PSNPs compared to PEG PSNPs (Figure 8C). This increase in uptake was corroborated by a FPC analysis performed on RAW macrophages incubated with NoPEG and PEG PSNPs, showing a 2-3 fold increase in uptake for the NoPEG PSNPs. (Supplementary data 3)

The PEG effect was also studied using 200 nm liposomes (Table 4, Figure 8D). Due to heavy aggregation of liposomes in cell medium both with and without serum this experiment had to be carried out in PBS. Liposomes in PBS were added to the RAW cells and incubated for 10 minutes. Confocal analysis indicated that NoPEG and PEG liposomes were taken up in similar amounts (Figure 8E). The quick uptake of liposomes into macrophages excluded them from reliable flow cytometry analysis.

However, these results show the potential of PEGylation of NPs in that attaching PEG on PSNPs indeed lowers the uptake by one of the biggest obstacles to obtain long circulating NPs; the macrophages.
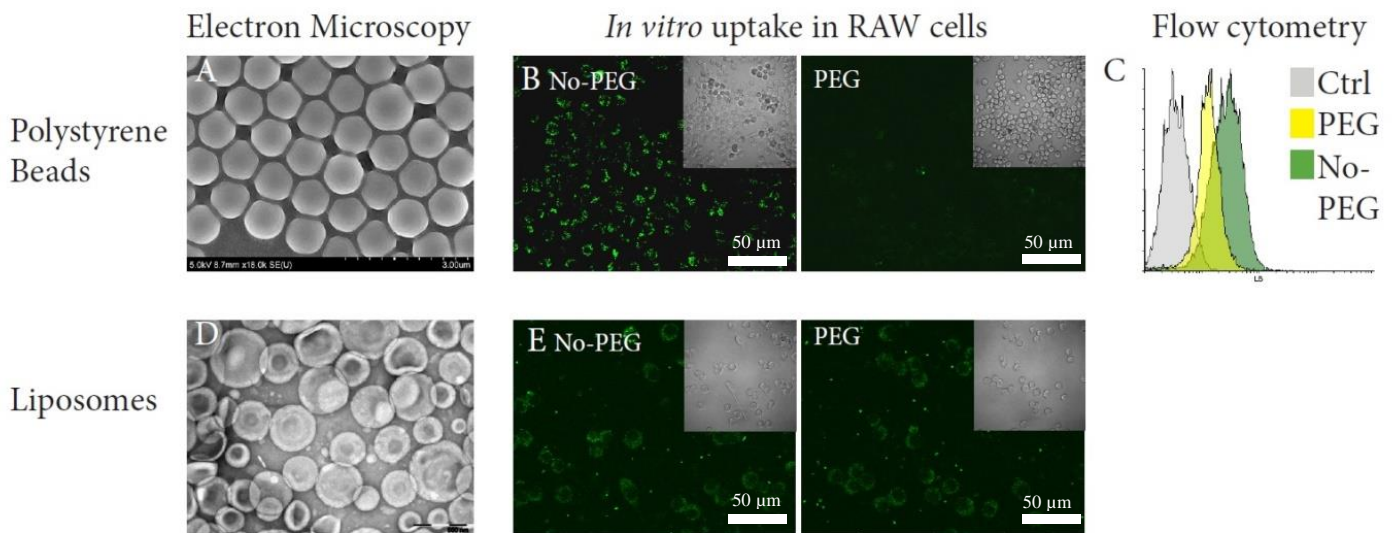

Figure 8. *In vitro* characterization of the PEGylation effect. (A) Electron microscopy (SEM) image showing the uniform size of the NoPEG 1000 nm beads PSNPs (Table 4). **(B)** No-PEG and PEG PSNP incubated with RAW macrophages for 4 h. A substantial uptake of NoPEG PSNPs by macrophages were observed (left panel) while PEG PSNPs were taken up in low levels (right panel). **(C)** The amount of NoPEG PSNPs taken up by RAW macrophages were 2-fold higher than PEG PSNPs, as quantified by flow cytometry. **(D)** Electron microscopy (TEM) images of PEG liposomes (Table 4). **(E)** NoPEG and PEG liposomes were incubated with RAW macrophages for 10 minutes in PBS. NoPEG (left panel) and PEG (right panel) liposomes were taken up in comparable amounts

Table 4. NP and liposome characteristics.

Particles	Zeta potential value with SD	Diameter Sizes (nm)	PEG (Surf. Conc.) (pmol/cm2)
PS	-35,3 ± 1,17	490	-
PS-PEG	-13,6 ± 1,09	518	37,4
PS	-20,48 ± 2,93	997	-
PS-PEG	-3,46 ± 0,08	1029	50,2
Liposomes	-33,26 ± 4,5	200	-
Liposomes-PEG	-14,22 ± 0,57	175	*

* The liposomes has ratio 1,81:1:0,15 (PC:Chol:PEG_PE), resulting in 5.1 % of the lipids being conjugated with PEG.

4.4 Quantification of the effect of PEGylation of NPs using optical tweezers

The data presented in the previous section showed that PEG reduces the uptake of PSNPs by macrophages. In order to analyze the interactions between cells and PSNPs in more detail we used controlled micromanipulation using optical tweezers (OT). The OT makes it possible to observe the interactions of NPs with cells under different conditions in real time and quantify how their interactions changes with different NP size and surface coating. OT uses an infrared laser to stably trap an object allowing us, in a controlled manner, to bring together NPs and cells to evaluate the interaction under different conditions. Only PSNPs were examined with OT, as the small size of the liposomes excluded them for this type of study.

First, we tested whether the size of the NoPEG PSNPs with or without PEG coating was proportional to the degree of adhesion. In these experiments there are three possible outcomes: 1) the OT is not strong enough to remove the NP from the cell, 2) the NP and cell can be moved apart but remain connected through a tether[124] or 3) the particle and cell can be moved apart as the connection between NP and cell is either not existing or not strong enough to prevent it. Here we included the tethered particle as adhered. The adhesion percentage is then defined as (the amount of adhered particles/ total amount of tests) x100%.

First, we tested whether the size of the NoPEG PSNPs was proportional to the degree of adhesion. Two sizes of PSNPs with a diameter of 1000 nm and 500 nm (Table 4) were used. We found that the 1000 nm NoPEG PSNP displayed a significantly higher binding affinity than the 500 nm NoPEG PSNPs (Figure 9A). NoPEG 500 nm PSNPs interacted strongly with RAW macrophages (85%) but compared to 1000 nm size it had a 10% reduction in the level of adhesion.

We next investigated whether PEGylation of the PSNPs would result in a lower adhesion to macrophages as was expected based on our earlier microscopy and flow cytometry experiments. Figure 9B shows snapshots of movies recorded as 1000 nm PSNPs, with or without PEG, were pushed against a RAW macrophage. The striking difference is that the NoPEG PSNPs already adhered to the macrophage surface within seconds after the first contact and the macrophage started to engulf it within

the first minute (Figure 9B, left panel, arrow, Supplementary Video 3). In contrast, a PEG PSNP did not stimulate such a response even after making transient, forced contacts with the RAW macrophage several times (Figure 9B, right panel, arrow, Supplementary Video 4).

When quantifying the degree of adhesion and comparing NoPEG vs PEG PSNPs we indeed found that PEG adds a measurable stealth effect to PSNPs *in vitro*. Coating the 1000 nm PSNP with PEG decreases the adhesion to macrophages significantly (Figure 9C). A similar decrease in adhesion to macrophages was observed when coating 500 nm PSNPs with PEG. By comparing the degree of adhesion for the 1000 nm and 500 nm PSNPs with PEG coating, the relevance of size for adhesion was eliminated as both the 1000 nm and 500 nm showed similar affinity for the macrophages (Figure 9C). Importantly, compared to the NoPEG PSNPs the degree of adhesion of the PEG PSNPs was reduced by 60-70 % (Figure 9A).

It is widely believed that the main effect of NP PEGylation *in vivo* is to reduce the binding of serum proteins and the process of opsonization; In the absence of PEG serum proteins such as IgG and complement bind to the NPs and allow binding to receptors on the surface of phagocytic cells such as macrophages.[125-127] To address the potential role of opsonization by serum proteins we pre-incubated one set of 1000 nm PSNPs with undiluted mouse serum (for mouse RAW macrophages). For controls two other sets of PSNPs were incubated in undiluted fetal bovine serum or phosphate-buffered saline (PBS) solution. The examination and evaluation of all the interactions between NPs and cells was carried out in PBS. All three sets of NoPEG PSNPs were quantified to have high levels of adhesion to macrophages as it was measured to be above 75%. Conversely, the level of adhesion for PEG PSNPs was below 5% for all three sets (Figure 9D). Using the OT assay we found that PEG lowered the interaction between PSNPs and RAW macrophages dramatically, but serum had no effect on NP interaction with the macrophages *in vitro*.

In a subsequent set of experiments, we determined the adhesion of 1000 nm PSNPs to the human Melmet 5 cancer cells. Therefore, one set of PSNPs was pre-incubated in undiluted human serum (HS). Here, as for the macrophages the PEGylation was found to lower the interaction between PSNPs and Melmet 5 cells. NoPEG PSNP had a degree of interaction above 65 % while the PEG PSNPs had very low levels of

40

interaction (Figure 9E). NoPEG PSNPs adheres much weaker to the Melmet 5 cells compared to RAW macrophages. Note that NoPEG PSNPs pre-incubated in PBS adhered stronger to Melmet 5 cells than NoPEG PSNPs pre-incubated with FBS and HS.

Another interesting observation made when applying the OT was that of increased adhesion of PEGylated NPs to both macrophages and cancer cells when the laser power was increased. This increased adhesion was observed for both FBS, PBS and serum conditions for both cells (Supplementary data 4)
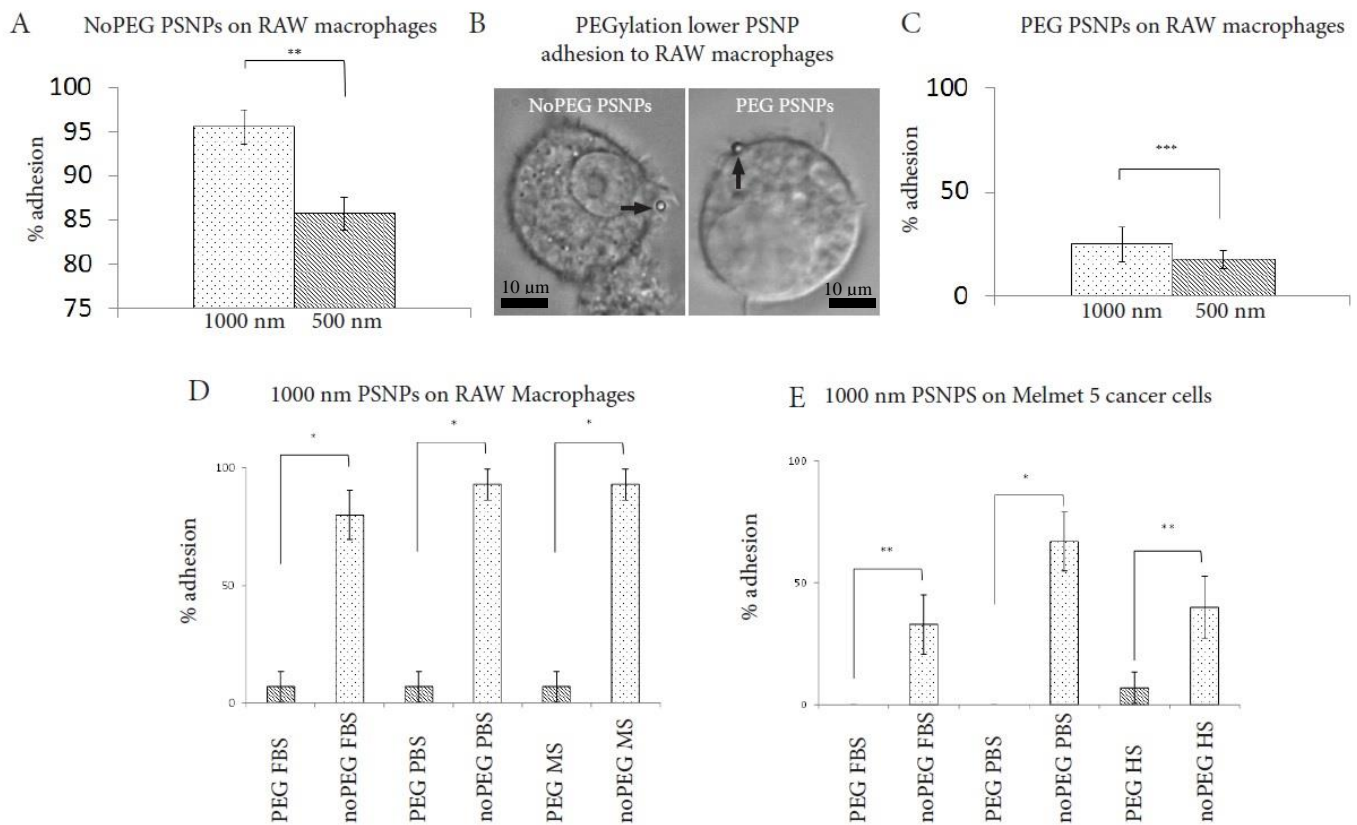
Figure 9. Quantification of the PEGylation effect using optical tweezers. (A) Quantification of the level of adhesion of 1000 nm and 500 nm NoPEG PSNPs to RAW macrophages. The bigger PSNP adhere stronger than the smaller one (p = <0.01). **(B)** Qualitative study showing a NoPEG 1000 nm PSNP stimulating a macrophage to engulf it within a minute after the first contact (left panel, arrow) while a PEG PSNP of the same size does not stimulate such a response (right panel, arrow). **(C)** The presence of PEG on the surface eliminate the size effect as 1000 nm and 500 nm PEG PSNPs show similar adhesion levels to RAW macrophages (p = >0.05). **(D)** Pre-incubation of PSNPs in serum does not affect binding profiles to RAW macrophages. PEG coating prevents binding while serum protein on NoPEG PSNPs does not result in increased binding as compared to (A) (p = <0.01). **(E)** Pre-incubation of PSNPs in serum does not interfere with the PEG-effect as all adhesion to Melmet 5 is blocked. Conversely, the presence of serum proteins lowers the binding of PSNPs to Melmet 5 as PBS-incubated PSNPs, lacking serum proteins, display higher level of adhesion.

4.5 PEGylation of NPs prolongs *in vivo* circulation time

We measured a clear stealth effect provided by PEG *in vitro* and wanted to investigate if PEG resulted in prolonged NP circulation time *in vivo*. The NoPEG PSNPs displayed undesirable properties shortly after injection, such as short circulation times and a high general affinity for the endothelium as they did not discriminate between the different blood vessels in the tail (Figure 7C). We therefore investigated if PEG could improve the quality of the PSNPs regarding these undesirable properties.

We injected 2 dpf wild type ZF embryos with green fluorescent 200 nm PEG PSNPs (Table 4) in the posterior cardinal vein (Figure 6A). Twenty seconds post injection PEG PSNPs circulated (Figure 10A, white asterisk, supplementary video 5) and displayed relative low affinity for the endothelium as they only adhered to the small vessels (Figure 10A, red arrow) in between the caudal artery (Figure 10A, yellow asterisk) and caudal vein (Figure 10A, red asterisk). 140 seconds post a relatively high amount, compared to 20 seconds post injection, of PEG PSNPs was still in circulation (Figure 10B, white asterisk). The PEG PSNPs indeed discriminated between the different blood vessels and the pattern was that blood vessels with strong blood flow did not attract PEG PSNPs; they did not adhere to the narrow DLAV vessels (Figure 10B, white arrow), the caudal artery (Figure 10B, yellow asterisk) or the caudal vein (Figure 10B, red asterisk). Thus, the affinity of the PEG PSNPs was for the most part directed towards the small blood vessels (Figure 10B, red arrow) with natural weaker blood flow (Supplementary video 6). The maximum detectable circulation time for PEG PSNPs was 60 minutes, as evident when we injected them into the mpeg cherry zebrafish line. At no time points did the green PEG PSNPs co-localize with the red fluorescent macrophages (Figure 10C), suggesting that clearance from circulation is due to adhesion to the endothelium.

We next carried out the same experiment with liposomes. The NoPEG version of the liposomes displayed good circulation properties as they did not stick to the endothelium, but were cleared from circulation within the first 20 h by macrophages (Figure 7F). The addition of PEG to liposomes showed a distinct improvement as they stayed in circulation 24 hours post injection, as observed by the complete visible

representation of the vasculature in the tail (Figure 10D, Supplementary Video 7). By this time macrophages had begun to clear PEG liposomes from circulation, as confirmed by using the ZF line with red fluorescent macrophages (Figure 10D, yellow, arrow). However, the majority of the PEG liposomes were still circulating. By 46 h post injections even more PEG liposomes were taken up by the macrophages (Figure 10E, green dots, arrows, Supplementary Video 8), but a considerable amount of liposomes were still circulating. From video time-lapse acquisition we estimated the circulation time to be between 50 and 70 h post injection. Inspection of the embryo by stereomicroscopy 70 h post injection showed a total clearance of PEG liposomes from blood circulation (Supplementary Video 9) as they were all taken up by macrophages (Figure 10F, arrow). No liposomes were observed to adhere to the endothelium. Importantly, the liposomes were not toxic as the embryo survived with liposomes present in the circulation for nearly three days.

The results collectively demonstrate the high suitability of the ZF embryo model to characterize novel NPs and provide an important foundation to identify NPs with stealth properties. The PEGylation of liposomes resulted in a substantial prolonged circulation time of at least 30 hours. For the PSNPs, the pattern of adhesion changed with the presence of PEG. PEGylation resulted in discrimination between vessels regarding adhesion as they only adhered to the blood vessels with weaker blood flow. The affinity of PEG PSNPs for the caudal vein, caudal artery and DLAV, which had a stronger circulation, was practically eliminated within the first minutes post injection; a clear detectable improvement compared to the NoPEG PSNPs.
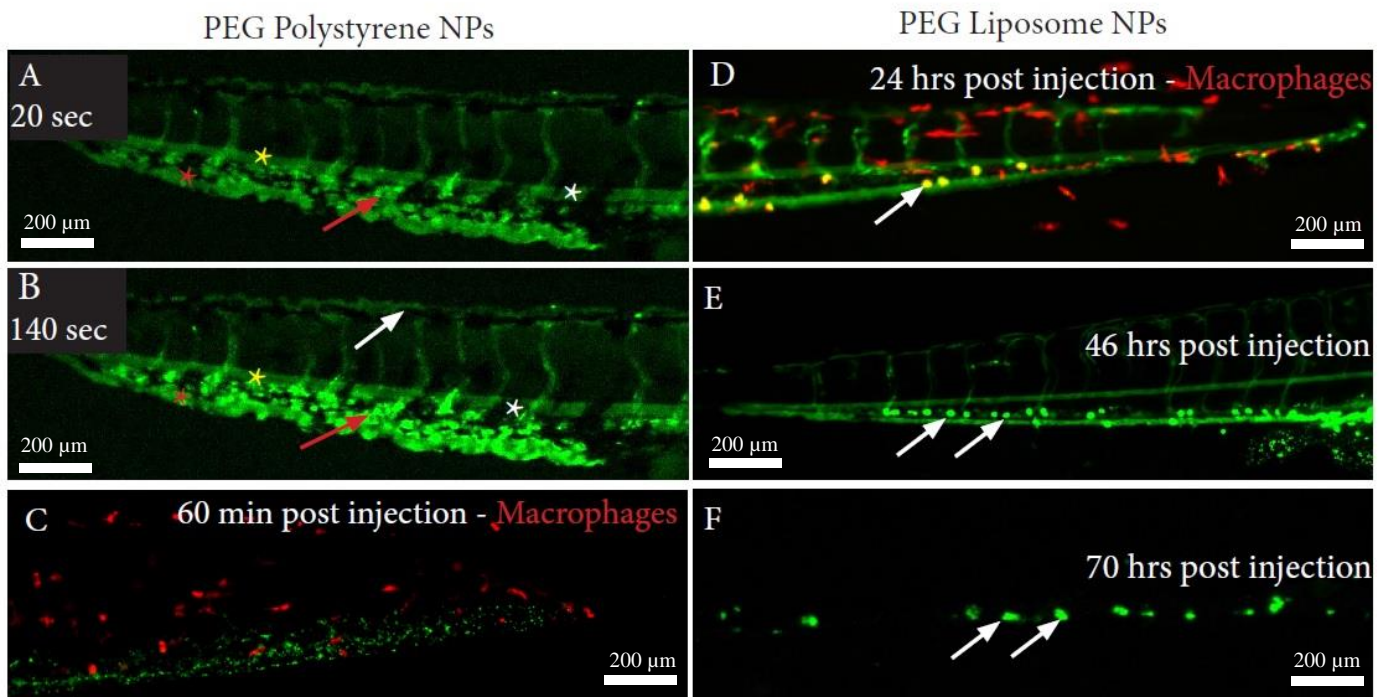
Figure 10. PEGylation prolongs NP circulation time. (A) 200 nm PEG PSNP (green) in the vasculature of a wt embryo 20 seconds post injection. They circulate (white asterisk) but are starting already to adhere to the small vessels (red arrow) between the caudal artery (yellow asterisk) and caudal vein (red asterisk) **(B)** 140 seconds post injection a relatively high level of PEG PSNPs are still in circulation (white asterisk). A striking observation is that they do not adhere to the DLAV (white arrow). Further, they do not adhere to the caudal artery (yellow asterisk) and caudal vein (red asterisk) but do stick to the small vessels between them (red arrow). **(C)** Maximum circulation time of PEG PSNPs (green) is 60 minutes. They stop to circulate due to adhesion to the endothelium as they are not associated or taken up by macrophages (red) in the mpeg cherry embryo. **(D)** PEG liposomes (green) injected into an mpeg cherry zebrafish embryo still circulates 24 h post injection. A fraction of liposomes are taken up by macrophages (yellow, arrow) but the majority is still in circulation. **(E)** 46 h post injection a full representation of the vasculature is observed as a consequence of circulating liposomes (green). However, compared to 24 h post injection the liposome level in circulation is much lower as they are continuously but slowly taken up by macrophages (green dots, arrows). **(F)** By 70 h post injection all PEG liposomes are cleared from circulation as they are taken up by macrophages (green dots, arrows). Importantly, no adhesion of liposomes to the endothelium is observed.

4.6 PEGylated liposomes accumulates passively and specifically in human tumor-like structures in ZF embryos

The observed long circulation time in ZF embryos for PEG liposomes made them a promising candidate for testing their ability for passive targeting to the human tumor-like structures. Given that the PSNPs were cleared so fast from circulation we did not investigate their possible accumulation in tumor-like structures. As shown in Figure 6, the tumor-like structures have a tight relation with the vasculature; injected long-circulating liposomes will pass through tumor-like tissues numerous times and potential accumulation can be studied via imaging.

Thus, the Melmet 5 human cancer cells were injected into 2 dpf wild type embryos and tumor-like structures were allowed to establish for two days. Embryos that fulfilled two selection criteria, a tumor-like structure in the tail and normal blood flow throughout the whole embryo, were then injected with PEG liposomes (Supplementary Video 10). Imaging indeed revealed a specific and rapid accumulation of liposomes into the tumor-like structures of the Melmet 5 cells. The Melmet 5 tumor-like structures showed a notable and fast ability to accumulate liposomes. The fastest observation of the green liposomes accumulating in a red tumor-like structure was already 2 hours post-injection (hpi) (Figure 11A). Liposomes seemed to accumulate specifically at the sites of tumor-like structures. There was no observed non-specific distribution of liposomes to macrophages or endothelium at this time-point. This argues that the liposomes escaped from the blood circulation at the site of the cancer cells before macrophages recognized them as foreign objects. Some embryos having multiple tumor-like structures exemplified the specificity of the accumulation of liposomes to areas with cancer cells in particular. Liposomes were observed to specifically accumulate at the precise sites of cancer cells in the tail tissue (Figure 11B, arrows, Supplementary Video 11). In Figure 11B, the tumor-like structure furthest to the right showed a pattern of liposomes sticking to the endothelium specifically in the area around cancer cells, opening up the possibility that Melmet 5 cells secrete factors that affect the vasculature locally.

A control embryo not injected with cancer cells shows the distribution of liposomes after 6 h of circulation (Figure 11C). The complete representation of the vasculature (in green) is evident due to the liposomes still in circulation. Some green "hotspots" can be observed (Figure 11C, arrows), referring to macrophages starting to clear liposomes from circulation. Notably, there are no accumulation elsewhere of liposomes in the absence of cancer cells.

To verify the profile of liposome accumulation in Melmet 5 tumor-like structures observed in Figure 11A, we performed confocal microscopy to study the pattern of liposomes in more detail. Embryos with tumor-like structures were examined by acquisition of confocal stacks. A 3D-view of the Melmet 5 tumor-like structure shows a tight association between liposomes and the Melmet 5 cells (Figure 11D, Supplementary Video 12). Some liposomes seem to have penetrated the tumor-like structure (Figure 11D, arrow) but the majority is located at the periphery. It is not clear if the liposomes are taken up by the Melmet 5 cells or if they are located on the surface of the cancer cells.
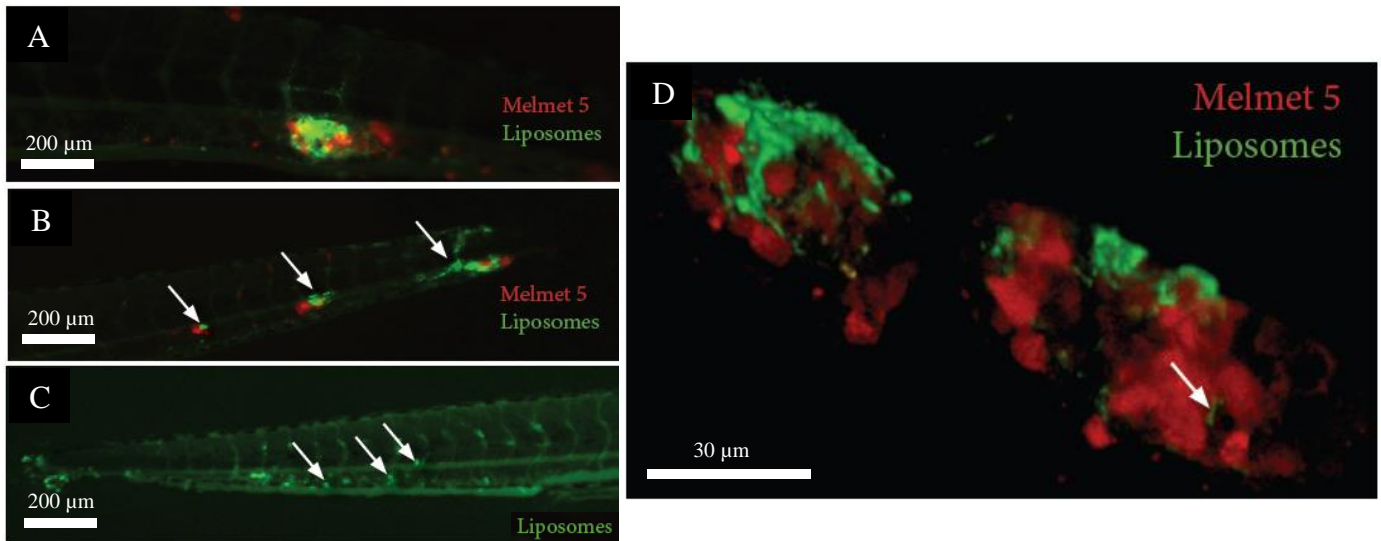
Figure 11. Liposomes accumulate passively into human tumor-like structures. **(A)** 2 dpi Melmet 5 tumor-like structures (red) accumulate liposomes (green) after 2 hrs of circulation. At this time point liposomes do not locate to other tissues or cells in the embryo. **(B)** The specificity is exemplified by an embryo with three Melmet 5 tumor-like structures (red). Liposomes exclusively accumulate in those three Melmet 5 tumor-like structures. **(C)** A control embryo only injected with liposomes (green), and not cancer cells, show the distribution of liposomes after 5 hours of circulation. Minute levels of liposomes are taken up by macrophages (arrows) but only visible at considerable longer exposure times than for the images in (a) and (b). **(D)** Confocal imaging of a 2 dpi Melmet 5 tumor-like structure (red) with accumulated liposomes (green) after 3 h of circulation. Liposomes seem to associate tightly with the cancer cells mostly at the periphery of the tumor-like structure. A sub-fraction of the liposomes are able to penetrate deeper into the tumor-like structure (arrow).

A method which has been widely used to follow circulation flow in ZF is to inject fluorescent dextran, which can infiltrate all chambers by fluid phase flow.[128, 129] When we injected fluorescent dextran into the circulation of embryos with Melmet 5 tumor-like structures, we could directly observe leakage of the dye into the areas of the tumor-like structures (Figure 12). Leakage was seen into Melmet 5 tumor-like structures, which could explain the tight association of liposomes with the Melmet 5 cells. *In vitro*, Melmet 5 cells have been shown to activate migration of HUVEC cells, stimulate HUVEC tube formation and induce expression of the angiogenic growth factors VEGFA and angiopoietin-2.[130] This suggests a local activation of endothelial cell in the ZF embryo leading to a destabilized and leaky vasculature. This loosening of the endothelium combined with the small liposome size and circulation properties allowed the liposomes to escape circulation specifically at the site of cancer cells.
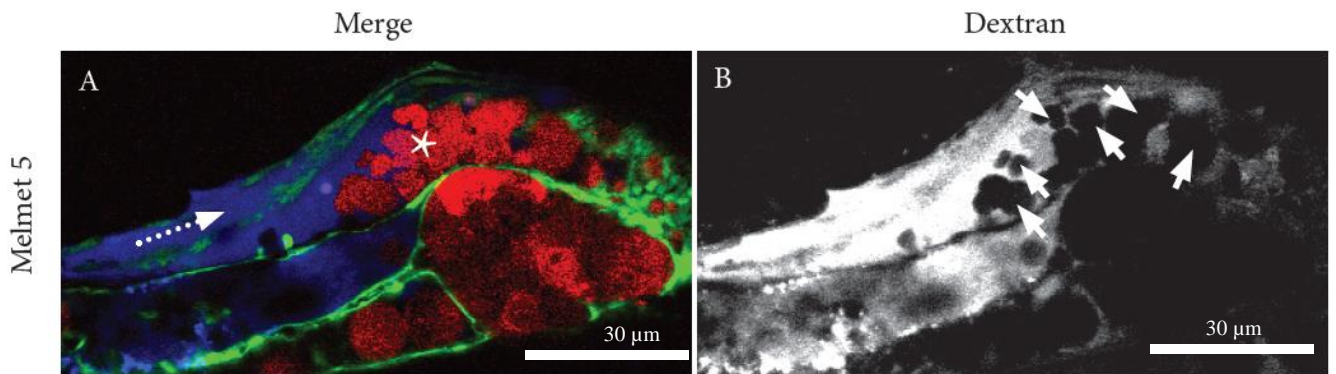
48

Figure 12. Leakage of Dextran into tumor-like structures. 2 dpf Fli1 embryos with green vasculature were injected with red fluorescent Melmet 5 cells and tumor-like structures were allowed to form for two days. Then blue fluorescent dextran (Mw 10 000) was injected into circulation and embryos were mounted in low melting point agar and imaged 20 minutes post injection of dextran by confocal microscopy. **(A)** A Melmet 5 tumor-like structure (red) reside close to the circulation surrounded by the vasculature (green) in which the dextran flows (blue). The dotted arrow indicates the direction of the blood flow. **(B)** A black and white image for best visualization of how dextran (white) leak into the Melmet 5 tumor-like structure. The arrows indicates the position of the Melmet 5 cancer cells where dextran is excluded, meaning that dextran is leaking out into the tumor-like structure already after 20 minutes in quite high amounts completely surrounding the cancer cells.

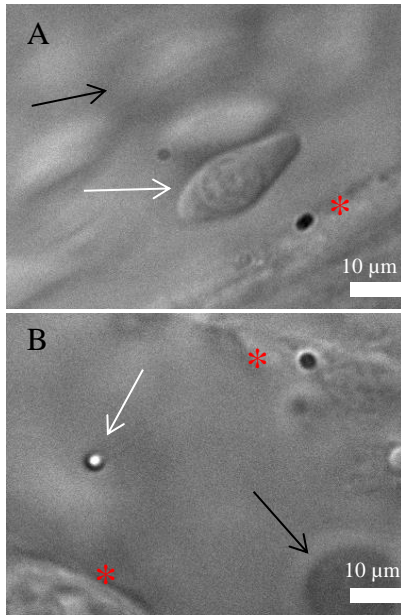## 4.7 *In vivo* manipulation of cells and NPs using OT

Figure 13: *In vivo* trapping of a red blood cell (RBC) and PSNP in the caudal vein of a 2 dpf ZF embryo. **(A)** Trapping of a RBC (white arrow) from the circulating blood flow. The rest of the RBCs (black arrow) continue to circulate. The trapped RBC is moved closer to the endothelial lining (red asterisk). **(B)** Trapping of a 1 µm NoPEG PSNP (white arrow). Endothelial cells indicated with red asterisk and RBC with black arrow.

The first use of OT for *in vivo* trapping was reported by Zhong et al. in 2013[131]. Here, red blood cells were trapped in sub dermal capillaries in the ears of living mice. This feat was easily reproduced in the ZF embryo, which because it is transparent and very thin, is well suited for trapping and *in vivo* manipulation of cells and PSNPs (Figure 13). By using the OT, trapping and manipulation of objects in the circulation of the ZF embryo was possible using a mounting system easily fashioned from coverslips and silicon (Materials and Methods).

This mounting system also allows for the ZF to be kept alive during and after the experiment, and anesthesia to be applied before starting the experiments. The tail region was found best suited for OT manipulation because of its thinness compared to other regions of the embryo. This causes less interference with the laser of the OT with the embryo tissue compared to thicker regions, as well as the PSNPs (table 4) consistently adhering to the vasculature in this region, thereby being easy to locate. The working distance inside the fish was typically between 20 - 100 µm. Trapping was possible inside the ZF vasculature using powers from 100mW up to 3000mW for an extended period of time without damaging the embryo. However, some areas of the ZF were apparently more susceptible to heat aggregation from the laser than most areas. These areas may be due to pigment, as they present as small black areas spread around the ZF embryo. When the laser was transiently moved over these areas the area dissolved/burnt away, damaging the ZF (Figure 14), and if the pigment was located near the circulatory system it caused leaking of blood from the embryo. By avoiding these areas however, power from 100mW to 3000mW caused no discernible damage to the embryo over the course of the experiments.
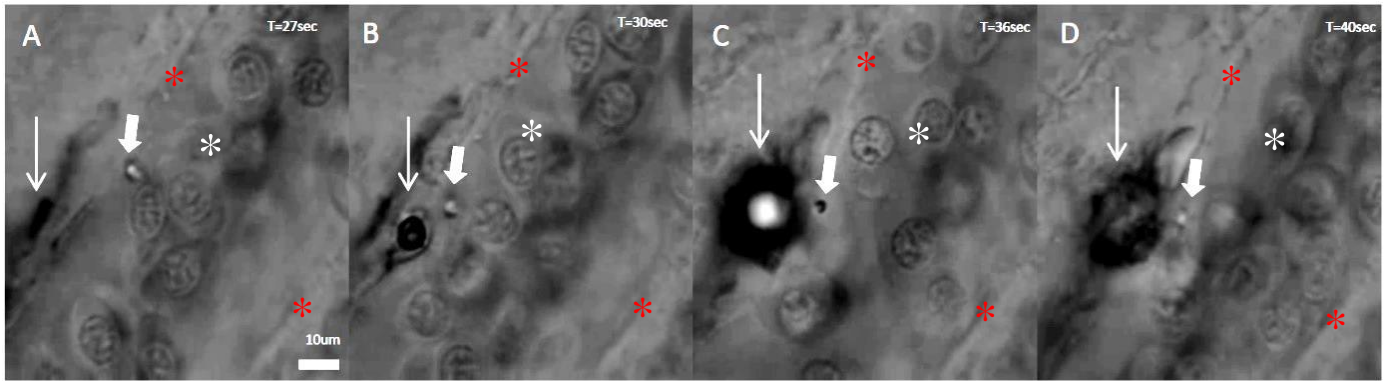
Figure 14. OT laser burns melanocyte in ZF. (A) A 1 µM NoPEG PNSP (thick arrow) stuck to an endothelial cells (red asterisk). RBCs are in circulation (asterisk) and Melanocytes (thin arrow) are seen as dark areas. **(B)** OT laser is in proximity to melanocyte, and energy transfer starts to burn the melanocyte cells, seen as an expansion of the dark areas. **(C)** OT laser in proximity to melanocyte for several seconds after initial contact. A further expansion of the dark area is seen as the burning continues **(D)** OT laser turned off and the burning of melanocyte stops.

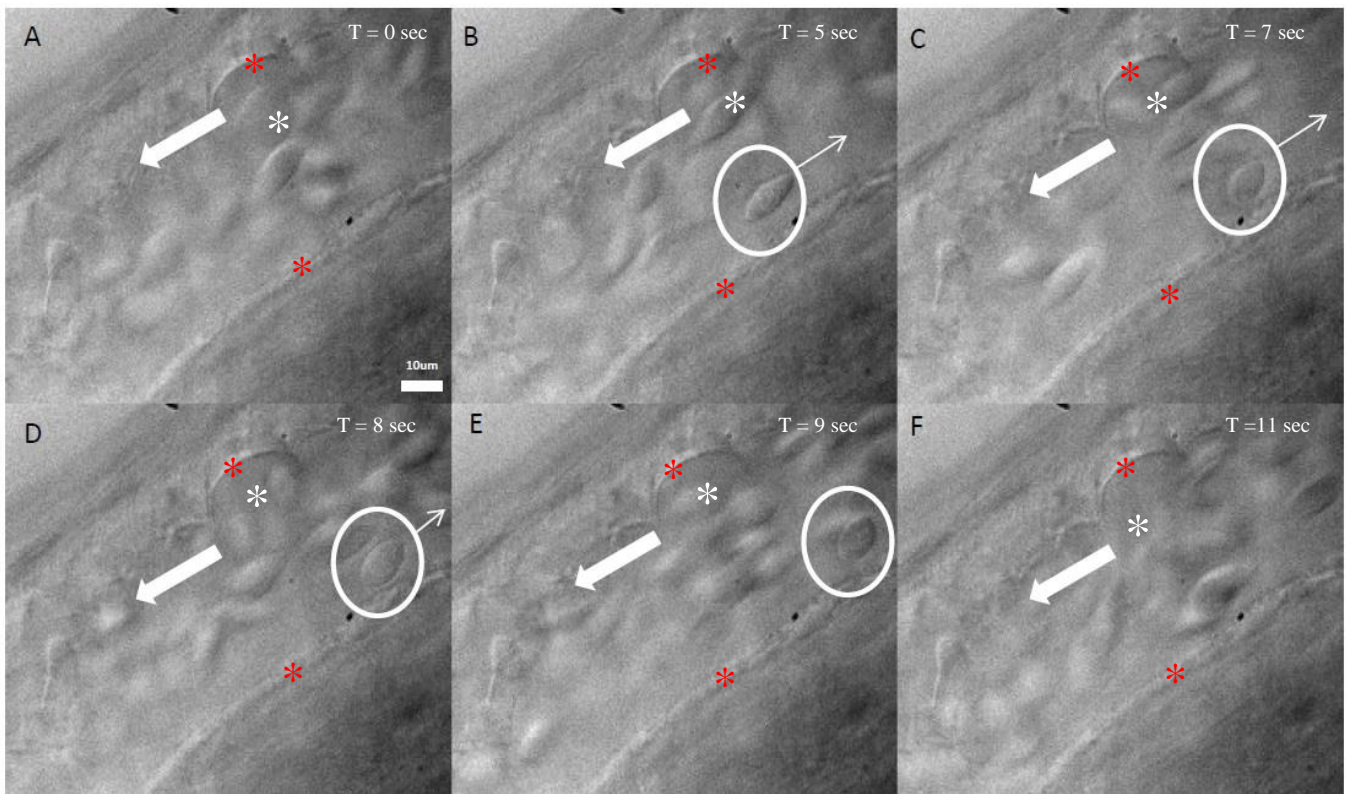**Figure 15. Trapping of red blood cell (RBC) in caudal vein of ZF. (A)** RBCs (white asterisk) in circulation. (Thick arrow shows direction of blood flow). **(B,C,D)** RBC trapped in OT (white circle) and being moved against the blood flow. (thin white arrow indicates direction). **(E)** RBC being held stationary in blood flow. **(F)** Red blood cell released back in circulation. Endothelial cells indicated with red asterisk.

trap stiffness for NP in optical tweezer

y = 0,6329x
y = 0,4796x

NP size(diameter, nm) 100 avg.
NP size(diameter, nm) 200 avg.
NP size(diameter, nm) 500 avg.
NP size(diameter, nm) 1000 avg.

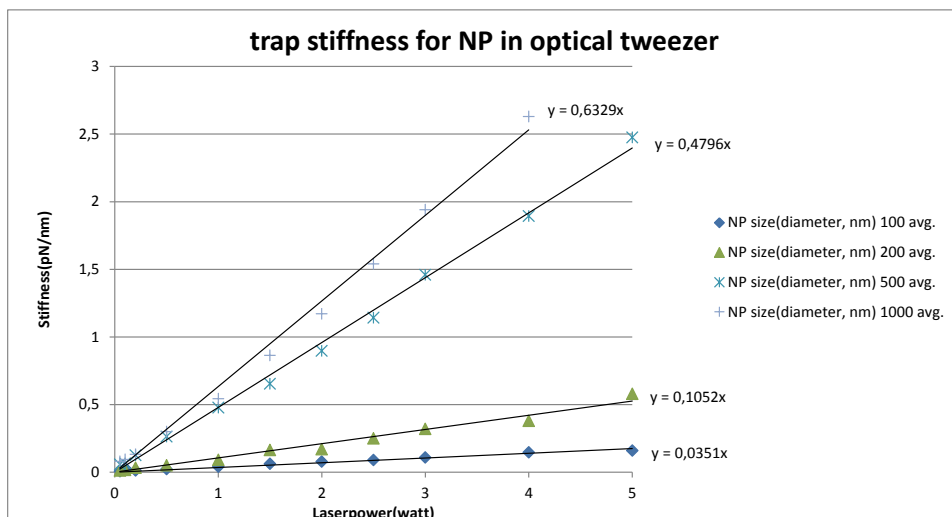y = 0,1052x
y = 0,0351x

Stiffness(pN/nm)
Laserpower(watt)

Figure 16. Graph showing trap stiffness when trapping NoPEG PSNP of different size at different laser powers. The force generated by the OT on the NP can generally be described by Hooke's law (F=-kx). The constant k, is what is represented here as stiffness. F = force (N) and x= distance. When we know the stiffness (k), measuring the displacement of the NP from the center of the optical trap allows us to determine the forces exerted on the NP.

When trapping cells in circulation they could be held in place inside larger veins or arteries (Figure 15B). The cells could also be moved with, or against the blood flow (Figure 15C-F, supplementary video 13). It was also possible to divert individual cells into new vessels. The cells however were not stable when trapped, and often the cells slipped out of the trap or was knocked out by another cell and escaped back into circulation. When this happened a new cell quickly took the place the escaped cell in the optical trap. This indicates that he composition of a cell, its shape and size makes them difficult to stably trap using OT *in vivo*.

Therefore PSNPs which *in vitro* display excellent trapping properties (Figure 16) were investigated *in vivo* using the OT. The PSNPs were more stable when trapped *in vitro* relative to cells and this made it possible to manipulate them without their escaping the optical trap. PSNPs are uniform in size and have a spherical shape, which makes them more stable during trapping than cells. The PSNPs were trapped both after adhering to endothelial cells of the caudal vein (CV) in the tail region of the embryo and directly from circulation in the same region, although the latter is difficult to achieve reliably, at least without slowing down the heart rate of the fish using increased levels of anesthesia. By trapping PSNPs adhering to the vasculature and manipulating them it was possible to try and pull them free of the endothelial cells (figure 17). We can also by slowing the blood stream down perform a sort of "spring cleaning" inside the vessels. By clearing the red blood cells out of the way using the optical trap, we were able to make a clean area for micromanipulation of NPs against endothelial cells of the blood vessels and to blood-resident macrophages

(Supplementary video 14). This 'cleaning' can be maintained by using the process of multiplexing, where a second laser can be divided into multiple (up to 200) separate laser on the system we employ, 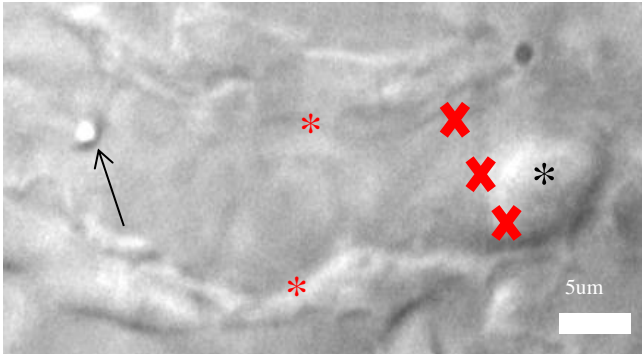that can be individually manipulated and used to create "fences" that prevent cells for entering the already cleared area(Figure 17). This process of "fencing" can provide areas to work within the living ZF where other unwanted cells and debris do not affect the experiment. The multiplexing can also be employed to manipulate several NPs simultaneously (Supplementary video 15).

Figure 17. Fencing off an area to manipulate PSNPs without unwanted cells interfering. By using the multiplexing function we can apply multiple optical traps (red cross) at once. This allows us to set up an optical fence where incoming cells (black asterisk) are stopped. This gives a area where we can manipulate the PSNPs (black arrow) adhered to the endothelial cells (red asterisk) without interference from other cells flowing by.

The pulling of PSNPs from the endothelial lining often resulted in the pulling of tethers from the endothelial cells. When the trap was turned off during the pulling of a tether, the PSNPs were dragged back towards the cell (Figure 18, Supplementary video 16).

The NP could also be pulled out of the optical trap by the force of the cell pulling back on the NP trough the tether, meaning the force exerted by the cell on the NP is higher than the force exerted by the optical trap in the NP. These results obtained with the OT confirm the observations made during normal fluorescent microscopy that the PSNPs indeed do adhere to the endothelial cells. The PSNPs adhere to the endothelial cells with such strength that they cannot be freed using the physical forces generated by the OT. The simplest interpretation of these results is that the NP has been internalized by the endothelial cell.

Preliminary experiments performed using this *in vivo* OT technique has also to some degree confirmed the observations that PEG PSNP adhere to a lesser degree to endothelial cells than do the NoPEG PSNPs (section 4.5). By trapping and manipulating the PSNPs *in vivo* we observed that it was possible to pull the PEG PSNPs free of the endothelium. In contrast this was not possible using the NoPEG

PSNPs. Using the NoPEG PSNPs pulling of tethers was possible, but we were not able to free them from the endothelium cells. It was also observed that higher laser powers were needed to pull tethers with the NoPEG PSNPs compared to the PEG PSNPs. This indicates that the NoPEG PSNPs adhere stronger to the endothelium cells than the PEG PSNPs.
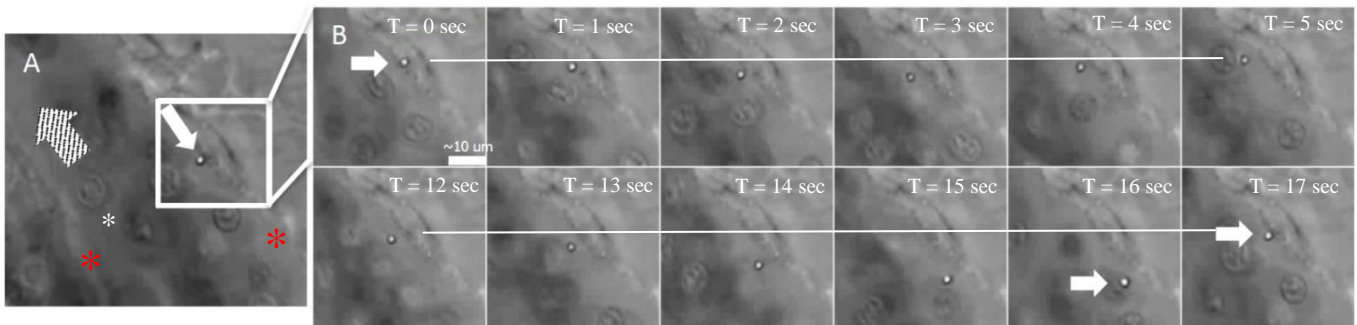

Figure 18. Pulling a tether with 1.0μm NoPEG PSNP adhered to endothelial cells in caudal vein of 2dpf ZF embryo. (A) NP (thick white arrow) adhered to endothelial cell (red asterisk). RBCs (white asterisk) circulate in the direction indicated (textured arrow). **(B)** Showing the NoPEG PSNP being pulled against blood stream. When the OT was turned off the NP was pulled back to the endothelial cell by the tether. The white line indicates the starting position of the NoPEG PSNP. Relative to this line, it is observed that the NoPEG PSNP is moved in a downward direction, against the blood flow, before the NoPEG PSNP was pulled back to its original position by a tether formed by the endothelial cells when the trap was turned off.

5 Discussion

The foundation of this study was the hypothesis that the ZF embryo model for human cancer could provide a powerful new fast screening tool for the development of NP therapies against cancer. This model has gained popularity due to its ability to support growth of human cancer cell lines that show many similarities to the behavior of tumors in mammalian models such as mice.[129, 132] In combination with the complete transparency of ZF embryos, that enables sophisticated imaging, this system allows exogenously injected human tumor cell growth and tumor formation to be monitored in real time with high spatial and temporal resolution. We show here that, relative to these tumors the ZF embryo further offers a unique system for following the fate of NPs whose ultimate goal is to selectively kill cancer cells. Moreover, transgenic ZF lines selectively expressing fluorescent proteins in the blood vessel endothelial cells or in immune cells such as macrophages, provides highly sophisticated tools for precise and detailed observation, in real time, of the behavior and tissue distribution of NPs.

For this study we focused on two quite different types of NPs, PSNP and liposomes. The commercial available PSNP were selected because they have a uniform size and have been widely used as model NPs[133] . In addition, the carboxylated surface can be modified by PEGylation. We also used liposomes, which are not as uniform in size as PSNPs, but have also been extensively studied. Moreover, some liposomes containing anti-cancer drugs, such as doxorubicin (Doxil) are in clinical use.[134] Liposomes can also be PEGylated and this parameter, a key feature of the commercial anti-cancer liposomes, was also investigated in our study.

Using both kinds of NPs we show clearly that the ZF embryo model allowed us to follow the NPs from the time of injection up to the point they are removed from circulation. By doing this we could easily monitor two undesirable localization sites where different NPs accumulated; the endothelium and the macrophages. The ability of endothelial cells to bind and to take up NPs has not been much studied in the field of NP therapy against cancer, even though it has been shown that the vasculature is indeed able to clear foreign objects from circulation[135]. The association of NPs with endothelial cells *in vivo* has been observed in mice[136], however the labor intensive

methods needed to visualize and study these NP-endothelium interactions in the mouse model means it has been largely overlooked, or not even considered to be studied, when considering the bio-distribution of NPs in vivo.[60, 83, 137-142] Earlier studies have described binding and uptake of latex particles (0.33 to 0.8 µm) to sinusoidal endothelial cells after perfusion of rat liver.[143] Thus, bio-distribution of NPs to the endothelium is a known phenomenon that has to be studied in more detail in order to obtain effective therapeutic NPs. NPs containing drugs that adheres in an unspecific manner to the vasculature will have a high probability for severe toxic side effects.

In contrast to the endothelial cells, the undesirable phenomenon of macrophage uptake of anti-cancer NPs from the circulation is a well-characterized one. In mice, NP injections is routinely followed by killing the animal, removal of body fluid at the site of injection to harvest macrophages, centrifugation and filtering the re-suspended cell suspension before flow cytometry analysis.[144] In the ZF embryo model it is easy to monitor macrophage uptake of NPs when using the fluorescently labeled macrophage fish lines (mpeg cherry).

Regarding the study of NPs and their interaction with cells we here introduced a new strategy to quantify the effect of surface coating and NP size. OT is a new and very powerful tool to study in detail the interaction between NPs and cells. It allows one to grip one single NP and move it towards a cell with different forces and study how size, surface coating and other tunable characteristics affects binding properties to for example macrophages and cancer cells. The level of adhesion is measured in great detail and the optimal bead can be found for different purposes by modification of the NPs.

Using OT we investigated whether size, coating with PEG or presence of serum proteins on the surface of PSNPs influenced how they interacted with RAW macrophages and cancer cells. The classical idea is that PEG prevents complement proteins from binding from serum. Implied in this idea is the fact that in the absence of PEG these serum opsonins are the main things responsible for binding. However, in our experiments we failed to see any increased binding of NPs that were incubated with serum. Nevertheless, our results with OT show that the NoPEG PSNPs show high affinity binding to the macrophages in the absence of serum. This agrees with

the data of Diakonova *et al.* who demonstrated that internalization of latex beads by macrophages occurs in serum free conditions [145]. Even though it is difficult to define the responsible molecular players scavenger receptors has been suggested to be responsible for the non-specific binding to particles [146]. However, the fact remains that macrophages do have high affinity receptors to clear nonspecific particles from circulation.

PEGylation of PSNPs significantly reduces binding to macrophages as shown by our OT experiments. This is also supported by flow cytometry data. This occurred regardless of presence of serum proteins on the surface of the PSNPs or not, suggesting that PEG directly inhibits interaction between the particle and the responsible receptors on the surface of the macrophages. A complication with the stealth hypothesis in practice is to be able to combine the exclusion of particles from macrophages but to allow uptake into cancer cells. We therefore also investigated the interactions of PSNPs with and without PEG, in the presence and absence of serum, with the human Melmet 5 cancer cells. The PSNPs without PEG or serum interacted less efficiently with Melmet cells than to macrophages. The addition of PEG completely blocked all measurable binding of PSNPs in this system. The effect of serum was also unpredictable. The data imply that serum reduces the ability of the NoPEG PSNPs to bind to Melmet 5 cells. The addition of serum had no effect on the inability of the PEG PSNPs to bind to the Melmet 5 cells. Therefore, our results with macrophages reveal a predictable stealth effect of PEG on PSNP binding and no significant effect of serum in this system. In contrast, it is more difficult to make general conclusions about serum or PEG in the binding of PSNPs to cancer cells.

Although more detailed studies are needed to make more definitive conclusions, the simplest interpretation of our data in RAW macrophages is that in the absence of PEG on the surface of the PSNP they bind directly to macrophage surface receptors. In the presence of PEG this molecule directly, rather than indirectly via serum proteins, lowers the interactions between the PSNPs and macrophage surface receptors. However, using the OT for studying NP-cell interactions we demonstrates the potential for this method and how it generates detail knowledge, on a level not possible before, about how cells interact with NPs with different characteristics. By examination of single NPs systematic studies can be performed to optimize them for

a certain biomedical application. In the future studies will be done in living zebrafish embryos to study how modification of NPs affects the interaction with for instance cancer tissues or endothelium.

When comparing NPs sizes, using the optical tweezers, we found that larger NPs without PEG adhered significantly stronger to RAW macrophages than did smaller NPs (Figure 8E). The size effect was eliminated by the presence of PEG, as both 1000 nm and 500 nm NPs adhered with similar strength to RAW macrophages.[133, 147] Our results also argue that PEG reduces the attachment of NPs to endothelial cells in the ZF embryos. Accordingly, we observed a significant increase in the overall circulation time of PEG-PSNPs and decreased adhesion to the endothelium relative to the NoPEG PSNPs (Figure 10 A-C). The prolonged circulation time with PEGylated PSNPs, that attached to the endothelium more than we desired, was even more pronounced with PEG liposomes, whose maximum circulation time was extended in the embryo for at least 30 hours. After this time the stealth effect of PEG appeared to be lost and the PEG liposomes were increasingly taken up by the macrophages. The PEG molecules need to have a certain structure and be oriented outwards from the NP to be effective. This structure is known to change over time and become non-functional which could explain the eventual uptake of PEG liposomes by macrophages.[148]

It is also likely that the liposomes are not stable and disintegrate after a certain time in circulation.[149] Regarding the PSNPs, both for the NoPEG and PEG versions, the circulation time appeared to be too short for the macrophages to be able to take them up. The affinity for the endothelium was of such a character that they adhered too quickly for the macrophages to interact with them.

Another advantage of the ZF model is that it is a sensitive indicator of toxic compounds [150]. Although this was not a major aspect of our study we noted a surprising aspect of those PSNPs that bound avidly to the blood vessels. These NPs were highly toxic since all embryos with high binding died within one day post injection. The reason for this toxicity remains to be determined. In contrast, the liposomes with or without PEG were completely non-toxic to the embryos having no increasing mortality relative to control embryos. The importance of the ZF model for

evaluating toxicity will become even more important when we test NPs encapsulating anti-cancer drugs such as doxorubicin.

The tumor-like structures comprised of human cells are supported by the ZF embryo and have a tight association with the vasculature, the route by which the NPs can reach the tumor. No other animal model currently exists where NP circulation through tumor tissues can be monitored so easily over time. The accumulation of liposomes in the tumor-like structures was especially rapid and apparently 'specific', in spite of the fact that our NPs did not contain molecules that could actively target the NPs to the tumor cells [151]. After only 2-5 hours a significant amount of PEG liposomes accumulated in the tissue where the Melmet 5 tumor-like structures were located. Tumor-like structures comprised of Melmet 5 cells were able to accumulate liposomes at the periphery and some liposomes even penetrated the tumor-like structure.

A plausible explanation for the leakage into the tumor-like structures is that the tumor cells secrete growth factors that manipulate the vasculature. These growth factors can include VEGF, which has been shown to be expressed in multiple cancer cells types. [152]. VEGF is the most powerful inducer of angiogenesis and could be responsible for loosening the interaction between endothelial cells at the site of the tumor-like structures, resulting in leakage of liposomes out of circulation and into the cancer tissue[153], as discussed in section 4.6.

When the optical tweezers was used to evaluate the adhesion of PEG and NoPEG PSNPs it was also observed an increased binding of PEG PSNPs to both macrophages and cancer cells when the laser power of the OT was increased from 20 mW, to 200 mW and finally 2000 mW (Supplementary data 4). This increase in laser power increases the stiffness of the optical trap (Figure 16), and affects how much force can be exerted on the NP before it is moved from the central position of the optical trap and eventually escapes it all together. The reasons for these observations of increased adhesion of PEGylated PSNPs at increased laser powers are not easily explained, but we have arrived at two hypothesis. First and most likely in our opinion is that the increased stiffness means that the NP is pushed more into the cell than at the lower laser powers. If we push the NP harder against the cell, the plasma membrane will bend more as the NP makes contact, and wrap around the

cell giving more surface contact and more possibility for adhesion. It is also possible that we push the NP trough some sort of glycocalyx on the cell surface, making the NPs adhere more strongly. The second hypothesis is that the 1064 nm infrared laser used to trap the NPs generates additional heat when the laser power is increased from 20 mW to 2000 mW [154]. This increase in temperature may affect the PEG layer, perhaps causing it to dehydrate and collapse, thereby loosing some of its effect, leading to more adhesion of the PEGylated NPs. The experiments where performed at 37^OC, and heat degradation of PEG is not observed until reaching approximately 80^OC[155], therefore degradation of the PEG is unlikely at the temperatures that are likely to be reached during the conditions used in these experiments, even with the heating of the OT taken into account [154]. However, the exact increase in temperature of the PSNPs in these experiments is not known. Several factors can influence the temperature, including size, what solution the PSNPs are in, and if there is fluorescent dyes present in the PSNPs [154, 156-158]. Because of these parameters it is difficult to say anything specific about the temperature parameters in our experiments without doing measurements of our own, and this is no trivial task, and falls outside the allotted time of this thesis.

Our results show that NPs made of different materials can in principle be tested in high-throughput screens for different sizes, variation in PEG-chain length and targeting molecules in the ZF model. Image-based high-throughput screens have been established where transgenic embryos are used in the search for new bioactive compounds.[159-161]. The experience and technology from these studies can be utilized to conduct high-throughput screens to identify leading NP candidates with long circulation times and an adequate biodistribution profile for the intended biomedical application. The most promising candidates, identified in the ZF embryo model, can subsequently be tested in more complex vertebrate models, such as mice.

Our application of optical tweezers in combination with the ZF and PSNP is a novel method allowing the precise examination of NP interactions with living organisms. The ability to micromanipulate particles and cells in ZF can give new insights into the largely unexplored area of nano-bio interactions, and give valuable information on how to design NPs and surface modifications in the future. The many mutant strains

of ZF expressing fluorescent cells, such as endothelial cells and macrophages makes the ZF even more suited for *in vivo* manipulation. Being able to easily locate and identify different cells *in vivo* is useful and also gives better contrast than normal light microscopy *in vivo*. Work on establishing the use of OT and fluorescent confocal microscopy is already underway in our lab, but is however outside the scope and time limit of this thesis to present it. However, by combining our *in vivo* and *in vitro* OT methods the field of NP research has a new arsenal of tools at their disposal.

Preliminary results have also indicated a difference in the degree of adhesion between NoPEG and PEG PSNPs to endothelial cells *in vivo*. What initially was only an observation of adhesion patterns in fluorescent microscopy with regards to the NoPEG and PEG adhesion is now possible to quantify using this *in vivo* OT technique.

The HepG2 data were moved out of the general results section and placed in a separate supplementary data sheet (supplementary data 2) attached to the thesis. A couple of weeks ago we were informed by our collaborators at the University of Leiden that the HepG2 cell line was contaminated with what are most likely HEK 293 cells. This makes the results from the experiments performed using this cell line unreliable to present as relevant for cancer treatment, since the cell line is of uncertain composition.

6   Conclusion

We here introduce the ZF embryo as a system for testing NPs in an *in vivo* vertebrate model for human cancer. In this system we introduce a way to screen for novel anti-cancer NPs with the aim to identify leading candidates for subsequent testing in more complex animal models. Undesirable anti-cancer NP properties such as uptake by macrophages and endothelium are easily identified. Conversely, the system also allows desirable properties to be monitored, such as NP accumulation in tumor tissues. We present *in vitro* experiments employing optical tweezers, which revealed detailed data regarding NP surface coating and how it affects interaction with macrophages and cancer cells.

We demonstrate the PEG effect *in vitro*, as macrophages do not adhere to PEG-coated NPs. This stealth effect could further be observed *in vivo* as PEG coated NPs had longer circulation times and lower affinity for endothelium in ZF embryos. Liposomes were shown to passively accumulate in tumor-like structures comprised of human cancer cells, further strengthening the ZF as a model for NP research. The presented *in vivo* model opens for future systematic studies of NPs in a dynamic model for human cancer. This will greatly facilitate the search for the best materials and coating to make NPs for tumor targeting purposes. Also, our results call for more attention and focus on how the endothelium interacts with NPs.

With chemists being able to create an increasingly diverse range of NPs with many different properties, this thesis presents a model along with several novel methods and techniques that will allow the biologist to study these NPs. The ZF model combined with the tools presented gives the opportunity to learn about NP behavior both at the single cell level, as well as on a whole organism level with remarkable precision thanks too the OT methods.

7   Future perspectives

The work done and the results obtained during the course of this thesis has illustrated that in the nanomedicine field, NPs, however promising they seem for use in cancer therapy, are still quite poorly characterized, both *in vitro* and *in vivo*. Little is known about their specific interactions with different cells and especially their interactions with living organisms.

The methods developed for *in vivo* manipulation, as well as *in vitro* characterization using OT show promise for further investigation, and opens up a new field of NP characterization. One exciting possibility is to investigate the interactions of liposomes with macrophages and cancer cells, as well as other cells. Conventional liposomes are usually too small to reliably measure and observe, but solid-core NPs coated with a lipid layer can offer an opportunity to perform these kinds of experiments. Combining the ZF model, OT, NPs and cancer cell transplantation is another promising way to go in the future. Learning more about how NPs interacts with tumors and tumor affected vasculature is important if one is to make the best possible NPs for treatment.

The FGT-T-MAE cells would be a good candidate for study NP interaction with angiogenic vessels using the methods described in this thesis. The FGF-T-MAE cells are suitable to use for studying tumor angiogenesis, as they as they generate tumor-like structures far from the host vasculature which are eventually vascularized due to FGF overexpression and secretion. It would be interesting to apply the OT in combination with NPs in these tumor vasculature areas to investigate the difference between healthy vasculature and vascularized tumor-like structures with regards to NP behavior.

The possibility to investigate other cell lines, possibly biopsied samples from patients and observe how they interact with NPs *in vivo* is important to possibly make a "map" over what kinds of cancers may be susceptible to NP treatment.

We believe these methods could also be used to open up new avenues of research for infectious diseases. One example that comes to mind is tuberculosis research. Our lab has already established the ZF model as a system for mycobacterium

marinum, a much used model bacteria for tuberculosis. If we can trap bacteria in the circulatory system of the ZF, we can measure the interaction forces between bacteria and macrophages, or we can possibly trap granulomas. If this is possible we can test their interactions with their environment or possibly their structural integrity by applying forces with the OT.

Given more time and resources these avenues would be interesting to pursue. The methods however still need to be refined and properly established in order to show its full promise, as well as its limitations.

Suffice it to say much of what has been presented in this thesis shows promise for further investigation by people in NP research, as well as for people in the ZF community.

8   Supplementary

8.1 Supplementary Protocol 1: Drop Volume Calibration for NP injection
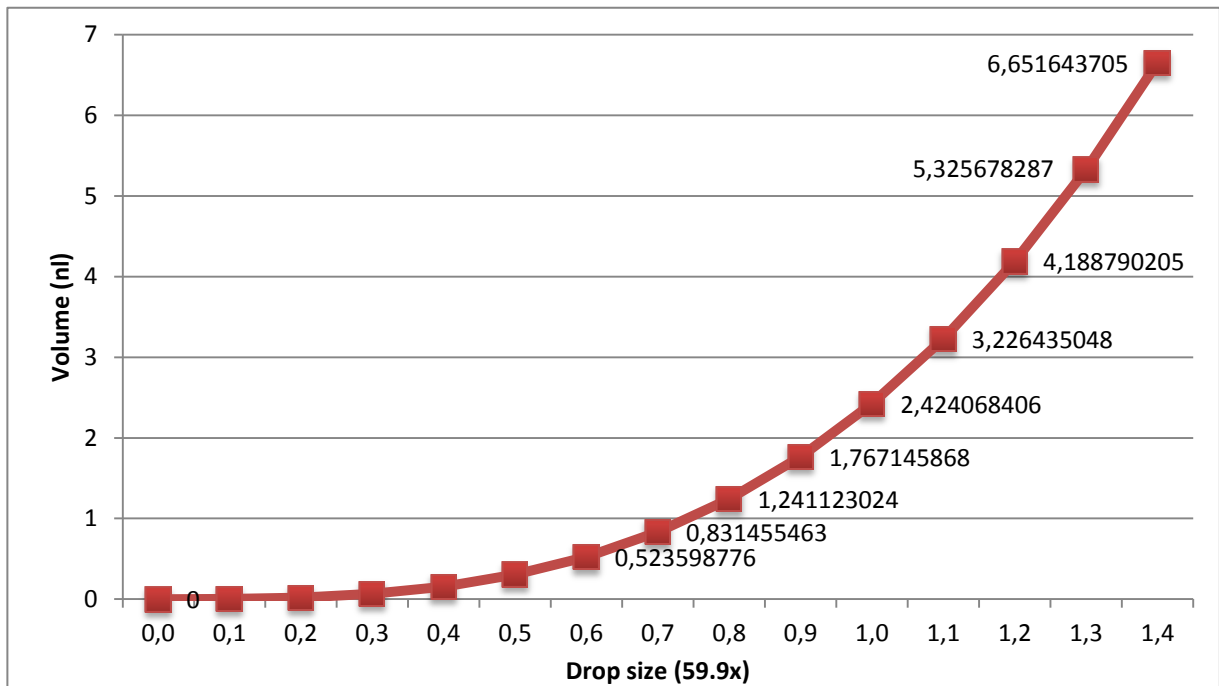
Graph used for calibration of volume for injection of NPs. For correct calibration the drop size must be measured a 60x magnification using an eyepiece with a ruler.

1 mm on eyepiece ruler = 6 units at 59.9x magnification (means a droplet of size 1 is actually 1/6 of a millimeter).

Volume of drop = $4/3*\pi r^3$, where r=radius, means that 1 nl = 0.001 cubic mm.

8.2 Supplementary Protocol 2: Fluorescent Pixel Count (FPC) Protocol using ImageJ

1. Import picture and convert to 16bit, then make a duplicate.
   a. **Image->Type->16-Bit**
   b. **Image-> Duplicate**
2. Set threshold to isolate the regions of interest (Check the "dark background" box). Use the sliders or the "Set"-function if you know the exact threshold levels. The areas marked in red will be counted during the pixel counting.
   a. **Image->Adjust->Threshold**

   Push the "**Apply**" button.
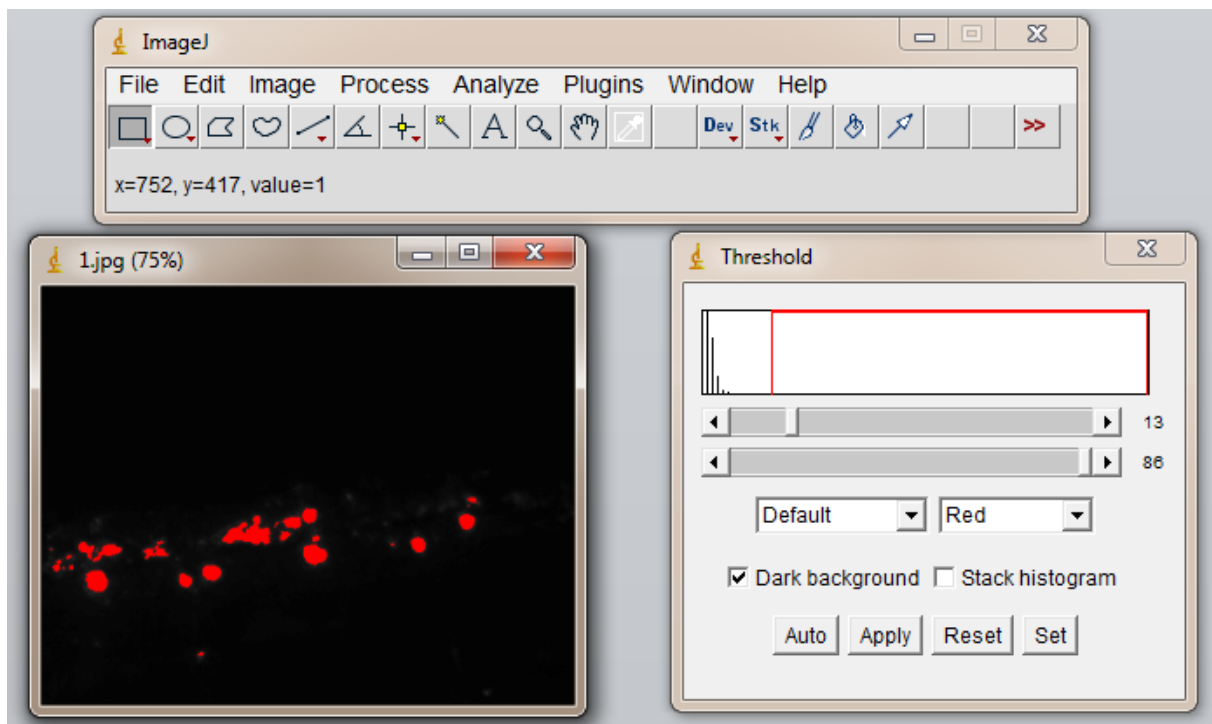
3. After pushing "**Apply**" ImageJ will generate an 8-bit image. Go to "**Set Measurements**" and redirect to the **duplicate** image generated in **Step 1**. Check the "**Limit to threshold**" box, then "OK". The other boxes checked in the picture should also be checked before proceeding.

   a. **Analyze-> Set Measurements**
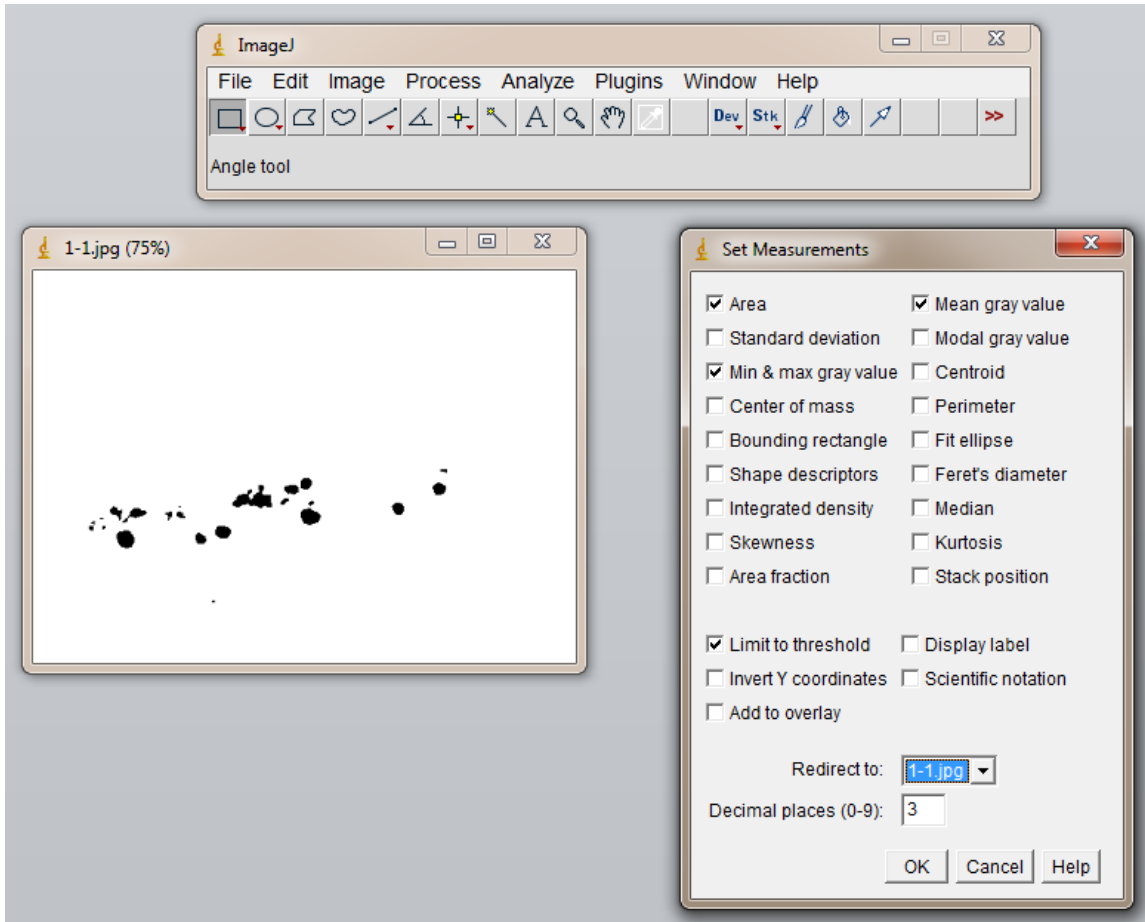
4. Go to the "**Analyze Particles**" section for the pixel count. Check the "**Display results**" box, then "**OK**". Use the **8-Bit** picture for the pixel counting. The "**Show**" option can be used to generate an additional picture in gray-scale with the areas used in the counting process outlined with area numbering which corresponds to the areas in the "**Results**"-table, use the "**Outline**" option.

   a. **Analyze->Analyze Particles**
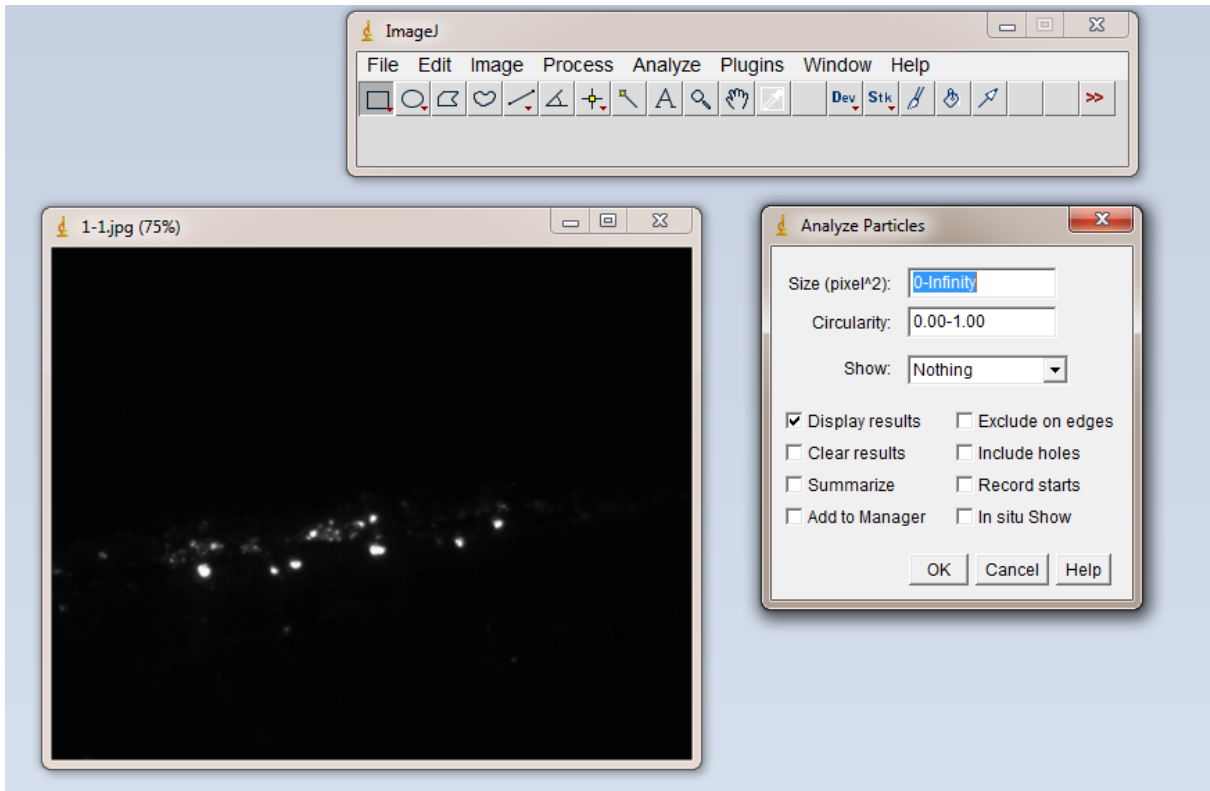
5. The "**Results**"-table will now appear. The data to be copy-pasted into the excel sheet are the two first rows. The first row indicates the sections counted, the numbers corresponds to the numbers in the picture obtained via the "**Show**" option. The second row, named "**Area**", is the number of pixels in the areas counted.
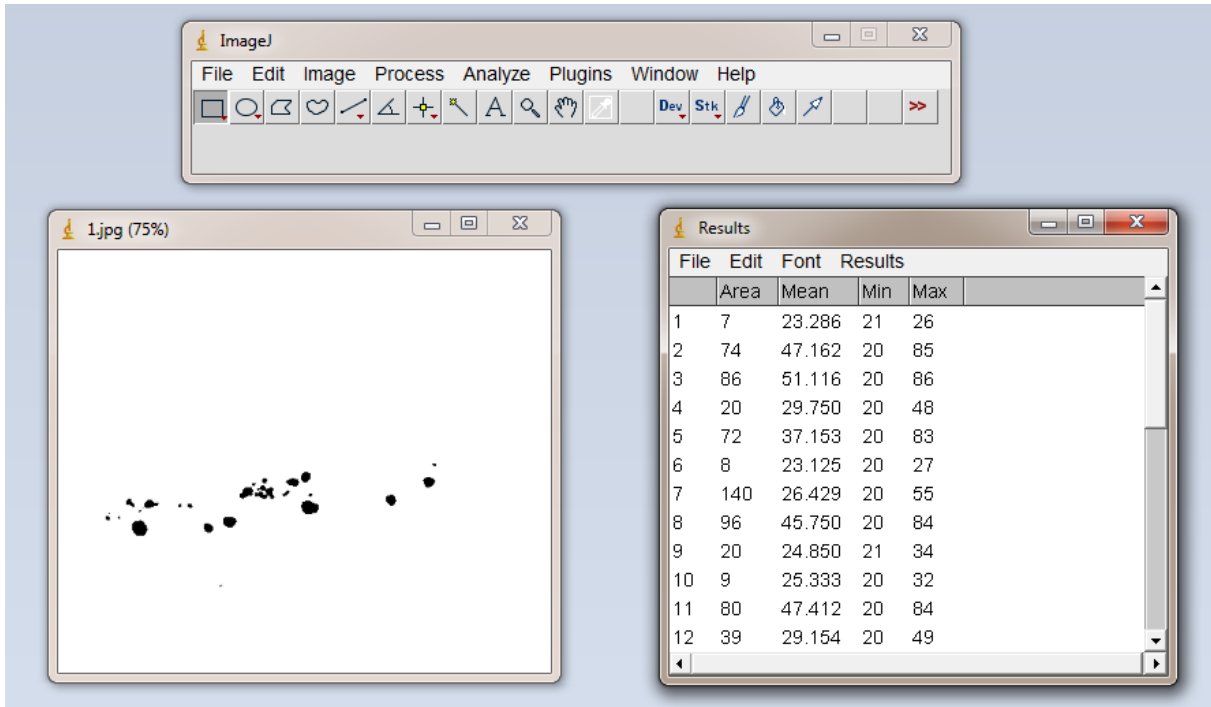
8.3 Supplementary Data 1: Information on cell lines

RAW macrophages
RAW 264.7 Cell Line murine, macrophage from blood.

Melmet 1 and 5
The Melmet 1 and 5 are metastatic melanoma cell lines established from the biopsies of metastatic melanoma patients at the Norwegian Radium Hospital. Both cell lines stably express a red fluorescent protein, DsRED. Both these cell lines where gifted to us from the group of Professor Gunhild M. Mælandsmo at the Norwegian Radium Hospital.

See" Effect of tumor microenvironment-derived factors on melanoma cell growth and drug response: an in vitro study in three dimensional cultures" by Maria Rist for further information on these cell lines.
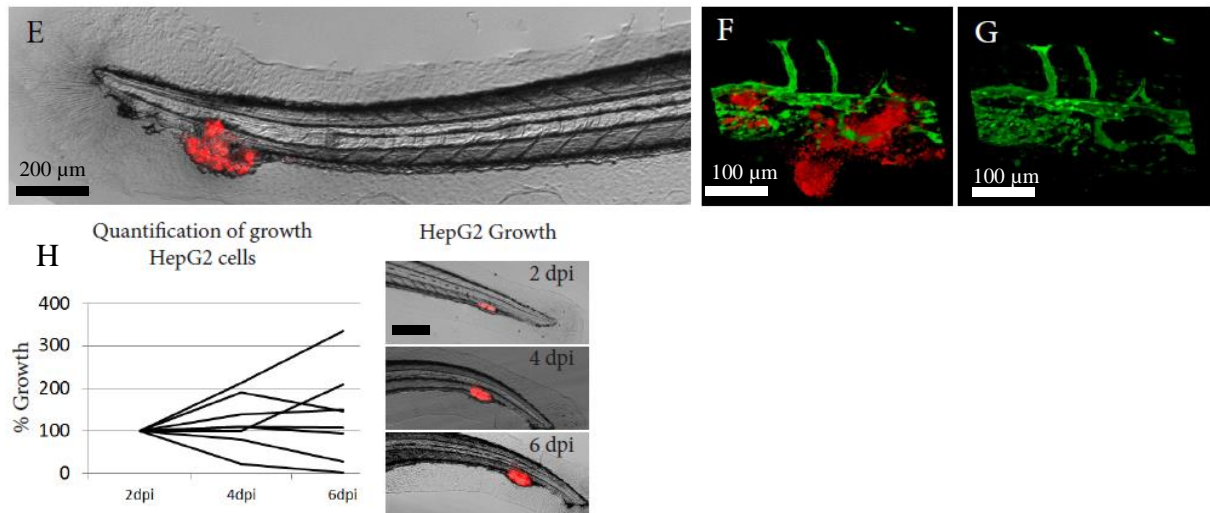
HepG2
HepG2 (ATCC No. HB-8065) is a human liver carcinoma cell line. The line used is this thesis was a gift from the lab of Dr. B. Ewa Snaar-Jagalska, Leiden University, Netherlands. This HepG2 line is virus transfected to stably express red fluorescent protein (RFP).

FGF-overexpressing murine aortic endothelial cells (FGF-T-MAE cells)
The FGF-T-MAE cell line was gifted to us from Marco Presta at the Department of Biomedical Sciences and Biotechnology, School of Medicine, University of Brescia, Italy.

8.4 Supplementary Data 2: HepG2 results

Supplementary figure 1. ZF injections and establishment of human tumor-like structures. (E) The human liver cancer cell line HepG2 established single tumor-like structures in the tail. **(F)** A HepG2 tumor-like structure and the orientation relative to the vasculature (green). The HepG2 tumor-like structures are mostly located around the blood vessels but also push the vasculature aside. **(G)** No endothelial (green) cells were observed to migrate into the tumor-like structure. **(H)** Quantification of HepG2 tumor-like structure sizes in individual embryos over a period of 6 dpi ($p>0.05$). Scale bar is 200 μm.

2 weeks before this thesis was due to be delivered, the lab in the Netherland which provided the HepG2 cell for these experiments reported that they had discovered the HepG2 cells to be contaminated with Human Embryonic Kidney 293 cells (HEK 293). This makes all data collected using this "HepG2"-cell line useless as a proof-of-principle cell line to establish a model system for the study of NPs in cancerous tissues in the ZF. The results of all experiments conducted using the HepG2 cells where therefore moved to a supplementary data sheet (Supplementary data 2).

The human liver cancer cell line HepG2 was tested based on its ability to establish solid tumors in mice.[89] Extravasation from the embryo blood vessels was observed within the first 24 h. The mechanism for the formation of a tumor-like structure appeared to be the same for the Melmet 5 cells; multiple HepG2 cells extravasated at

the same location. However, in contrast, a striking characteristic of these cells in the embryos was the generation of a single, prominent tumor-like structure in the tail (Supplementary Figure 1 A). The relative location of the HepG2 tumor-like structure to the vasculature was different from the Melmet 5 phenotype, as it was located more around the vasculature in a, in a toroid shape, rather than in between blood vessels (Supplementary Figure 1B-C). Also here, the blood flow was unaffected and no endothelial cells were observed to migrate into the tumor-like structure.

The growth of the tumor-like structures was quantified every second day over a period of six days post-injection (Supplementary Figure 1 D). The HepG2 cells had a average growth (34 %), and a high degree of variation from 2 dpi to 6 dpi. The variation ranged from a 97 % decrease in size to a 250 % increase in size for the HepG2 cells.
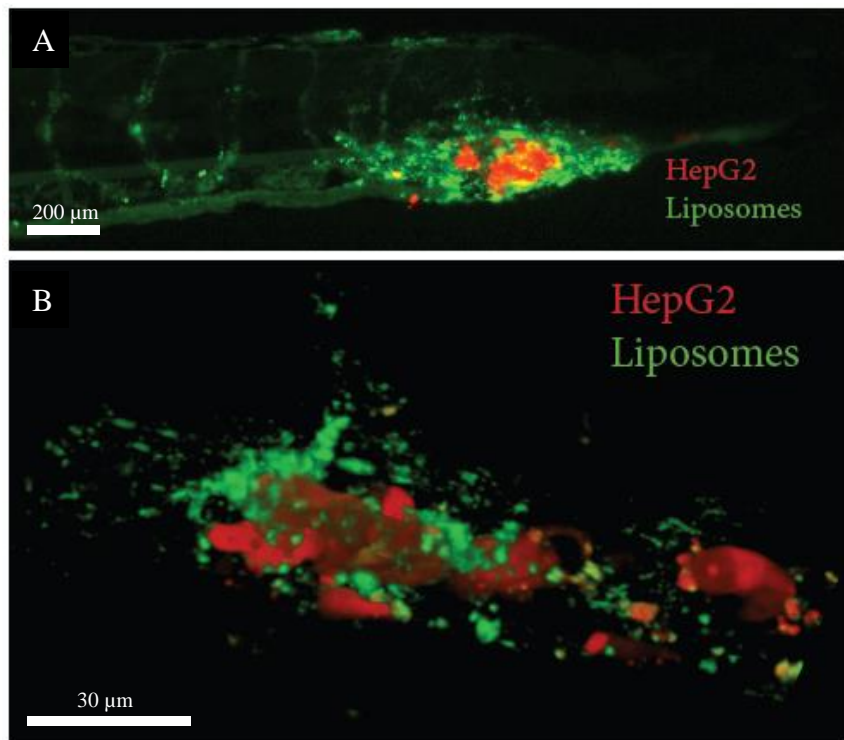
Supplementary Figure 2. Liposomes accumulates passively into HepG2 human tumor-like structures. (A) Tumor-like structures comprised of HepG2 cells (red) also showed the capacity to accumulate liposomes (green) specifically after 5 hours of circulation as liposomes does not bind to any other locations in the tail. **(B)** Confocal imaging of a 2 dpi HepG2 tumor-like structure with accumulated liposomes after 5 h of circulation. The liposomes have a loose association with the tumor-like structure as they concentrate in the area around the cancer cells, and do not interact with the cancer cells directly.

Tumor-like structures comprised of HepG2 were also able to accumulate PEG liposomes quickly and specifically, as we observed strong accumulation of liposomes after 5 h (Supplementary Figure 2 A). However, liposomes seemed to accumulate more around the HepG2 tumor-like structure; this was in contrast to the tumor-like structures consisting of Melmet 5 cells, where liposomes seemed to accumulate inside the tumor-like structure. A control embryo not injected with cancer cells shows the distribution of liposomes after 6 h of circulation (Figure 11C). The complete representation of the vasculature (in green) is evident due to the liposomes still in circulation. Some green "hotspots" can be observed (Figure 11C, arrows), referring to

macrophages starting to clear liposomes from circulation. Notably, there are no accumulation elsewhere of liposomes in the absence of cancer cells.

We performed confocal microscopy to study the pattern of liposomes in more detail. Two embryos with tumor-like structures were examined by acquisition of confocal stacks. The HepG2 tumor-like structure showed a loose association between liposomes and the HepG2 cells (Supplementary Figure 2A). Liposomes are indeed located to the area around the tumor-like structure but are definitely not taken up by the cancer cells. This image could suggest that most liposomes are not yet fully out of circulation and are still attached to the vasculature, which is both above and underneath the tumor-like structure.
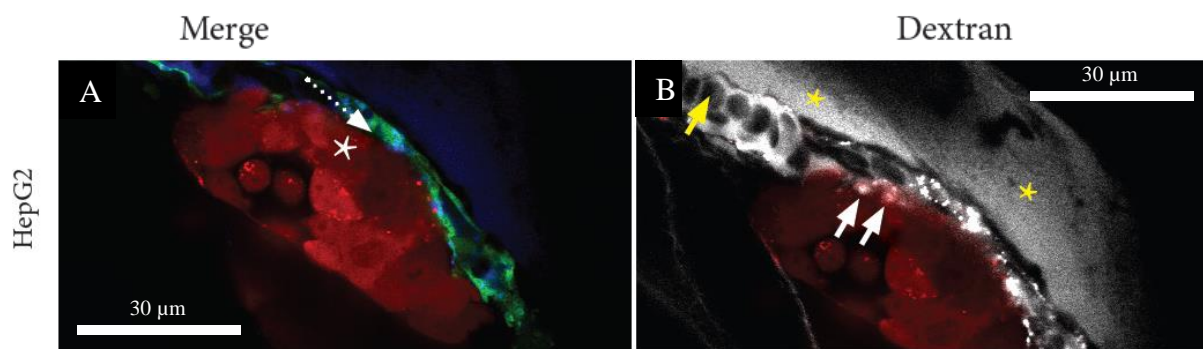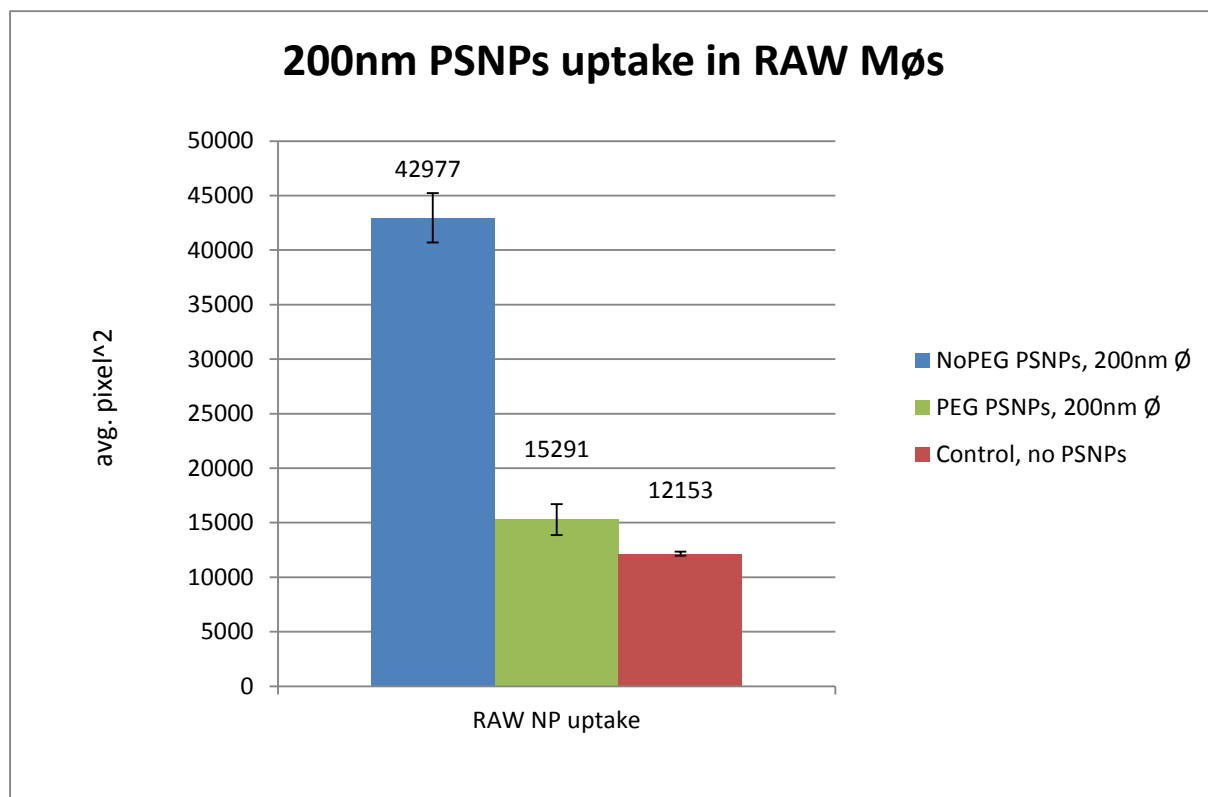

Supplementary Figure 3. Leakage of Dextran into HepG2 tumor-like structures. (A) A HepG2 tumor-like structure (red, asterisk) located next to a blood vessel (green) where dextran flows (blue). The dotted arrow indicates the direction of the blood flow. **(B)** Dextran (white) flowing in the vessel at the periphery of the HepG2 tumor-like structure (red). The yellow asterisks mark areas of autofluorescence. In the circulation erythrocytes exclude dextran (yellow arrow). At the border of the tumor-like structure and the blood vessel there are overlapping signals from the dextran and the HepG2 cells (white arrows). This indicates that after 20 minutes dextran are leaking into the periphery of the turmor-like structure in small amounts.

When we injected fluorescent dextran into the circulation of embryos with HepG2 tumor-like structures, we could after 20 min observe leakage of the dye into the HepG2 tumor-like structure (Supplementary Figure 3A). This suggests a local

activation of endothelial cell in the ZF embryo leading to a destabilized and leaky vasculature. The accumulation of dextran into HepG2 cells (supplementary Figure A-B), could be explained by growth factors secreted by the cells, which locally activate the endothelial cells. This loosening of the endothelium combined with the small liposome size and circulation properties allowed the liposomes to escape circulation specifically at the site of cancer cells.

8.5 Supplementary Data 3: FPC of PSNP incubation with RAW macrophages

200nm PSNPs uptake in RAW Møs

- NoPEG PSNPs, 200nm Ø
- PEG PSNPs, 200nm Ø
- Control, no PSNPs

y-axis: avg. pixel^2

x-axis: RAW NP uptake

Values shown: 42977, 15291, 12153

Supplementary Data 3. FPC on PSNP incubation with RAW macrophages. An approximate 3-fold increase in fluorescence is seen in the NoPEG PSNPs sample compared to the PEG PSNPs and the control. The small difference seen between the PEG PSNPS sample and the control indicates very little uptake of the PEG PSNPs by the RAW macrophages.

8.6 **Supplementary Data 4: Optical tweezers used to quantify the effect of PEG *in vitro***

1.0um NP binding to cancer cells using optical tweezers

(laserpower: 20mW)

1.0um NP binding to cancer cells using optical tweezers

(laserpower: 200mW)

1.0um NP binding to cancer cells using optical tweezers

(laserpower: 2000mW)
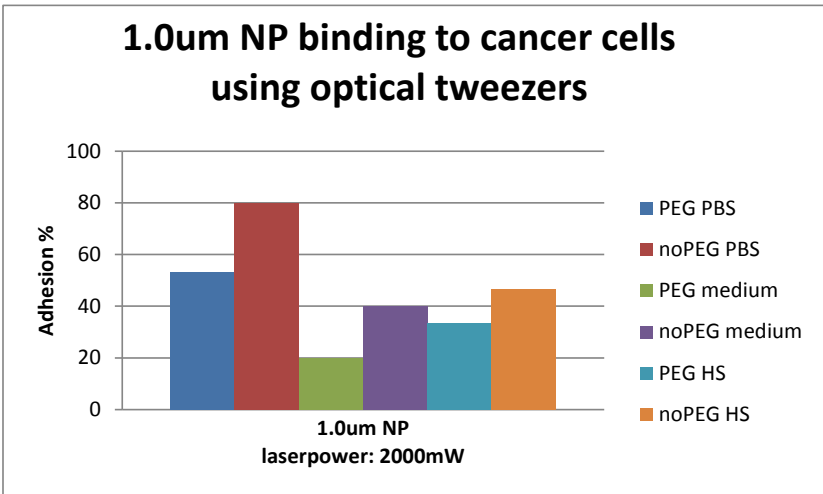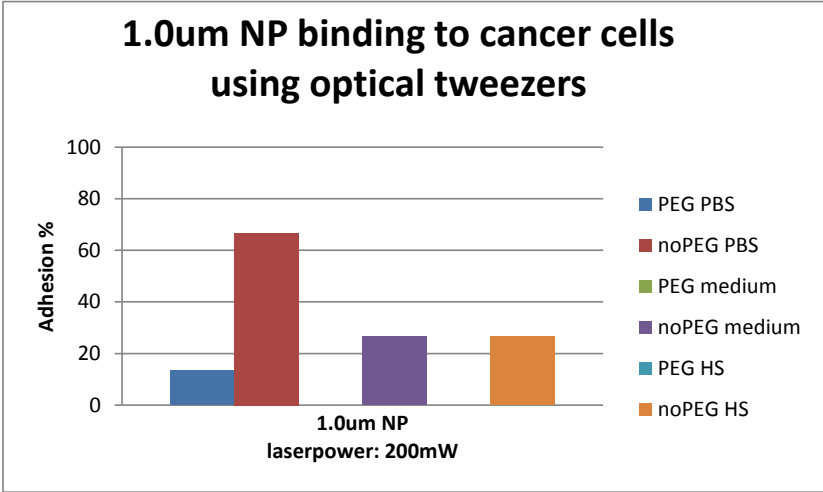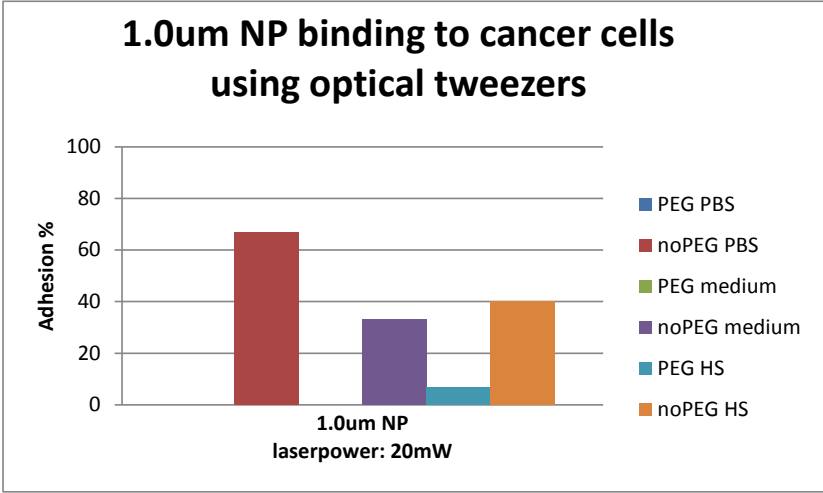
Supplementary Data 4. Optical tweezers used to quantify the effect of PEG on Melmet 5 cancer cells *in vitro*.
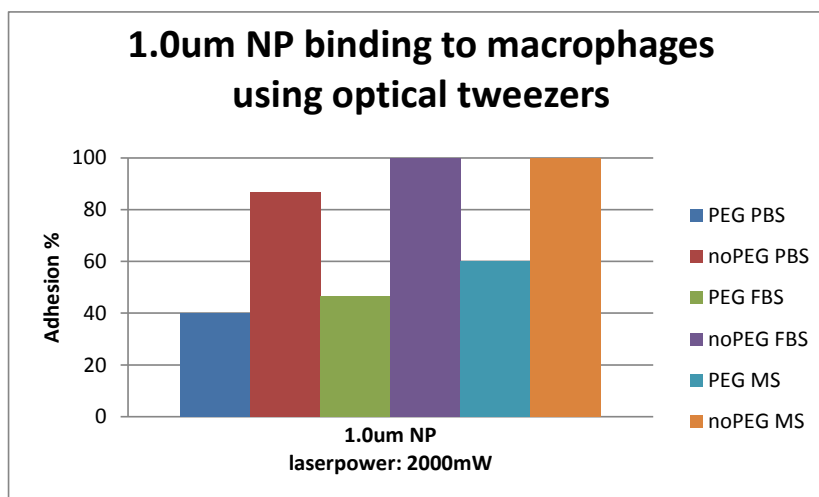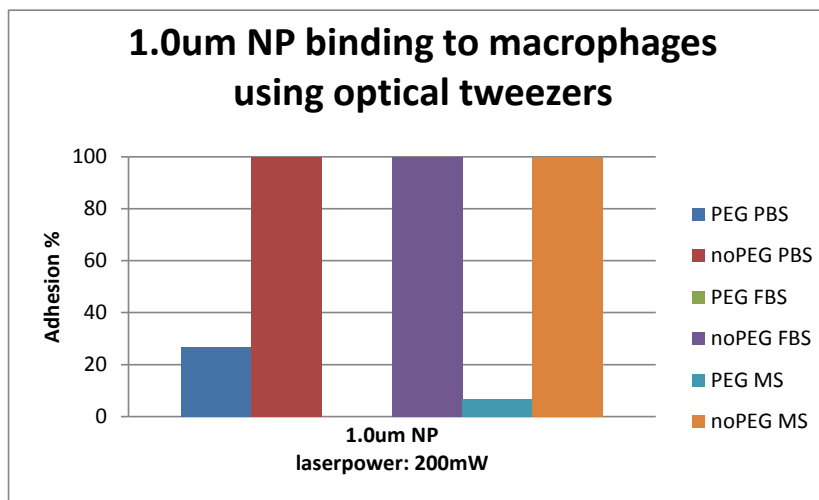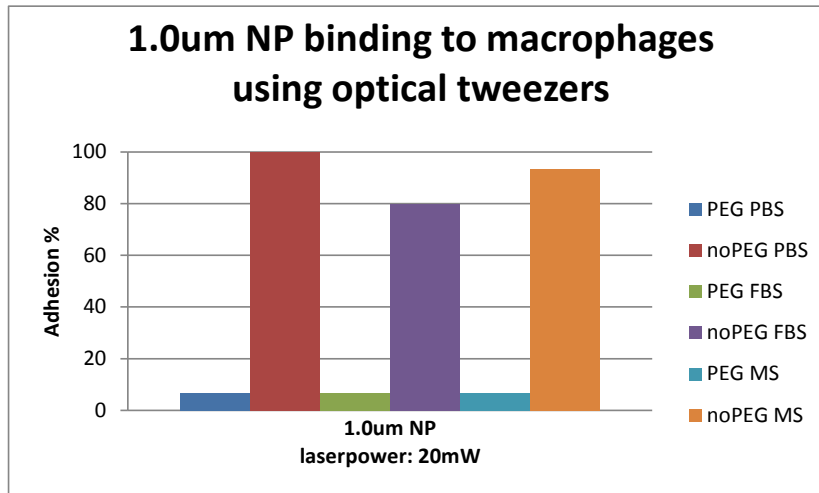
Supplementary Data 4. Optical tweezers used to quantify the effect of PEG on RAW macrophages *in vitro*.

8.7 **Supplementary data 5: SDS-PAGE gels for confirmation of protein presence on NPs after incubation with serum**

Top: Gel for human serum.

Bottom: Gel for mouse serum

well #	human/mouse serum
1	PEG 1000 + serum
2	PEG 1000 + PBS
3	NoPEG 1000 + serum
4	NoPEG 1000 + PBS
5	PEG 500 + serum
6	PEG 500 + PBS
7	NoPEG 500 + serum
8	NoPEG 500 + PBS
9	Control
10	Ladder

Key for well number

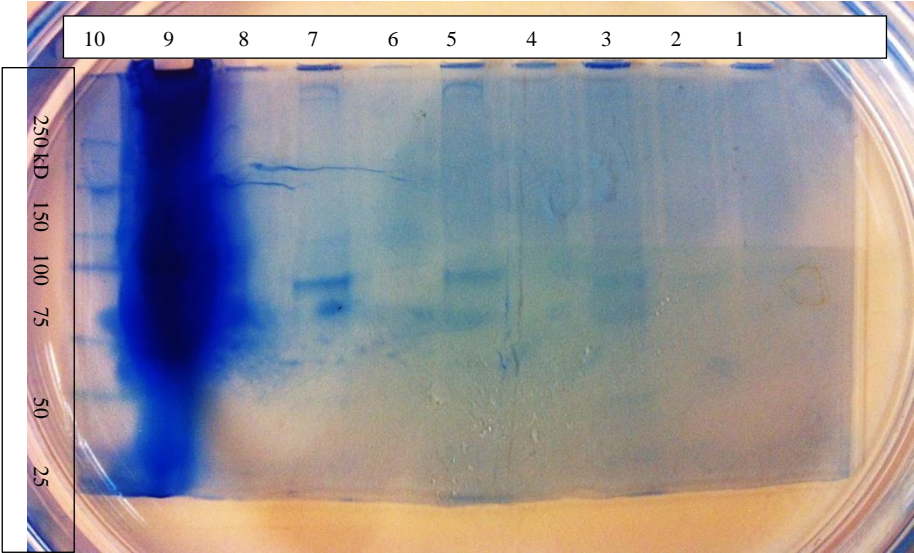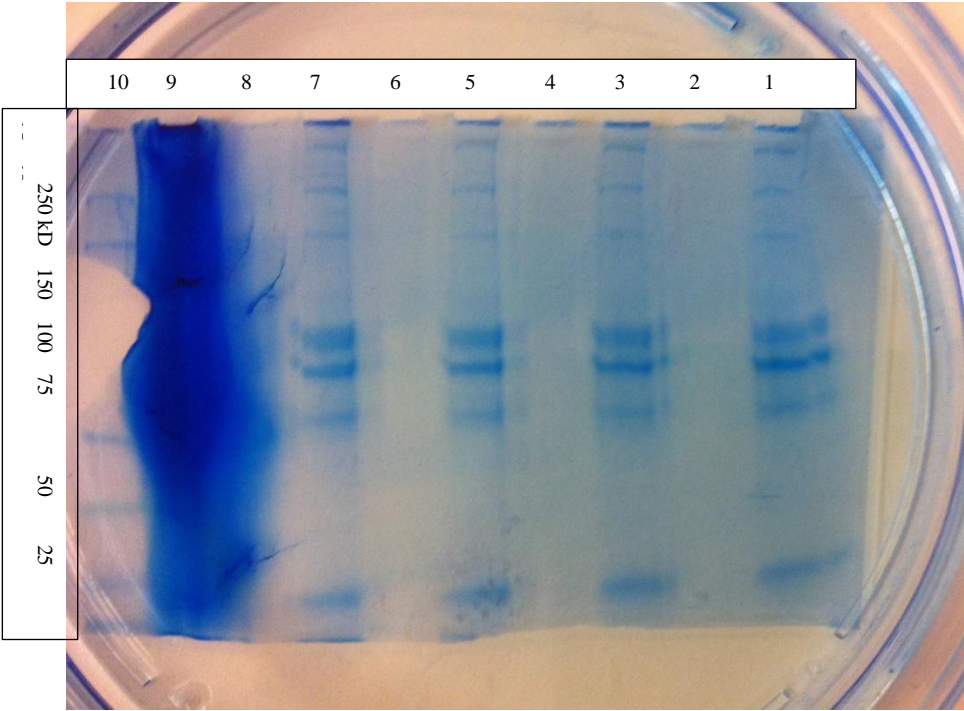## 8.8 **Supplementary Videos**

Supplementary video 1. 200 nm green fluorescent NoPEG PSNPs in zebrafish embryo circulation 20 seconds post injection.

Supplementary video 2. 200 nm green fluorescent NoPEG PSNPs in zebrafish embryo circulation 140 seconds post injection

Supplementary video 3. 1000 nm NoPEG PSNP adhering to a RAW macrophage *in vitro*.

Supplementary video 4. 1000 nm PEG PSNP do not adhere to a RAW macrophage *in vitro*.

Supplementary video 5. 200 nm green fluorescent PEG PSNPs in zebrafish circulation 20 seconds post injection

Supplementary video 6. 200 nm green fluorescent PEG PSNPs in zebrafish circulation 140 seconds post injection

Supplementary video 7. 200 nm green PEG liposomes in zebrafish embryo circulation 24 h post injection.

Supplementary video 8. 200 nm PEG green liposomes in zebrafish embryo circulation 46 h post injection.

Supplementary video 9. 200 nm PEG green liposomes taken up by macrophages 70 h post injection

Supplementary video 10. 200 nm green PEG liposomes circulating in zebrafish embryo with red tumor-like structures.

Supplementary video 11. 200 nm green liposomes accumulated in Melmet 5 tumor-like structure. Tumor-like structures are invisible but the embryo is the same as in Figure 6B where the tumor-like structures can be seen.

Supplementary video 12. 3D view of a confocal stack (ImageJ) of a red Melmet 5 tumor-like structure with accumulated green liposomes.

Supplementary video 13. Transmission light microscopy using OT to trap and manipulate red blood cells *in vivo*.

Supplementary video 14. Transmission light microscopy using OT showing how we can remove cells from an area, "fence" it off using the multi-plexing function and manipulate NPs.

Supplementary video 15. Transmission light microscopy using OT showing how we can manipulate several NPs simultaneously using the multi-plexing function.

Supplementary video 16. Transmission light microscopy using OT showing how we can trap 1.0um NPs in vivo and pull on them after they have attached to the endothelial cells. This video show the pulling of a tether and the release of the NP from the optical trap, resulting in the NP being pulled back to the cell via the tether.

8.9 **Recipes**

Deionized, distilled water was used in all recipes and protocol steps.

Tricaine stock solution

Adapted from Cosma et.al 2006.

400 mg tricaine (Argent Laboratories)

97.9mL H2O

~2.1mL 1 M Tris·Cl, pH 9

Adjust pH to ~7

Store up to 1 month at 4∘C

Zebrafish embryo medium

Adapted from Westerfield 2000.

1.0mL Hanks' stock solution #1 (see recipe)

0.1mL Hanks' stock solution #2 (see recipe)

1.0mL Hanks' stock solution #4 (see recipe)

95.9mL H2O

1.0mL Hanks' stock solution #5 (see recipe)

1.0mL Hanks' stock solution #6 (see recipe)

Use about ten drops 1 M NaOH to pH 7.2. Store indefinitely at 4∘C

Hanks' stock solutions

Stock #1:

8.0 g NaCl

0.4 g KCl

100mL H_2O

Stock #2:

0.358 g Na_2HPO_4 anhydrous

0.60 g KH_2PO_4

100mL H_2O

Stock #4:

0.72 g $CaCl_2$

50mL H_2O

Stock #5:

1.23 g $MgSO_4 \cdot 7H_2O$

50mL H_2O

Stock #6:

0.35 g $NaHCO_3$

10mL H_2O

All of Hanks' stock solutions should be stored indefinitely at 4∘C.

Dulbecco's Modified Eagle's medium (DMEM)

500mL DMEM (Sigma-Aldrich product # D6429)

50mL Fetal Calf Serum (FCS), Heat inactivated (Sigma-Aldrich)

5mL Pen-Strep (Lonza)

Store at 40C.

RPMI-1640 Medium

RPMI-1640 Medium (Sigma-Aldrich product # R5886)

50mL Fetal Calf Serum (FCS), Heat inactivated (Sigma-Aldrich)

5mL Pen-Strep (Lonza)

5mL L-glutamin 200mM (Sigma-Aldrich)

Store at 40C.

PTU solution

Adapted from Cosma et.al 2006.

0.06g 1-phenyl-2-thiourea (PTU) (Sigma Aldrich)

100mL zebrafish embryo medium (see recipes)

Store up to 1 month at 40C.

PTU may take several hours to dissolve completely with constant stirring using a stir bar.

Store at room temperature.

References

1. Amsterdam, V.U.M.C. *EBV realted cancers*. Available from: http://www.vumc.com/branch/pathology/4947029/4947095/4947989/.
2. Prevention, C.f.D.C.a. *Human Papillomavirus*. Available from: http://www.cdc.gov/hpv/cancer.html.
3. Insititute, N.C. *Patient`s Genetic Background*. Available from: http://www.cancer.gov/cancertopics/understandingcancer/geneticbackground/page24.
4. Hajdu, S.I., *A note from history: landmarks in history of cancer, part 1*. Cancer, 2011. **117**(5): p. 1097-102.
5. Hajdu, S.I., *A note from history: landmarks in history of cancer, part 2*. Cancer, 2011. **117**(12): p. 2811-20.
6. Hajdu, S.I., *A note from history: landmarks in history of cancer, part 3*. Cancer, 2012. **118**(4): p. 1155-68.
7. Hajdu, S.I., *A note from history: landmarks in history of cancer, part 4*. Cancer, 2012. **118**(20): p. 4914-28.
8. Hajdu, S.I. and F. Darvishian, *A note from history: landmarks in history of cancer, part 5*. Cancer, 2013. **119**(8): p. 1450-66.
9. Hajdu, S.I. and M. Vadmal, *A note from history: Landmarks in history of cancer, Part 6*. Cancer, 2013. **119**(23): p. 4058-82.
10. Hanahan, D. and R.A. Weinberg, *The Hallmarks of Cancer*. Cell, 2000. **100**(1): p. 57-70.
11. UK, C.R. *How can cancer kill you?* 2014; Available from: http://www.cancerresearchuk.org/about-cancer/cancers-in-general/cancer-questions/how-can-cancer-kill-you.
12. Mehlen, P. and A. Puisieux, *Metastasis: a question of life or death*. Nat Rev Cancer, 2006. **6**(6): p. 449-458.
13. Institute, N.C. *Metastatic cancer*. 2014; Available from: http://www.cancer.gov/cancertopics/what-is-cancer/metastatic-fact-sheet.
14. Yokota, J., *Tumor progression and metastasis*. Carcinogenesis, 2000. **21**(3): p. 497-503.
15. Hanahan, D. and Robert A. Weinberg, *Hallmarks of Cancer: The Next Generation*. Cell, 2011. **144**(5): p. 646-674.
16. *The metabolism of tumours. Investigations from the Kaiser-Wilhelm Institute for Biology, Berlin-Dahlem. Edited by Otto Warburg, Kaiser-Wilhelm Institute for Biology, Berlin-Dahlem. Translated from the German edition, with accounts of additional recent researches, by Frank Dickens, M.A., Ph.D., whole-time worker for the Medical Research Council, Courtauld Institute of Biochemistry, Middlesex Hospital, London. Demy 8vo. Pp. 327 + xxix. Illustrated. 1930. London: Constable & Co. Ltd. 40s. net.* British Journal of Surgery, 1931. **19**(73): p. 168-168.
17. Warburg, O., *On respiratory impairment in cancer cells*. Science, 1956. **124**(3215): p. 269-270.
18. DeBerardinis, R.J., et al., *The biology of cancer: metabolic reprogramming fuels cell growth and proliferation*. Cell Metab, 2008. **7**(1): p. 11-20.
19. Hsu, P.P. and D.M. Sabatini, *Cancer Cell Metabolism: Warburg and Beyond*. Cell. **134**(5): p. 703-707.
20. Jones, R.G. and C.B. Thompson, *Tumor suppressors and cell metabolism: a recipe for cancer growth*. Genes Dev, 2009. **23**(5): p. 537-48.

21. Potter, V.R., *The biochemical approach to the cancer problem.* Fed Proc, 1958. **17**(2): p. 691-7.
22. Vander Heiden, M.G., L.C. Cantley, and C.B. Thompson, *Understanding the Warburg effect: the metabolic requirements of cell proliferation.* Science, 2009. **324**(5930): p. 1029-33.
23. Feron, O., *Pyruvate into lactate and back: from the Warburg effect to symbiotic energy fuel exchange in cancer cells.* Radiother Oncol, 2009. **92**(3): p. 329-33.
24. Semenza, G.L., *Tumor metabolism: cancer cells give and take lactate.* J Clin Invest, 2008. **118**(12): p. 3835-7.
25. Bindea, G., et al., *Natural immunity to cancer in humans.* Curr Opin Immunol, 2010. **22**(2): p. 215-22.
26. Vajdic, C.M. and M.T. van Leeuwen, *Cancer incidence and risk factors after solid organ transplantation.* Int J Cancer, 2009. **125**(8): p. 1747-54.
27. Schuell, B., et al., *Side effects during chemotherapy predict tumour response in advanced colorectal cancer.* Br J Cancer, 2005. **93**(7): p. 744-748.
28. Srinivas, P.R., B.S. Kramer, and S. Srivastava, *Trends in biomarker research for cancer detection.* The Lancet Oncology, 2001. **2**(11): p. 698-704.
29. Institute, N.C., *Cancer Staging.* 2014.
30. Cooper, W.A., et al., *What's new in non-small cell lung cancer for pathologists: the importance of accurate subtyping, EGFR mutations and ALK rearrangements.* Pathology, 2011. **43**(2): p. 103-15.
31. Ramaswamy, S., et al., *Multiclass cancer diagnosis using tumor gene expression signatures.* Proceedings of the National Academy of Sciences, 2001. **98**(26): p. 15149-15154.
32. Zhu, H., M. Bilgin, and M. Snyder, *Proteomics.* Annu Rev Biochem, 2003. **72**: p. 783-812.
33. Arango, B.A., C.L. Rivera, and S. Gluck, *Gene expression profiling in breast cancer.* Am J Transl Res, 2013. **5**(2): p. 132-8.
34. Institute, N.C. *SEER Stat Fact Sheets: Prostate Cancer*. Available from: http://seer.cancer.gov/statfacts/html/prost.html.
35. Institute, N.C. *SEER Stat Fact Sheets: Liver and Intrahepatic Bile Duct Cancer*. Available from: http://seer.cancer.gov/statfacts/html/livibd.html.
36. Jemal, A., et al., *Cancer statistics, 2005.* CA Cancer J Clin, 2005. **55**(1): p. 10-30.
37. Institute, N.C. *SEER Cancer Statistics Review 1975-2011*. Available from: http://seer.cancer.gov/csr/1975_2011/browse_csr.php?sectionSEL=1&pageSEL=sect_01_table.03.html.
38. Rothenberg, M.L., et al., *Mortality associated with irinotecan plus bolus fluorouracil/leucovorin: summary findings of an independent panel.* J Clin Oncol, 2001. **19**(18): p. 3801-7.
39. van Kuilenburg, A.B., et al., *Lethal outcome of a patient with a complete dihydropyrimidine dehydrogenase (DPD) deficiency after administration of 5-fluorouracil: frequency of the common IVS14+1G>A mutation causing DPD deficiency.* Clin Cancer Res, 2001. **7**(5): p. 1149-53.
40. Cattel, L., M. Ceruti, and F. Dosio, *From conventional to stealth liposomes: a new frontier in cancer chemotherapy.* Tumori, 2003. **89**(3): p. 237-49.
41. Laroui, H., et al., *Nanomedicine in GI.* Am J Physiol Gastrointest Liver Physiol, 2011. **300**(3): p. G371-83.
42. Lu, J.M., et al., *Current advances in research and clinical applications of PLGA-based nanotechnology.* Expert Rev Mol Diagn, 2009. **9**(4): p. 325-41.

43.   Mousavi, S.R. and M. Rezaei, *Nanotechnology in agriculture and food production.* J Appl Environ Biol Sci, 2011. **1**(10): p. 414-419.

44.   Cheng, Y., et al., *Highly Efficient Drug Delivery with Gold Nanoparticle Vectors for in Vivo Photodynamic Therapy of Cancer.* Journal of the American Chemical Society, 2008. **130**(32): p. 10643-10647.

45.   Malam, Y., M. Loizidou, and A.M. Seifalian, *Liposomes and nanoparticles: nanosized vehicles for drug delivery in cancer.* Trends in Pharmacological Sciences, 2009. **30**(11): p. 592-599.

46.   Shukla, A.K., S. Patra, and V.K. Dubey, *Nanospheres Encapsulating Anti-Leishmanial Drugs for Their Specific Macrophage Targeting, Reduced Toxicity, and Deliberate Intracellular Release.* Vector Borne and Zoonotic Diseases, 2012. **12**(11): p. 953-960.

47.   Partridge, A.H., H.J. Burstein, and E.P. Winer, *Side effects of chemotherapy and combined chemohormonal therapy in women with early-stage breast cancer.* J Natl Cancer Inst Monogr, 2001(30): p. 135-42.

48.   Singla, A.K., A. Garg, and D. Aggarwal, *Paclitaxel and its formulations.* Int J Pharm, 2002. **235**(1-2): p. 179-92.

49.   Acharya, S. and S.K. Sahoo, *PLGA nanoparticles containing various anticancer agents and tumour delivery by EPR effect.* Adv Drug Deliv Rev, 2011. **63**(3): p. 170-83.

50.   Farokhzad, O.C., et al., *Targeted nanoparticle-aptamer bioconjugates for cancer chemotherapy in vivo.* Proceedings of the National Academy of Sciences, 2006. **103**(16): p. 6315-6320.

51.   Klibanov, A.L., et al., *Amphipathic polyethyleneglycols effectively prolong the circulation time of liposomes.* FEBS Lett, 1990. **268**(1): p. 235-7.

52.   Torchilin, V.P., *Polymer-coated long-circulating microparticulate pharmaceuticals.* J Microencapsul, 1998. **15**(1): p. 1-19.

53.   Meyers, J.D., et al., *Nanoparticles for imaging and treating brain cancer.* Nanomedicine (London, England), 2013. **8**(1): p. 123-143.

54.   Yu, M.K., J. Park, and S. Jon, *Targeting Strategies for Multifunctional Nanoparticles in Cancer Imaging and Therapy.* Theranostics, 2012. **2**(1): p. 3-44.

55.   Chen, J., et al., *Enhanced cellular uptake of folic acid-conjugated PLGA-PEG nanoparticles loaded with vincristine sulfate in human breast cancer.* Drug Dev Ind Pharm, 2011. **37**(11): p. 1339-46.

56.   Kim, D.-H. and D.C. Martin, *Sustained release of dexamethasone from hydrophilic matrices using PLGA nanoparticles for neural drug delivery.* Biomaterials, 2006. **27**(15): p. 3031-3037.

57.   Soppimath, K.S., et al., *Biodegradable polymeric nanoparticles as drug delivery devices.* Journal of Controlled Release, 2001. **70**(1–2): p. 1-20.

58.   Albanese, A., P.S. Tang, and W.C. Chan, *The effect of nanoparticle size, shape, and surface chemistry on biological systems.* Annu Rev Biomed Eng, 2012. **14**: p. 1-16.

59.   Alexis, F., et al., *Factors Affecting the Clearance and Biodistribution of Polymeric Nanoparticles.* Molecular Pharmaceutics, 2008. **5**(4): p. 505-515.

60.   Balasubramanian, S.K., et al., *The effect of primary particle size on biodistribution of inhaled gold nano-agglomerates.* Biomaterials, 2013. **34**(22): p. 5439-52.

61.   Basha, R., et al., *Targeted nanoparticles for pediatric leukemia therapy.* Front Oncol, 2014. **4**: p. 101.

62.   Adams, R.H. and K. Alitalo, *Molecular regulation of angiogenesis and lymphangiogenesis.* Nat Rev Mol Cell Biol, 2007. **8**(6): p. 464-478.

63. Maeda, H., et al., *Tumor vascular permeability and the EPR effect in macromolecular therapeutics: a review.* Journal of Controlled Release, 2000. **65**(1–2): p. 271-284.

64. Gao, H., et al., *Ligand modified nanoparticles increases cell uptake, alters endocytosis and elevates glioma distribution and internalization.* Sci. Rep., 2013. **3**.

65. Lu, J., et al., *Light-Activated Nanoimpeller-Controlled Drug Release in Cancer Cells.* Small (Weinheim an der Bergstrasse, Germany), 2008. **4**(4): p. 421-426.

66. Meng, F., et al., *Intracellular drug release nanosystems.* Materials Today, 2012. **15**(10): p. 436-442.

67. Matsumura, Y. and H. Maeda, *A new concept for macromolecular therapeutics in cancer chemotherapy: mechanism of tumoritropic accumulation of proteins and the antitumor agent smancs.* Cancer Res, 1986. **46**(12 Pt 1): p. 6387-92.

68. Greish, K., *Enhanced permeability and retention (EPR) effect for anticancer nanomedicine drug targeting.* Methods Mol Biol, 2010. **624**: p. 25-37.

69. Gazit, Y., et al., *Fractal characteristics of tumor vascular architecture during tumor growth and regression.* Microcirculation, 1997. **4**(4): p. 395-402.

70. Narang, A.S. and S. Varia, *Role of tumor vascular architecture in drug delivery.* Adv Drug Deliv Rev, 2011. **63**(8): p. 640-58.

71. Maeda, H., et al., *Vascular permeability enhancement in solid tumor: various factors, mechanisms involved and its implications.* Int Immunopharmacol, 2003. **3**(3): p. 319-28.

72. Wu, J., et al., *Enhanced vascular permeability in solid tumor involving peroxynitrite and matrix metalloproteinases.* Jpn J Cancer Res, 2001. **92**(4): p. 439-51.

73. Wu, J., T. Akaike, and H. Maeda, *Modulation of enhanced vascular permeability in tumors by a bradykinin antagonist, a cyclooxygenase inhibitor, and a nitric oxide scavenger.* Cancer Res, 1998. **58**(1): p. 159-65.

74. Lever, M.J. and M.T. Jay, *Convective and diffusive transport of plasma proteins across the walls of large blood vessels.* Front Med Biol Eng, 1993. **5**(1): p. 45-50.

75. Mann, M.J., et al., *Pressure-mediated oligonucleotide transfection of rat and human cardiovascular tissues.* Proc Natl Acad Sci U S A, 1999. **96**(11): p. 6411-6.

76. Longmire, M., P.L. Choyke, and H. Kobayashi, *Clearance Properties of Nano-sized Particles and Molecules as Imaging Agents: Considerations and Caveats.* Nanomedicine (London, England), 2008. **3**(5): p. 703-717.

77. van Furth, R., et al., *The mononuclear phagocyte system: a new classification of macrophages, monocytes, and their precursor cells.* Bull World Health Organ, 1972. **46**(6): p. 845-52.

78. Longmire, M., P.L. Choyke, and H. Kobayashi, *Clearance properties of nano-sized particles and molecules as imaging agents: considerations and caveats.* Nanomedicine, 2008. **3**(5): p. 703-717.

79. Soo Choi, H., et al., *Renal clearance of quantum dots.* Nat Biotech, 2007. **25**(10): p. 1165-1170.

80. Storm, G., et al., *Surface modification of nanoparticles to oppose uptake by the mononuclear phagocyte system.* Advanced Drug Delivery Reviews, 1995. **17**(1): p. 31-48.

81. Fenaroli, F., et al., *Nanoparticles as Drug Delivery System against Tuberculosis in Zebrafish Embryos: Direct Visualization and Treatment.* ACS Nano, 2014. **8**(7): p. 7014-7026.

82. Frohlich, E., *The role of surface charge in cellular uptake and cytotoxicity of medical nanoparticles.* Int J Nanomedicine, 2012. **7**: p. 5577-91.

83. Pasut, G., et al., *Polyethylene glycol (PEG)-dendron phospholipids as innovative constructs for the preparation of super stealth liposomes for anticancer therapy.* J Control Release, 2015. **199**: p. 106-13.

84. Niikura, K., et al., *Gold nanoparticles as a vaccine platform: influence of size and shape on immunological responses in vitro and in vivo.* ACS Nano, 2013. **7**(5): p. 3926-38.

85. van Vlerken, L.E., T.K. Vyas, and M.M. Amiji, *Poly(ethylene glycol)-modified nanocarriers for tumor-targeted and intracellular delivery.* Pharm Res, 2007. **24**(8): p. 1405-14.

86. Gref, R., et al., *Biodegradable long-circulating polymeric nanospheres.* Science, 1994. **263**(5153): p. 1600-3.

87. Kommareddy, S. and M. Amiji, *Biodistribution and pharmacokinetic analysis of long-circulating thiolated gelatin nanoparticles following systemic administration in breast cancer-bearing mice.* J Pharm Sci, 2007. **96**(2): p. 397-407.

88. Hamidi, M., A. Azadi, and P. Rafiei, *Pharmacokinetic consequences of pegylation.* Drug Deliv, 2006. **13**(6): p. 399-409.

89. Kommareddy, S., S.B. Tiwari, and M.M. Amiji, *Long-circulating polymeric nanovectors for tumor-selective gene delivery.* Technol Cancer Res Treat, 2005. **4**(6): p. 615-25.

90. Veronese, F.M. and G. Pasut, *PEGylation, successful approach to drug delivery.* Drug Discov Today, 2005. **10**(21): p. 1451-8.

91. Moghimi, S.M., et al., *An investigation of the filtration capacity and the fate of large filtered sterically-stabilized microspheres in rat spleen.* Biochim Biophys Acta, 1993. **1157**(3): p. 233-40.

92. Thorek, D.L. and A. Tsourkas, *Size, charge and concentration dependent uptake of iron oxide particles by non-phagocytic cells.* Biomaterials, 2008. **29**(26): p. 3583-90.

93. Ishida, T. and H. Kiwada, *Accelerated blood clearance (ABC) phenomenon upon repeated injection of PEGylated liposomes.* Int J Pharm, 2008. **354**(1-2): p. 56-62.

94. Abu Lila, A.S., H. Kiwada, and T. Ishida, *The accelerated blood clearance (ABC) phenomenon: Clinical challenge and approaches to manage.* Journal of Controlled Release, 2013. **172**(1): p. 38-47.

95. Alestrom, P., J.L. Holter, and R. Nourizadeh-Lillabadi, *Zebrafish in functional genomics and aquatic biomedicine.* Trends Biotechnol, 2006. **24**(1): p. 15-21.

96. Dahm, R. and R. Geisler, *Learning from small fry: the zebrafish as a genetic model organism for aquaculture fish species.* Mar Biotechnol (NY), 2006. **8**(4): p. 329-45.

97. Howe, K., et al., *The zebrafish reference genome sequence and its relationship to the human genome.* Nature, 2013. **496**(7446): p. 498-503.

98. Kimmel, C.B., *Genetics and early development of zebrafish.* Trends Genet, 1989. **5**(8): p. 283-8.

99. Westerfield, M., *The Zebrafish Book. A Guide for the Laboratory Use of Zebrafish (Danio rerio).* 2000. **4th Edition**.

100. Corey, D.R. and J.M. Abrams, *Morpholino antisense oligonucleotides: tools for investigating vertebrate development.* Genome Biol, 2001. **2**(5): p. Reviews1015.

101. Meng, X., et al., *Targeted gene inactivation in zebrafish using engineered zinc-finger nucleases.* Nat Biotechnol, 2008. **26**(6): p. 695-701.

102. Kinth, P., G. Mahesh, and Y. Panwar, *Mapping of zebrafish research: a global outlook.* Zebrafish, 2013. **10**(4): p. 510-7.

103. Etchin, J., J.P. Kanki, and A.T. Look, *Chapter 13 - Zebrafish as a Model for the Study of Human Cancer*, in *Methods in Cell Biology*, M.W. H. William Detrich and I.Z. Leonard, Editors. 2011, Academic Press. p. 309-337.

104. Haldi, M., et al., *Human melanoma cells transplanted into zebrafish proliferate, migrate, produce melanin, form masses and stimulate angiogenesis in zebrafish.* Angiogenesis, 2006. **9**(3): p. 139-51.

105. Lee, L.M., et al., *The fate of human malignant melanoma cells transplanted into zebrafish embryos: assessment of migration and cell division in the absence of tumor formation.* Dev Dyn, 2005. **233**(4): p. 1560-70.

106. Lawson, N.D. and B.M. Weinstein, *In vivo imaging of embryonic vascular development using transgenic zebrafish.* Dev Biol, 2002. **248**(2): p. 307-18.

107. Tobin, D.M., R.C. May, and R.T. Wheeler, *Zebrafish: A See-Through Host and a Fluorescent Toolbox to Probe Host–Pathogen Interaction.* PLoS Pathog, 2012. **8**(1): p. e1002349.

108. Taylor, A.M. and L.I. Zon, *Zebrafish Tumor Assays: The State of Transplantation.* Zebrafish, 2009. **6**(4): p. 339-346.

109. Fenaroli, F., et al., *Nanoparticles as drug delivery system against tuberculosis in zebrafish embryos: direct visualization and treatment.* ACS Nano, 2014. **8**(7): p. 7014-26.

110. Lundqvist, M., et al., *Nanoparticle size and surface properties determine the protein corona with possible implications for biological impacts.* Proc Natl Acad Sci U S A, 2008. **105**(38): p. 14265-70.

111. Peng, Q., et al., *Preformed albumin corona, a protective coating for nanoparticles based drug delivery system.* Biomaterials, 2013. **34**(33): p. 8521-30.

112. Myhren, L., et al., *Efficacy of multi-functional liposomes containing daunorubicin and emetine for treatment of acute myeloid leukaemia.* Eur J Pharm Biopharm, 2014. **88**(1): p. 186-93.

113. Xu, H., F. Meng, and Z. Zhong, *Reversibly crosslinked temperature-responsive nano-sized polymersomes: synthesis and triggered drug release.* Journal of Materials Chemistry, 2009. **19**(24): p. 4183-4190.

114. Meng, F., G.H. Engbers, and J. Feijen, *Polyethylene glycol-grafted polystyrene particles.* J Biomed Mater Res A, 2004. **70**(1): p. 49-58.

115. Meng, F., et al., *Pegylated polystyrene particles as a model system for artificial cells.* J Biomed Mater Res A, 2004. **70**(1): p. 97-106.

116. Gao, L.Y. and J. Manoranjan, *Laboratory maintenance of Mycobacterium marinum.* Curr Protoc Microbiol, 2005. **Chapter 10**: p. Unit 10B.1.

117. Nygaard, V., et al., *Melanoma brain colonization involves the emergence of a brain-adaptive phenotype.* Oncoscience, 2014. **1**(1): p. 82-94.

118. Prasmickaite, L., et al., *Human malignant melanoma harbours a large fraction of highly clonogenic cells that do not express markers associated with cancer stem cells.* Pigment Cell & Melanoma Research, 2010. **23**(3): p. 449-451.

119. van der Eb, M.M., et al., *Gene therapy with apoptin induces regression of xenografted human hepatomas.* Cancer Gene Ther, 2002. **9**(1): p. 53-61.

120. Dell'Era, P., et al., *Gene expression profile in fibroblast growth factor 2-transformed endothelial cells.* Oncogene, 2002. **21**(15): p. 2433-40.

121. Jokerst, J.V., et al., *Nanoparticle PEGylation for imaging and therapy.* Nanomedicine (Lond), 2011. **6**(4): p. 715-28.

122. Torchilin, V.P., *Recent advances with liposomes as pharmaceutical carriers.* Nat Rev Drug Discov, 2005. **4**(2): p. 145-60.

123. Wang, A.Z., R. Langer, and O.C. Farokhzad, *Nanoparticle delivery of cancer drugs.* Annu Rev Med, 2012. **63**: p. 185-98.

124. Li, Z., et al., *Membrane tether formation from outer hair cells with optical tweezers.* Biophys J, 2002. **82**(3): p. 1386-95.

125. Beduneau, A., et al., *Facilitated monocyte-macrophage uptake and tissue distribution of superparmagnetic iron-oxide nanoparticles.* PLoS One, 2009. **4**(2): p. e4343.

126. Beningo, K.A. and Y.L. Wang, *Fc-receptor-mediated phagocytosis is regulated by mechanical properties of the target.* J Cell Sci, 2002. **115**(Pt 4): p. 849-56.

127. Pacheco, P., D. White, and T. Sulchek, *Effects of microparticle size and Fc density on macrophage phagocytosis.* PLoS One, 2013. **8**(4): p. e60989.

128. Gerlach, G.F. and R.A. Wingert, *Zebrafish pronephros tubulogenesis and epithelial identity maintenance are reliant on the polarity proteins Prkc iota and zeta.* Dev Biol, 2014. **396**(2): p. 183-200.

129. He, S., et al., *Neutrophil-mediated experimental metastasis is enhanced by VEGFR inhibition in a zebrafish xenograft model.* J Pathol, 2012. **227**(4): p. 431-45.

130. Bettum, I.J., et al., *Metastasis-associated protein S100A4 induces a network of inflammatory cytokines that activate stromal cells to acquire pro-tumorigenic properties.* Cancer Lett, 2014. **344**(1): p. 28-39.

131. Zhong, M.-C., et al., *Trapping red blood cells in living animals using optical tweezers.* Nat Commun, 2013. **4**: p. 1768.

132. Teng, Y., et al., *Evaluating human cancer cell metastasis in zebrafish.* BMC Cancer, 2013. **13**(1): p. 453.

133. Alexis, F., et al., *Factors affecting the clearance and biodistribution of polymeric nanoparticles.* Mol Pharm, 2008. **5**(4): p. 505-15.

134. Allen, T.M. and P.R. Cullis, *Liposomal drug delivery systems: from concept to clinical applications.* Adv Drug Deliv Rev, 2013. **65**(1): p. 36-48.

135. Isogai, S., M. Horiguchi, and B.M. Weinstein, *The vascular anatomy of the developing zebrafish: an atlas of embryonic and early larval development.* Dev Biol, 2001. **230**(2): p. 278-301.

136. Moghimi, S.M., A.C. Hunter, and J.C. Murray, *Nanomedicine: current status and future prospects.* Faseb j, 2005. **19**(3): p. 311-30.

137. Lee, M.J., et al., *Rapid pharmacokinetic and biodistribution studies using cholorotoxin-conjugated iron oxide nanoparticles: a novel non-radioactive method.* PLoS One, 2010. **5**(3): p. e9536.

138. Liao, W.Y., et al., *Comprehensive characterizations of nanoparticle biodistribution following systemic injection in mice.* Nanoscale, 2013. **5**(22): p. 11079-86.

139. Mohammad, A.K., et al., *Rapid lymph accumulation of polystyrene nanoparticles following pulmonary administration.* Pharm Res, 2013. **30**(2): p. 424-34.

140. Palko, H.A., J.Y. Fung, and A.Y. Louie, *Positron emission tomography: a novel technique for investigating the biodistribution and transport of nanoparticles.* Inhal Toxicol, 2010. **22**(8): p. 657-88.

141. Simon, B.H., H.Y. Ando, and P.K. Gupta, *Circulation time and body distribution of 14C-labeled amino-modified polystyrene nanoparticles in mice.* J Pharm Sci, 1995. **84**(10): p. 1249-53.

142. Tamba, B.I., et al., *Silica nanoparticles: Preparation, characterization and in vitro/in vivo biodistribution studies.* Eur J Pharm Sci, 2015. **71**: p. 46-55.

143. Dan, C. and K. Wake, *Modes of endocytosis of latex particles in sinusoidal endothelial and Kupffer cells of normal and perfused rat liver.* Exp Cell Res, 1985. **158**(1): p. 75-85.

144. Wang, Y. and W. Wu, *In situ evading of phagocytic uptake of stealth solid lipid nanoparticles by mouse peritoneal macrophages.* Drug Deliv, 2006. **13**(3): p. 189-92.

145. Diakonova, M., et al., *Localization of five annexins in J774 macrophages and on isolated phagosomes.* J Cell Sci, 1997. **110 (Pt 10)**: p. 1199-213.

146. Sulahian, T.H., et al., *Signaling pathways required for macrophage scavenger receptor-mediated phagocytosis: analysis by scanning cytometry.* Respir Res, 2008. **9**: p. 59.
147. Sheng, Y., et al., *In vitro macrophage uptake and in vivo biodistribution of PLA-PEG nanoparticles loaded with hemoglobin as blood substitutes: effect of PEG content.* J Mater Sci Mater Med, 2009. **20**(9): p. 1881-91.
148. Mehne, J., et al., *Characterisation of morphology of self-assembled PEG monolayers: a comparison of mixed and pure coatings optimised for biosensor applications.* Anal Bioanal Chem, 2008. **391**(5): p. 1783-91.
149. Gabizon, A. and D. Papahadjopoulos, *Liposome formulations with prolonged circulation time in blood and enhanced uptake by tumors.* Proc Natl Acad Sci U S A, 1988. **85**(18): p. 6949-53.
150. Parng, C., et al., *Zebrafish: a preclinical model for drug screening.* Assay Drug Dev Technol, 2002. **1**(1 Pt 1): p. 41-8.
151. Perche, F. and V.P. Torchilin, *Recent trends in multifunctional liposomal nanocarriers for enhanced tumor targeting.* J Drug Deliv, 2013. **2013**: p. 705265.
152. Tian, T., et al., *PTEN regulates angiogenesis and VEGF expression through phosphatase-dependent and -independent mechanisms in HepG2 cells.* Carcinogenesis, 2010. **31**(7): p. 1211-9.
153. Wallez, Y., I. Vilgrain, and P. Huber, *Angiogenesis: the VE-cadherin switch.* Trends Cardiovasc Med, 2006. **16**(2): p. 55-9.
154. Peterman, E.J.G., F. Gittes, and C.F. Schmidt, *Laser-Induced Heating in Optical Traps.* Biophysical Journal, 2003. **84**(2): p. 1308-1316.
155. Han, S., C. Kim, and D. Kwon, *Thermal/oxidative degradation and stabilization of polyethylene glycol.* Polymer, 1997. **38**(2): p. 317-323.
156. Ebert, S., et al., *Fluorescence ratio thermometry in a microfluidic dual-beam laser trap.* Opt Express, 2007. **15**(23): p. 15493-9.
157. Estrada-Perez, C.E., Y.A. Hassan, and S. Tan, *Experimental characterization of temperature sensitive dyes for laser induced fluorescence thermometry.* Rev Sci Instrum, 2011. **82**(7): p. 074901.
158. Shah, J.J., M. Gaitan, and J. Geist, *Generalized Temperature Measurement Equations for Rhodamine B Dye Solution and Its Application to Microfluidics.* Analytical Chemistry, 2009. **81**(19): p. 8260-8263.
159. Evensen, L., et al., *Contextual compound screening for improved therapeutic discovery.* Chembiochem, 2013. **14**(18): p. 2512-8.
160. Pardo-Martin, C., et al., *High-throughput in vivo vertebrate screening.* Nat Methods, 2010. **7**(8): p. 634-6.
161. Spaink, H.P., et al., *Robotic injection of zebrafish embryos for high-throughput screening in disease models.* Methods, 2013. **62**(3): p. 246-254.